TOWARD IMPROVED CHARACTERIZATION OF HUMAN MESENCHYMAL STEM CELLS FOR USE IN CELLULAR THERAPIES: A REGULATORY SCIENCE PERSPECTIVE

by

Jessica L. Lo Surdo

BS, Syracuse University, 2005

MS, University of Pittsburgh, 2008

Submitted to the Graduate Faculty of

Swanson School of Engineering in partial fulfillment

of the requirements for the degree of

Doctor of Philosophy

University of Pittsburgh

2013

UNIVERSITY OF PITTSBURGH

SWANSON SCHOOL OF ENGINEERING

This dissertation was presented

by

Jessica L. Lo Surdo

It was defended on

April 26, 2013

and approved by

Johnny Huard, PhD, Professor, Departments of Orthopaedic Surgery, Molecular Genetics, Biochemistry, Pathology and Bioengineering

Kacey Marra, PhD, Associate Professor, Departments of Surgery and Bioengineering

Partha Roy, PhD, Associate Professor, Departments of Pathology and Bioengineering

Dissertation Director: Steven R. Bauer, PhD, Adjunct Professor, Department of Bioengineering

TOWARD IMPROVED CHARACTERIZATION OF HUMAN MESENCHYMAL STEM CELLS FOR USE IN CELLULAR THERAPIES: A REGULATORY SCIENCE PERSPECTIVE

Jessica L. Lo Surdo, PhD

University of Pittsburgh, 2013

Cellular therapies hold great potential to treat a variety of medical conditions. Product characterization of cellular therapies is particularly difficult, as they pose regulatory challenges due to donor heterogeneity and a lack of standard lot release tests that can reliably predict *in vivo* outcomes. In particular, multipotent stromal cells, also called mesenchymal stem cells (MSCs), are potentially valuable as a cellular therapy due to their regenerative capacity and immunosuppressive function. Due to the required expansion and inherent heterogeneity of MSCs, quantitative approaches capable of measuring differentiation capacity and immunosuppressive function between donors and passages on a per cell basis are needed. To address this unmet need, a sample set of human MSCs comprised of eight donors was created, cultured to early and late passages, and novel quantitative bioassays were established capable of measuring adipogenic and osteogenic differentiation on a per cell basis, as well as an *in vitro* assay to measure immunosuppressive function. Based on existing bioassays, MSCs demonstrate a decrease in overall proliferative potential and colony forming unit capacity, while expression of hallmark MSC surface markers remain unchanged. Utilizing automated microscopy techniques, adipogenic and osteogenic differentiation potential was quantified on a per cell basis, allowing us to directly assess the role of donor variability and *in vitro* culture on MSC function. Overall,

donor variability and a decrease in differentiation potential with passage was demonstrated based on these quantitative assays. Since culture-expanded MSCs increase in cell size, this parameter was utilized to enrich for small cells, which demonstrated that the small cell population is more stem-like based on these applied quantitative bioassays. Lastly, immunosuppressive function of human MSCs on murine-derived clonal T cells was assessed utilizing a novel *in vitro* xenogeneic model system. Human MSCs can inhibit murine T cell activation, rendering this an ideal system to assess immunosuppressive function of MSCs *in vitro.* In conclusion, novel methods were established to quantify MSC function, and these findings were correlated with other previously-established quantitative bioassays to better understand the role of donor variability and passaging on MSC potency. Taken together, these quantitative approaches provide valuable tools to measure MSC quality, and supports continued efforts to improve characterization strategies for cellular therapies.

TABLE OF CONTENTS

LIST OF TABLES

LIST OF FIGURES

NOMENCLATURE

ALP – alkaline phosphatase (enzymatic activity)

ALPL – alkaline phosphatase (gene)

CFU – colony forming unit

FSC – forward scatter

IFN-γ – interferon gamma

MFI – mean fluorescence intensity

MSCs – mesenchymal stem cells or marrow stromal cells

P3 – passage 3

P5 – passage 5

P7 – passage 7

sFRP-1 – secreted frizzled-related protein 1

SSC – side scatter

TNF-α – tumor necrosis factor alpha

PREFACE

I would like to express my sincerest gratitude and appreciation to my mentor and PI, Dr. Steven Bauer. I appreciate your willingness to take me on as a student, and sharing your enthusiasm for research. Thank you for your support and guidance, for always being my biggest advocate, and for believing in my abilities as a scientist. I feel honored to have worked for you, and I cannot thank you enough. You truly are 'mahvelous'.

To Dr. Borovetz, thank you for giving me the opportunity to finish pursuing my graduate studies at the FDA. Although unconventional, you still made this possible, and I greatly appreciate the opportunity. I'd also like to say a special thank you to Lynette Spataro for all your help and assistance from afar!

To Drs Huard, Marra and Roy, thank you for serving on my dissertation committee. I truly appreciate your time, guidance and scientific expertise.

I would like to thank current and past members of the Bauer laboratory for all your help and assistance in the lab. To Eva Rudikoff, thank you for all of your help in expanding cells, and most of all, for always sticking your neck out on my behalf. To Heba Degheidy and Edyta Pawelczyk, you both truly exemplify what it means to be a woman in science, and near or far, you will always give me something to aspire to. Thank you!

To my fiancé Bryan, thank you for being everything you've done for me during this whole process. Your love and support helped me through, so I thank you for everything.

I'd like to say a special thank you to my Nonna for your daily well wishes, love and encouragement. To my Aunt Marie and Uncle Tony, you are always so supportive and find a way to be a part of my life, so thank you for sharing this with me. To Andie, Sam and Janelle, thanks for your sibling love and support. To my dear friend Christy, thank you for your friendship since we started graduate school. I'm so happy you're all a part of my life and that I'm able to share this experience with you!

To my loving parents, I would not be where I am without you. Thank you from the bottom of my heart for all your love, encouragement, and support, and for always believing in me and my academic goals. You are so special to me; I love you both and I cannot thank you enough for everything you've done for me.

Lastly, I would like to acknowledge my funding sources. This project was supported in part by an appointment to the Research Participation Program at CBER administered by the Oak Ridge Institute for Science and Education through US DOE and US FDA. This work was also supported in part by the FDA Modernizing Science grant program, a BARDA grant, a grant from the Medical Countermeasures Initiative, and research funds from the Division of Cell and Gene Therapies.

1.0 BACKGROUND

Stem cell therapy holds great therapeutic potential to address a range of unmet medical needs. Adult stem cells include bone marrow stromal cells, or mesenchymal stem cells (MSCs), and are of great interest for their potential clinical use as cellular therapies to treat many diseases based on their innate reparative and immunosuppressive functions. There are currently over 300 trials underway using MSCs to treat a variety of clinical conditions, including Crohn's disease, heart failure, osteoarthritis, osteogenesis imperfecta, multiple sclerosis and several others (1). MSCs are particularly promising as they are free of ethical concerns typically associated with embryonic stem cells, would not be expected to form teratomas, and are immune-privileged.

The use of biologic therapies such as MSCs provides a unique challenge. While drugs are well characterized and provide an established mode of action, biologics and cell therapies in general are less understood. MSCs may come from either an autologous or allogeneic cell source, which means cells can come from several donors. Cells derived from different donors may vary in their potency, or their ability to carry out a desired function. Further, their potency may also decline due to the often required cell expansion before treatment. Taken together, this establishes a need to develop assays that are capable of identifying potency based on the ability of MSCs to repair and immunosuppress.

This section will focus on the basic biology of MSCs and the underlying molecular mechanisms involving differentiation and immunosuppression. An understanding of the

biological processes behind differentiation capacity and immunosuppression will enhance our ability to establish bioassays capable of measuring potency in MSCs based on donor differences and *in vitro* culturing.

1.1 BASIC BIOLOGY OF MSCS

1.1.1 MSC niche

The idea of a stem cell niche was first described in the late 1970s by Schofield, and is described as the microenvironment in which stem cells are retained in their naïve state through the influence of local cytokines, growth factors and extracellular matrix by which they are surrounded (2).

The bone marrow is a dynamic tissue comprised of the stroma and stromal cells, whose primary function *in vivo* is to support hematopoiesis and bone formation through the secretion of extracellular matrix components and various cytokines and growth factors. The bone marrow provides support for hematopoiesis through cell signaling that drives lineage commitment and differentiation of hematopoietic stem cells (3-5). The MSCs are presumed to be the stromal cells that reside in the bone marrow, and were first discovered by Friedenstein, who described these stromal cells as adherent, clonogenic populations that are capable of self-renewal and differentiation (6). The self-renewal capacity of MSCs that promote maintenance of the undifferentiated state involves various cytokines and growth factors, including leukemia inhibitory factor (LIF) (7,8) and fibroblast growth factor (FGF) (9,10). Likewise, it has also

been suggested that Wnt signaling may be involved in maintenance and self-renewal in MSCs (11,12).

MSCs are typically isolated by density gradient centrifugation from a bone marrow aspirate. Once placed in culture, adherent cells persist as fibroblast-like cells capable of an initial doubling time of 12-24 hours, which is density-dependent (13).

While MSCs can be derived from a variety of sources, the original tissue from which they were derived plays a role in their ability to carry out a desired function. MSCs may not only be derived from bone marrow, but from many other sources, including adipose (14-16), skeletal muscle (17-20), umbilical cord blood (21-24) and dental pulp (25-28). Further, they have also been shown to be derived from non-mesoderm tissues, however the focus of this work will be on human bone-marrow derived MSCs.

1.1.2 MSC Phenotype

The minimum criteria as defined by the ISCT requires that MSCs be plastic adherent, capable of trilineage differentiation, and ≥ 95% positive for CD73, CD90 and CD105, and lack expression of (≤ 2%) of CD14 or CD11b, CD79a or CD19, CD34, CD45, and HLA Class II (29). However, there is currently no hallmark MSC marker, and they are therefore typically assessed using a panel of cell surface markers. Identification of novel markers in the future to further define a multipotent, stem-like phenotype will be a useful tool in characterizing MSCs.

1.1.2.1 Cell surface marker expression – positive markers

CD29 is an integrin β1 or fibronectin receptor involved in cell adhesion, hemostasis, tissue repair and the immune response. Loss of integrin β1 leads to disrupted cell differentiation, as it is the major adhesion receptor for several extracellular matrix components (30). CD44 is a cell surface glycoprotein that is the receptor for hyaluronic acid. It is involved with cell adhesion, migration and cell-cell interactions, while also mediating interactions with ligands including osteopontin, collagens and matrix metalloproteinases (31). CD73, otherwise known as ecto 5'-nucleotidase, is a plasma membrane protein that is associated with lymphocyte differentiation. It catalyzes the dephosphorylation of extracellular nucleoside 5' monophosphates for cell metabolic purposes. Defects in the ecto 5'-nucleotidase gene may result in calcification of joints and arteries. Thy-1 antigen (CD90), is a membrane glycoprotein expressed in cord blood cells, bone marrow and human fetal liver cells. Expression of this surface antigen has been shown to correlate with highly proliferating progenitor cells (32). CD105, otherwise known as endoglin, is a component of the TGF-beta receptor complex. CD105 is a glycoprotein of the vascular endothelium, and has been reported to play a crucial role in embryonic angiogenesis. CD105 has been shown to be expressed ovary, uterus, fibroblasts, as well as heart, muscle and stromal cells (33). Vascular cell adhesion moledule-1 (VCAM1), also known as CD106, is a cell surface sialoglycoprotein that is expressed in cytokine-activated endothelium, and is potentially involved in atherosclerosis and rheumatoid arthritis, while also mediating cell adhesion and signal transduction (34). Activated leukocyte adhesion molecule (ALCAM, CD166), is involved in cell adhesion and migration between thymic epithelial cells and $CD6^{+}$ cells during T-cell development. CD166 is expressed in several cell types, including activated T cells and monocytes, epithelial cells, fibroblasts, and neurons (35).

1.1.2.2 Cell surface marker expression – negative markers

Following bone marrow aspiration and subsequent culture, MSCs exist amongst other cell types with a variety of expression profiles. During expansion *in vitro*, it is necessary to distinguish between hematopoietic stem cell (HSCs) contaminants, as well as other cell types seen in the bone marrow (i.e. osteoblasts, osteocytes, etc.). MSCs should be $\leq$ 2% positive for HSC markers, including CD34 (a primitive HSC marker) and CD45 (a positive marker of all hematopoietic cells). MSCs should also be negative for an endothelial/HSC marker CD31, as well as CD117 (a marker for hematopoietic progenitors). Further, MSCs should also not express CD14 (a monocyte/macrophage marker), CD79α (recognizes a membrane glycoprotein present on B lymphocytes), and HLA-DR (binds to MHC class II, and is present on antigen presenting cells).

1.1.2.3 Cell surface marker expression – other markers

The STRO-1^{+} fraction in bone marrow was previously demonstrated to contain early osteogenic precursors in MSCs (36). Expression of STRO-1 has been shown to enhance CFU capacity, however, its expression by flow cytometry has been shown to be variable, and may be lost with *in vitro* culture (37). More recently, CD271, otherwise known as nerve growth factor receptor (NGFR), has been shown to be expressed in a small population of MSCs. Buhring *et al.* previously demonstrated that the $CD271^{bright}$ population contained the CFU-forming cell population (38). Further, the CD271 positive population was also shown to express higher levels of Wnt-related genes (39).

1.1.3 Trilineage differentiation capacity

MSCs are capable of trilineage differentiation, and therefore have potential clinical applicability related to regenerative therapies. MSCs can be easily differentiated *in vitro* provided they are cultured in the appropriate environment. Interestingly, MSCs have now been shown to differentiate to tissue types outside the mesoderm, including hepatic and neural lineages (16,40-45). For the purpose of this work, we will focus only on mesoderm-specific lineage pathways, including adipogenic, osteogenic and chondrogenic differentiation potential.

1.1.3.1 Adipogenesis

Adipogenesis is the process by which an MSC undergoes differentiation to a mature adipocyte. MSCs can be induced *in vitro* through the addition of exogenous factors to the culture media, including isobutyl methyl xanthine (IBMX), indomethacin and insulin (46). The presence of IBMX, a phosphodiesterase inhibitor, blocks the conversion of cAMP to 5'AMP, which leads to upregulation of protein kinase A (PKA), and in turn increasing expression of hormone sensitive lipase (HSL). Triacylglycerides are converted to glycerol and ultimately free fatty acids through the effect of HSL. Indomethacin is an anti-inflammatory drug that promotes adipogenesis through peroxisome proliferator-activated receptor gamma (PPARγ) (47). Insulin promotes adipogenesis through binding insulin-like growth factor 1 (IGF-1), resulting in phosphorylation of cAMP response element–binding protein (CREB) through phosphatylinositol-3 kinase (PI3K) and cAMP (48). CREB is an early regulator of major players in adipogenesis, including CCAAT/enhancer binding protein (C/EBPα) and PPARγ (49).

MSCs undergo terminal differentiation into a mature adipocyte following growth arrest, and expression of mRNAs including lipoprotein lipase (LPL), which is involved in lipogenesis

(50). This is followed by activation of transcriptional factors including CCAAT/enhancer binding protein alpha (C/EBPα) and peroxisome proliferator-activated receptor gamma (PPARγ) (51). Other markers of adipogenesis include adipsin, a protease involved in glucose transport stimulation, and adiponectin, a protein in involved in insulin sensitivity regulation (52), and acyl-CoA synthetase short-chain family member 2 (ACSS2), which is involved in lipid synthesis (50). The terminally-differentiated adipocyte adopts a lipid-laden, spherical morphology and expresses mature differentiation markers, including C/EBPα, PPARγ, adiponectin adipocyte protein 2 and adipsin (53).

1.1.3.2 Osteogenesis

A crucial role of MSCs *in vivo* is osteogenic differentiation and bone formation. *In vitro* differentiation of MSCs typically involves the addition of ascorbic acid, β-glycerophosphate, and dexamethasone to the culture media for 14-21 days. Ascorbic acid and β-glycerophosphate stimulate collagen type I secretion (54), while dexamethasone stimulates osteogenesis by inducing expression of osteogenesis-related genes, including runt-related transcription factor 2 (Runx2) Osterix (Osx) and bone matrix proteins (55). Runx2 is the earliest marker of osteogenesis, and regulates differentiation through transforming growth factor beta 1 (TGF-β1) and bone morphogenic protein 2 (BMP2) (56,57). Commitment to the pre-osteogenic lineage involves increases in proliferative capacity and morphological changes, and involves expression of earlier bone markers, including ALPL, type I collagen and osteopontin. ALPL is a regulator of bone mineralization expressed in preosteoblasts. β-catenin, osterix and Runx2 promotes differentiation of preosteoblasts into immature osteoblasts that express bone matrix protein, osteopontin, and bone sialoprotein (58). A fully terminally-differentiated osteoblast adopts a

cuboidal morphology capable of increased mineralization and protein production (59). Osterix promotes differentiation of mature osteoblasts through osteocalcin expression (60), and is also associated with increased expression of ALPL, collagen type I and osteocalcin in the mature osteoblast phenotype (61,62).

1.1.3.3 Chondrogenesis

The regulation of articular cartilage formation through chondrogenesis is the first developmental step of skeletal development in mammalian organisms, and is controlled by a variety growth factors and signaling molecules. Initiation of chondrogenesis is mediated through paracrine factors and predominantly by a transcription factor, Sox9. Expression of N-cadherin and Sox9 is upregulated by paracrine factors such as FGF, TGF-β, BMPs, while Wnts negatively regulate chondrogenesis by blocking expression of Sox9. Sox9 positively induces other genes involved in chondrogenesis, namely Sox5, Sox6, and Col2A1. L-Sox5 and Sox6 are also required for expression of Col2A1 and aggrecan expression, which is the most abundant proteoglycan in cartilage (63).

1.1.4 MSC heterogeneity

MSCs are a heterogeneous population of adult stem cells, both in regards to their morphology as well as biological function. MSC heterogeneity can be discussed in terms of their "inter-population" heterogeneity, or differences between different populations, sources or donors, or in terms of "intra-population" heterogeneity, clonal heterogeneity within an individual population of MSCs (64). In regards to morphological heterogeneity, MSCs *in vitro* co-exist as either small, rapidly dividing cells, termed recycling stem cells (RS cells), or large, slowly dividing mature

cells (mMSCs). Changes in biological function in MSCs may be closely tied to this morphological heterogeneity, and this phenomenon will be discussed more extensively in Chapter 4.

1.1.5 Wnt signaling in MSCs

Understanding signaling mechanisms underlying MSC function may allow for the identification of novel molecular targets to improve measurement of MSC function. While many signaling pathways are involved in different aspects of MSC function, Wnt signaling may be the fundamental mechanism by which MSCs are capable of self renewal and differentiation. Specifically, canonical Wnt signaling is involved in cell fate decisions and regulating stemness in many stem cell types (12).

In the presence of Wnt ligand, Wnt binds to Frizzled (Fz) and co-receptors LRP-5 and LRP-6, leading to the activation of cytoplasmic Disheveled (Dv1). The presence of Disheveled blocks phosphorylation of β-catenin by glycogen synthase kinase (GSK-3β). This allows accumulation of β-catenin and subsequent nuclear translocation, where it binds to T-cell factor (TCF) and lymphoid enhancer factor (LEF) to regulate downstream targets. In the absence of Wnt, β-catenin is phosphorylated by GSK-3β, targeting it for ubiquitination and subsequent proteosomal degradation (65). The role of Wnt signaling in differentiation will be discussed in greater detail in Chapter 4.

1.1.6 Immunosuppressive function

MSCs may not only have a potential therapeutic effect because of their regenerative properties, but also due to their capacity for immunosuppression. This immunoprivileged status has therefore extended their potential clinical relevancy to treat several autoimmune diseases, including type 1 diabetes, Crohn's disease, multiple sclerosis, and others (66-69). The ability of MSCs to escape the immune response may be in part due to their lack of HLA Class II antigens on the cell surface. Mechanisms of immunomodulation include inhibition of proliferation and differentiation of T cells, B cells, natural killer cells and dendritic cells, however the focus of this work will be the effect of MSCs on T cells. A more detailed background of the immunosuppressive function of MSCs will be reviewed in Chapter 5.

1.2 CELLULAR THERAPIES USING MSCS AND THE REGULATORY PERSPECTIVE

Adult bone marrow derived MSCs hold great therapeutic potential based on their capacity to differentiate, regenerate and support hematopoiesis, as well as their immunomodulatory functions. Because of their immune-privileged status, they may be used both in autologous and allogeneic settings. Over 300 clinical trials are underway using MSCs, and which are primarily centered around;. differentiation capacity toward osteogenic and chondrogenic lineages; stromal support in the hematopoietic microenvironment; immunomodulatory function; and secretory profile of trophic factors involved in tissue regeneration (1).

Cell based therapies are being actively developed as evidenced by several hundred Investigational New Drug (IND) applications at the Center for Biologics Evaluation and Research (CBER). While these therapies have great promise to treat a wide variety of medical conditions, cellular therapies as a whole are so novel that product characterization is particularly challenging. In general, optimal approaches to evaluate and select in-process or lot-release tests that are capable of predicting *in vivo* performance of cell-based therapies are still unknown. At CBER, a consortium has been assembled to address the needs of product characterization in cell-based therapies as it relates to MSC potency.

Regulatory science is defined as the science of developing tools, standards and approaches to assess the safety, efficacy, quality and performance of Food and Drug Administration (FDA)-regulated products. CBER research priorities include improving or developing new methods to measure, and ideally quantify, biologic product quality, safety and efficacy. Reviewers help to identify issues and set research priorities applicable to concrete product issues, with the goal of developing and integrating novel scientific technologies that could be used to improve biologics product characterization, availability, and quality. Unlike academic or industry-based research institutions, the research focus at the FDA and CBER is unique, with a goal in identifying solutions related to product development challenges. Key regulatory considerations as it relates to cellular therapies include the following: (a) can biomarkers be identified that predict quality, potency and safety of stem-cell based products reliably? (b) by what mechanisms do stem cells function?, and (c) what adverse effects, such as migration to an ectopic location, inappropriate differentiation or tumorigenicity are likely to occur? And more specifically, as it relates to the field of MSC biology, our goals are also to

address the needs of the field, including quantitative measures of differentiation capacity on a per cell basis to assess stemness potential in MSCs.

1.3 PROJECT OBJECTIVES

The overarching goal of this project is to improve characterization of bone marrow-derived MSCs by determining the role of donor variability and *in vitro* expansion as it relates their differentiation potential and immunosuppressive function. Further, we seek to correlate these characteristics with Wnt signaling to identify a mode of action, while also improving MSC function by enriching for a more biologically active MSC population.

1.3.1 Objective #1: To evaluate the role of donor variability and *in vitro* expansion on MSC characteristics.

Hypothesis: MSC characteristics, including cell size, CFU and proliferative capacity, and MSC cell surface marker expression will vary between donor cell lines, and physical and functional characteristics will change as a result of passaging.

Due to the low percentage of MSCs in the bone marrow, MSCs will require *in vitro* expansion to obtain sufficient numbers for treatment in cellular therapies. Further, this will also require cells from multiple donors. Because of the inherent heterogeneity associated with an individual population of MSCs, as well as donor differences, there is a need to utilize existing and establish

novel quantitative assays to assess MSC characteristics that are predictive of MSC function *in vivo.*

Studies looking at different donors have been focused on understanding the role of *in vivo* (donor age) or *in vitro* (passaging) on MSC quality. Decreases in proliferative capacity were more highly associated with passaging as opposed to donor age, which correlated with increased beta-galactosidase staining, a measurement of senescence.

Current assays to assess biological function of MSCs include colony forming units, proliferation capacity and flow cytometry to measure expression of cell surface markers. In this chapter, we will utilize these assays and others to assess a baseline of biological function of the MSCs used in this thesis. We have expanded cells from 8 male or female donors of a range of ages, to further examine MSC quality. We will further-correlate these endpoints with differentiation capacity as discussed in the next chapter.

1.3.2 Objective #2: To establish quantitative bioassays to measure differentiation capacity in MSCs.

Hypothesis: Novel assays to measure differentiation can quantify changes in differentiation potential between donors and passages.

MSCs are partially defined by their ability to differentiate to adipocytes, osteoblasts and chondrocytes *in vitro.* To assess differentiation, staining is typically used to identify a differentiated phenotype. While staining is sufficient, these methods are inherently qualitative, and do not take into account the heterogeneity associated with MSCs. Further, these qualitative

assays cannot be used to assess differences between donors or as a result of passaging. There is therefore a need to establish quantitative assays that are capable of detecting changes in MSC characteristics.

Where applicable, we employed novel quantitative bioassays to measure differentiation on a per cell basis. Adipogenesis will be measured using two methods; limiting dilution and automated microscopy. Osteogenesis will be quantified by ALP staining. Chondrogenesis will assessed qualitatively by the presence of sulfated glycosaminoglycans via Alcian Blue staining. Differentiation potential by donor and passage will be correlated with changes in gene expression of lineage-specific markers.

1.3.3 Objective #3: Determination of the role of cell size and Wnt signaling in differentiation and senescence of MSCs using quantitative bioassays

Hypothesis: The small cell-size population contains more stem-like progenitors, and may correlate with decreased Wnt activity and senescence.

The canonical Wnt signaling pathway is intrinsic to regulating stem cell function and cell fate decisions, and elicits various functions on many stem cell types (12,70). Wnt signaling has different roles in differentiation and senescence. Blocking signaling through the addition Wnt antagonists have previously demonstrated increased adipogenesis and improved proliferative capacity, while its effect on osteogenesis is more controversial (70-73). Identifying the role of signaling mechanisms involved in MSC differentiation and senescence may allow for the discovery of novel therapeutic targets.

MSCs are a heterogeneous population of adult stem cells that contain small, agranular proliferating cells and large, granular senescent cells. Changes in cell size following *in vitro* expansion have been previously documented (74-76). However, there has been little effort in the field to enrich for purified cell size populations to study them individually and elucidate the role of cell size in MSC function.

To better understand the role of passaging, and to correlate noted changes in cell size, we separated MSCs by size to apply quantitative assays to measure changes in size-associated biological function. To further elucidate a mode of action, we evaluated the role of Wnt signaling by adding specific pathway stimuli to unsorted MSC populations.

1.3.4 Objective #4: To measure immunosuppressive activity in MSCs *in vitro*

Hypothesis: Human MSCs will exert an immunosuppressive effect on mouse T cells in a novel *in vitro* assay system.

MSCs possess the ability to immunosuppress, and therefore there is ongoing interest in exploring their therapeutic potential in treating immune disorders such as Graft versus Host Disease (GvHD), Crohn's Disease, multiple sclerosis and type II diabetes. Their immune-privileged status is due to, at least in part, their lack of major histocompatibility complex II (MHC-II), as well as paracrine effects that inhibit secretion of pro-inflammatory cytokines, allowing them to evade the immune response. This allows for MSCs to be used allogeneically based on this immunosuppressive function, and therefore can be expanded in large volumes to treat a variety of diseases. Further, MSCs may therefore be expanded from multiple donors for cellular therapy trials. There is therefore a need to establish quantitative *in vitro* bioassays to assess

immunosuppressive function that are predictive of *in vivo* outcomes to determine the role of donor and passage differences.

In this chapter, we will utilize a novel *in vitro* xenogeneic model system to assess immunosuppressive capacity of human MSCs on mouse T cells. Immunosuppression will be measured by reduced expression of inflammatory and activation markers such as CD25, CD62L and CD69 by flow cytometry. Secretion of pro-inflammatory cytokines TNF-α and IFN-γ will be assessed by cytokine arrays, and expression of activation markers Tbet and GATA3 will be assessed by digital droplet PCR.

2.0 EVALUATION OF MSC CHARACTERISTICS BASED ON DONOR VARIABILITY AND *IN VITRO* CULTURING

2.1 INTRODUCTION

MSCs have proven to be easy to expand and differentiate in culture. MSCs are characterized by their adherent properties, expression of several surface antigens including CD73, CD105 and CD90, and tri-lineage differentiation capacity (29); however, investigators are continually trying to improve characterization due to MSC heterogeneity. Within a population of MSCs, variability in cell properties such as proliferation, morphology, differentiation capacity and cell surface marker expression profiles have been widely observed (77). These "intra-population" MSC heterogeneities and their innate plasticity may arise due to the *in vivo* microenvironment or also due to long-term *in vitro* culture (64). It is this heterogeneous nature of MSCs that may allow them to respond effectively to a wide variety of cues in their local microenvironment to carry out a particular biological function.

As these cells are extensively being tested for clinical applications, it would be useful to develop new quantitative bioassays to measure donor variability and the effect of passaging. Such tools could help to determine the suitability of a particular population of MSCs in treating a particular disease. Further, these quantitative tools could be used to assess differences in parameters such as cell source (fat, bone marrow, muscle), cell selection for enrichment (STRO-

1, CD271), culture media, cell density, and the effects of different protocols for expansion of MSCs. Finally, these tools could enhance our understanding of MSC heterogeneity. As stated by Wagner and Ho (77), there is an urgent need for more precise cellular and molecular markers to define subsets of MSCs.

In this chapter, we utilize several existing quantitative bioassays to measure differences in donors and passage number in a systematic fashion in order to establish a baseline of biological activity for the cell lines used in this thesis. The overall goal in this chapter is to employ quantitative measurements that will improve characterization MSCs by determining the role of donor variability and passage number as it relates to the biological properties of MSCs *in vitro*.

2.2 MATERIALS AND METHODS

2.2.1 Expansion of MSCs

Human bone marrow-derived MSCs from 8 different donors were purchased from either All Cells (Emeryville, California) (PCBM1641, PCBM1632, PCBM1662, PCBM1655) or Lonza (Walkersville, MD) (167696, 110877, 8F3560, 127756) at passage 1 (see Table 2.1 for donor specifications). MSCs were plated in T175 flasks (Cellstar) at a cell density of 60 cells/cm^2, and expanded in complete medium containing α-MEM, l-glutamine, penicillin-streptomycin (Invitrogen), and 16.5% lot-selected fetal bovine serum (FBS, JM Bioscience) at 37°C and 5% CO_2. All cell lines were expanded and cryopreserved in the same serum-selected media with uniform handling throughout culture, as outlined in Lo Surdo and Bauer (74).

Table 2-1. Summary of cell line specifications.

Designation	PCBM1632	110877	167696	PCBM1641	PCBM1662	8F3560	127756	PCBM1655
Gender	M	M	F	F	F	F	M	F
Age	24	22	22	23	31	24	43	47

MSCs from each donor were thawed and cultured at passage 1. When the cultures reached 80% confluence, cells were removed by trypsin (0.25% Trypsin/EDTA, Invitrogen) and replated into flasks at passage 2. Once passage 2 cells became 80% confluent, MSCs were trypsinized, and the resulting passage 3 cells were cryopreserved in freezing medium containing 30% FBS (JM Bioscience), 5% dimethyl sulfoxide (Sigma-Aldrich), 1% l-glutamine, and 1% penicillin (100 units/ml) and streptomycin (100ug/ml; Invitrogen). An aliquot of cells was

removed prior to cryopreservation to allow for continuous expansion to passages 3 (P3), 5 (P5) and 7 (P7) without any freezing in between. Therefore, once MSCs were expanded to a particular passage, they were only frozen one time; at that passage. Each passage is considered to be the number of times the cells were trypsinized up until cryopreservation. The time to reach 80% confluence varied between cell lines and passages, and is outlined in the results section in Table 2.2.

2.2.2 Authentication of cell lines by STR profiling

MSCs were thawed at P3, cultured until 80% confluent, then trypsinized, counted, and resuspended in PBS at 1 x 10^6 cells/ml. 20µl of cell suspension was spotted on FTA sample collection cards and were allowed to dry. Sample collection cards were submitted to ATCC for their STR-based Cell Authentication Testing Service. As per the methodology provided by ATCC, seventeen short tandem repeat (STR) loci, including the gender determining loci Amelogenin, were amplified using commercially available Powerplex 18D Kit from Promega. Cell line samples were processed using the ABI Prism 3500xl Genetic Analyzer, and data was analyzed using GeneMapper IDX v3.1 software from Applied Biosystems with suitable positive and negative controls.

2.2.3 Cell proliferation

MSCs from all donors at P3, P5 and P7 were plated at 1000 cells/cm^2 in 24-well plates (Corning). Following cell adhesion, cells were placed in an Incucyte Live Cell Imager (Essen

Bioscience). Nine images per well were taken every 3-4 hours. Percent confluence measurements were averaged for each well (n=9) and then at each passage (n=4) and plotted as a function of time to measure proliferation capacity.

2.2.4 Flow cytometry

MSCs were thawed and cultured to 80% confluence, trypsinized and resuspended in FACS buffer containing 1% FBS and 0.2% sodium azide in 1X PBS. Cells were incubated with 2.4G2 antibody (ATCC) at 4°C for 30 minutes to block non-specific binding. Cells were then labeled with the following at 4°C for 30 min: Positive MSC markers: anti-CD29-PE-Cy5, anti-CD44-APC, anti-CD73-PE-Cy7, anti-CD90-FITC, anti-CD166-PE (BD Pharmingen), anti-CD105-PE (Beckman Coulter). Negative MSC markers: anti-CD14-Alexa Fluor 488, anti-CD34-PE, anti-CD45-PE, HLA-DR-FITC (BD Pharmingen), anti-CD79α-PE-Cy5, anti-CD117-APC (Beckman Coulter). Flow cytometry data was recorded using the FACS Canto II (BD Biosciences), and analysis was completed using Flow Jo Analysis Software. Forward (FSC) and side scatter (SSC) data was recorded and analyzed to determine changes in cell size and granularity, and percent positive cells was measured for all markers mentioned above.

2.2.5 Cell size measurements

Following trypsinization, an aliquot of cells from 5 to 13 pooled T175 flasks (from one cell line and one passage) were counted using an automated cell counter (Nexcelom Cellometer). MSCs were diluted 1:1 in trypan blue, and MSCs from each donor were cyropreserved at P3, P5 and P7 at $1x10^6$ cells/ml/vial. Cell lines 127756 and PCBM1655 could not be expanded past P5 and P3

respectively. The Cellometer measures the pixel area of the cells, converts that measurement to a surface area, and calculates a cell diameter based on the assumption that the cells are circular within user-defined parameters. The minimum and maximum size range was determined, and the frequency of cell sizes falling within a 1μm diameter bin was calculated and graphed to determine the size distribution of each donor and passage number.

2.2.6 Colony forming units

MSCs for all donors and passages were plated at 100 cells/dish in 10-cm dishes (BD Falcon) in triplicate for all cell lines and passages. Cells were cultured for 14 days at 37°C and 5% CO_2 with no media changes. At day 14, plates were washed with PBS, and stained with 3% Crystal Violet (Sigma-Aldrich) in 100% methanol for 10 minutes at room temperature. Plates were rinsed with tap water until clear and allowed to dry. Colonies that were greater than 2mm in diameter were counted, and the percent CFUs was reported per 100 cells seeded.

2.2.7 Statistical analyses

Statistical analyses for percent CFU data were completed using GraphPad Prism 5. Data was grouped for comparisons between cell lines and between passages. For colony forming unit quantification (n=3), two-way ANOVA was preformed with a Bonferroni post-hoc analysis. CFU data was expressed as the mean ± standard deviation. Statistical analyses for average cell diameter measurements ($n \geq 6$) were completed in IBM SPSS using one-way ANOVA followed by a Bonferroni post-hoc analysis to assess differences within cell lines relative to P3. Average

cell diameter data was expressed as the mean ± standard error of the mean. P-values < 0.05 were considered significant.

2.3 RESULTS

2.3.1 STR profiling

For all donors, the submitted sample profile is human, and does not match any profile in the ATCC 8-loci STR database, indicating each sample is unique.

2.3.2 Expansion potential of MSCs

MSCs were cultured from donors varying in age by up to 25 years (Table 2.1), and were expanded to 80% confluence under identical growth conditions to ensure continuity between cell lines and passages. We observed interesting differences in growth potential between different cell lines and passages (Table 2.2). The overall proliferative capacity of MSCs from 127756 (43 y/o) and PCBM1655 (47 y/o) was limited, as they were not capable of expansion beyond passage 5 and passage 3 respectively. However, PCBM1632 (24 y/o) shows limited growth potential by passage 7, requiring 17 days to become 80% confluent. Other cell lines show a general trend toward increasing in time required to reach 80% confluence with increasing passage.

Table 2-2. Number of days to 80% confluence during expansion.

	P2 to P3	P4 to P5	P6 to P7
PCBM1632	7	9	17
110877	8	9	10
167696	8	10	12
PCBM1641	7	8	8
PCBM1662	10	9	12
8F3560	9	10	9
127756	9	11	n/a
PCBM1655	14	n/a	n/a

2.3.3 MSC proliferative potential decreases due to passaging and varies between donors

MSCs were plated at identical densities to measure proliferation potential in normal expansion medium using a live cell imager, and percent confluence was measured as a function of time. MSCs decrease in proliferative potential in all donors (where applicable) by P7. Cell lines which were not capable of expansion past P5 (127756) and P3 (PCBM1655) revealed decreased potential when compared to other donors which were expanded to P7. Cell line 8F3560 demonstrated the smallest change in proliferation with passage, while PCBM1632 and 167696 revealed a substantial drop in proliferation capacity by P7 (Figure 2-1A). The confluence at the 4-day (96-hr) time point (Figure 2-1B) from the same dataset further demonstrates the decrease in proliferation potential with passage, and the variability seen between donors.

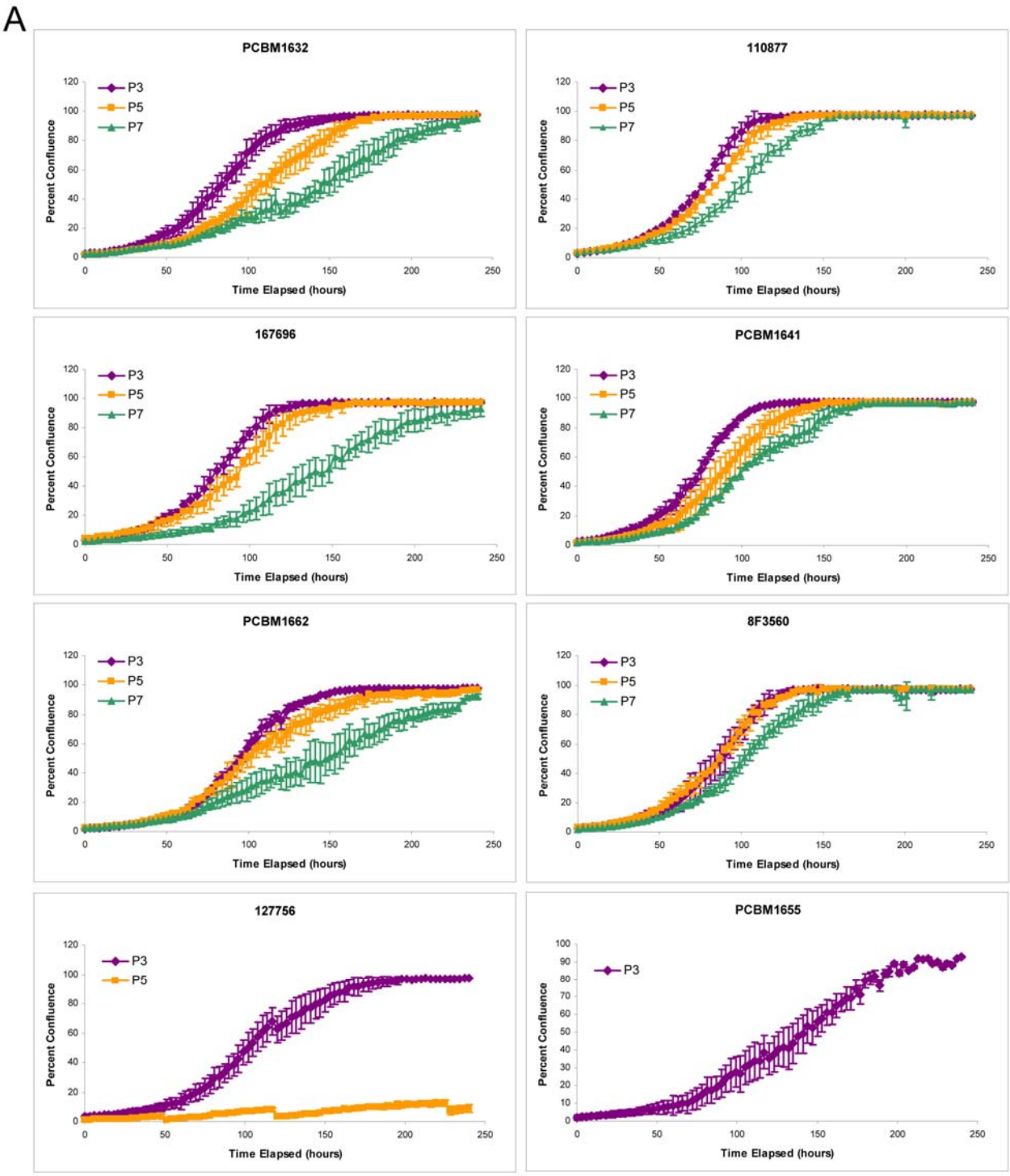

Figure 2-1. Legend on following page.

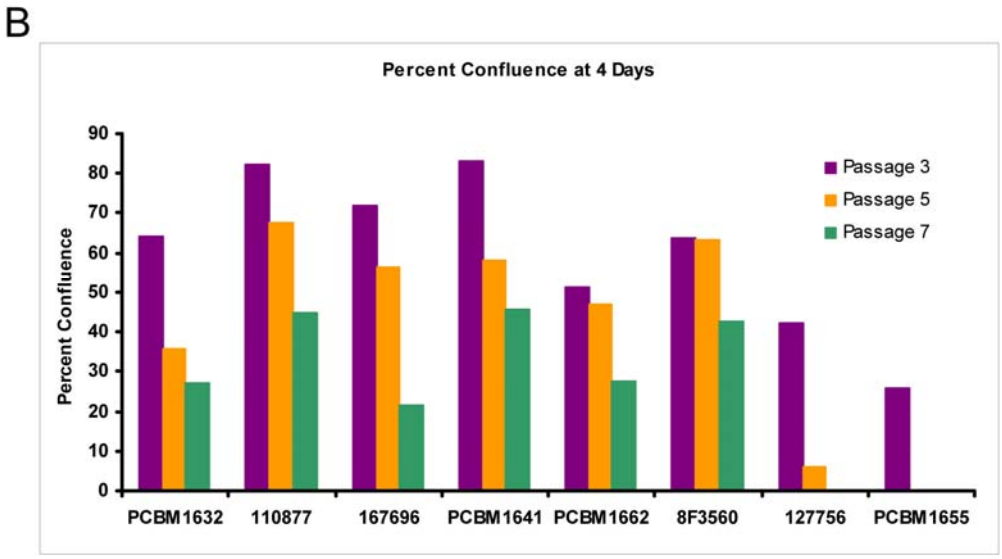

Figure 2-1. MSCs decrease in proliferative potential with passage and vary between donors. MSCs were plated at 2000 cells/well in 24-well plates, and percent confluence was measured every 3-4 hours in a live cell imager. (A) Percent confluence as function of time for all donors at P3, P5 and P7. Error bars represent standard deviation; n=4. (B) Percent confluence at 4 day time point for all donors at P3, P5 and P7.

2.3.4 Surface marker expression remains constant following passaging and between donors

MSCs have been characterized by their positive expression profile, including but not limited to, CD29, CD44, CD73, CD90, CD105 and CD166. MSCs for all cell lines and passages were analyzed by flow cytometry based on this set of markers, to determine any changes in expression as a function of donor variability or culturing. All staining was done with the same antibodies, and events for all cell lines and passages were collected using the same cytometer settings. Gating analysis was based on unstained controls for each donor and each passage, to account for changes in forward and side scatter properties that are seen with increasing passage. Averaged percent positive expression for all cell lines within a passage was not significantly different between passages. Expression of CD44, CD73 and CD105 were consistently greater than 95%

positive, while expression of CD29 remained above 90%. Slightly lower expression of CD90 was seen in PCBM1632 at 88.9%, 91.6%, and 92.4% at P3, P5, and P7 respectively; all other cell lines and passages showed greater than 95% expression. Cell line 127756 showed decreased expression of CD166 by passage 5 at 89.8%, however all other cell lines remained above 90% expression (Figure 2-2).

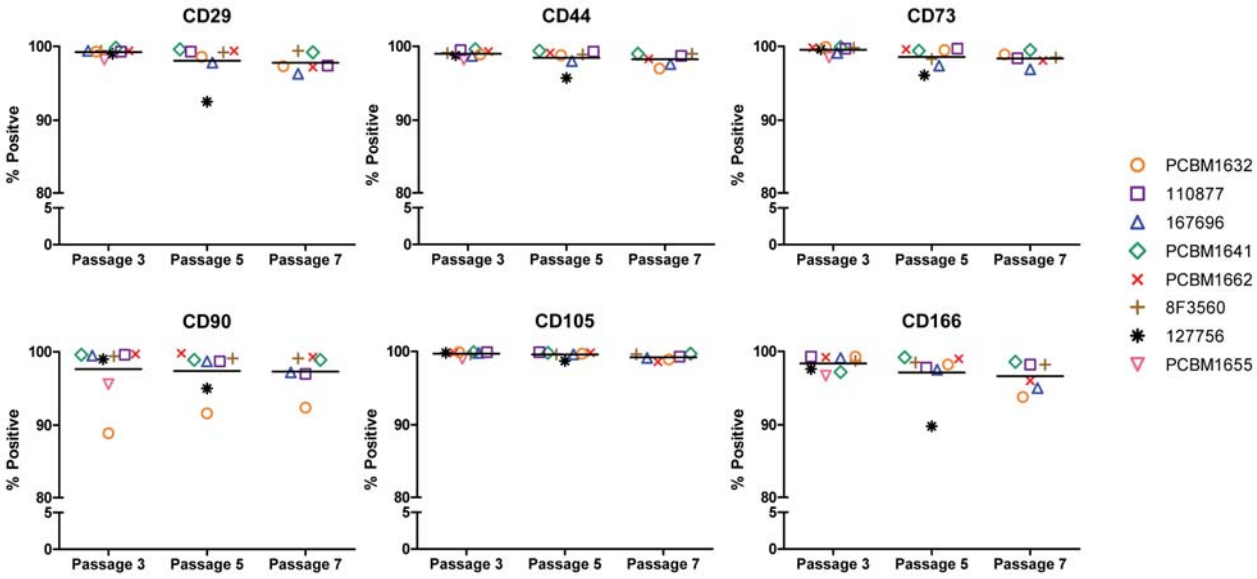

Figure 2-2. MSCs maintain expression of cell surface markers through passages. MSCs were stained for CD29, CD44, CD73, CD90, CD105 and CD166 at P3, P5 and P7. Gating was applied to unstained controls at each passage for each donor, and the percent positive was reported. Data is grouped by passage number, and horizontal bars indicate the average percent positive expression of all (applicable) cell lines at that passage. Each donor is represented as a unique symbol and color, as seen in the figure legend.

2.3.5 MSC cell size increases with increasing passage and varies between donors

Acquisition of forward and side scatter data using flow cytometry allows for cell size (FSC) and granularity (SSC) parameters to be measured. Quadrant gating was determined for P3 MSCs for one particular cell line, and then applied to P5 and P7 for that same cell line; therefore, each cell line has its own individual P3 gate. The percent positive cells with high forward and side scatter

in the upper right quadrant (URQ) was recorded, and plotted as seen in Figure 2-3 (n=1). An example of the FSC/SSC gating can be seen for cell line 167696 at P3 (left), P5 (center) and P7 (right) in Figure 2-3B. Most cell lines showed a trend toward increasing in FSC and SSC with increasing passage. Both 127756 and PCBM1655 (oldest donors) showed a higher percentage (11.2 and 17% respectively) at P3 then the other cell lines. 8F3560 remained at a relatively stable value, varying between 8.4% (P3), 10.1% (P5) and 9.7% (P7).

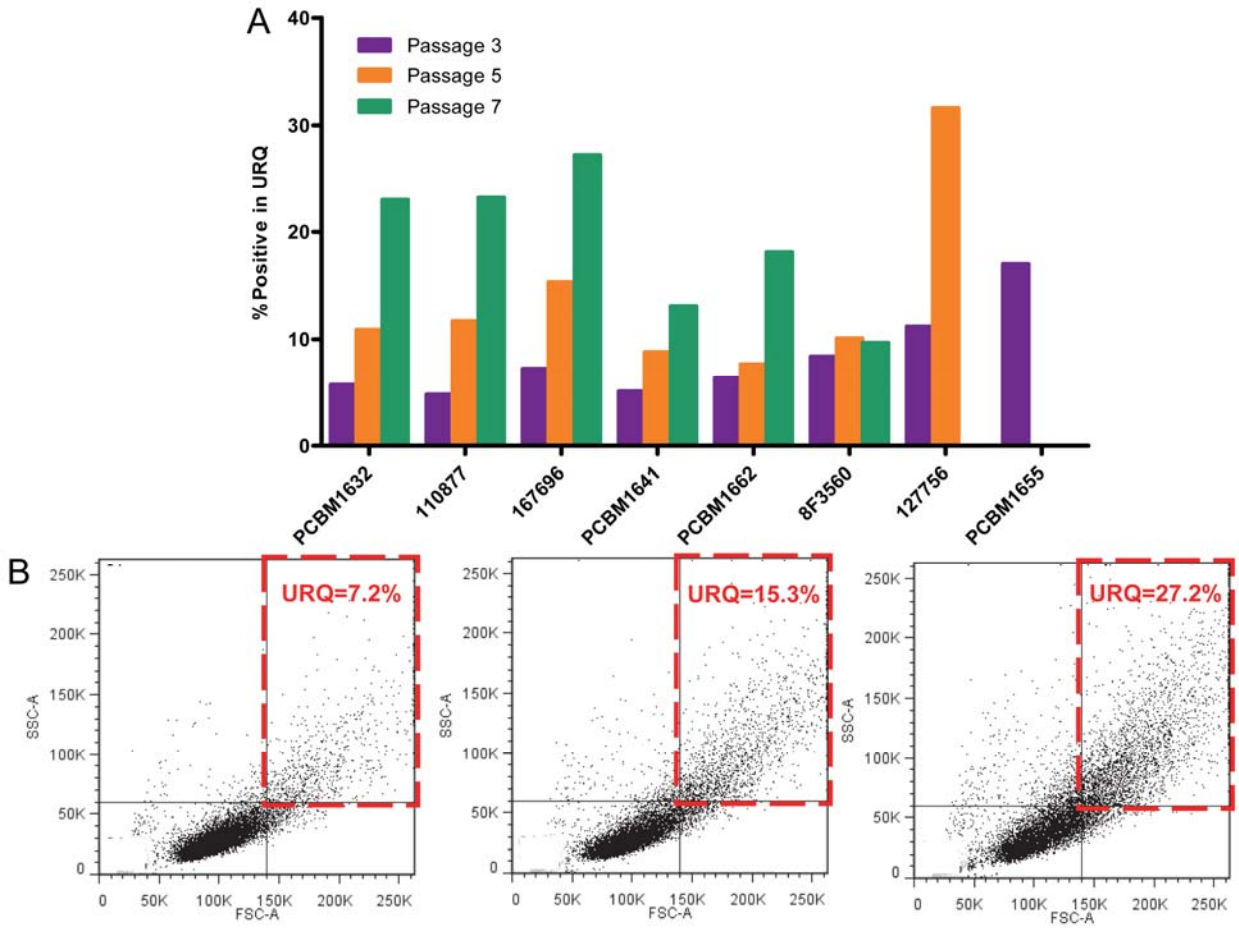

Figure 2-3. MSCs increase in forward and side scatter with increasing passage. (A) FSC/SSC quadrant gating was applied to each individual dot plot at P3. The P3 gates were applied to P5 and P7 for each particular cell line. Changes in percent positive cells in the Upper Right Quadrant (URQ) were recorded, plotted, and grouped by cell line; n=1. Purple bar = P3; orange bar = P5; green bar = P7. (B) Example of quadrant gating analysis on FSC/SSC dot plots from donor 167696 at P3 (left), P5 (center) and P7 (right). Percent positive in URQ is shown in the red dashed line following gating analysis.

Changes in cell size were also measured using a Cellometer, which measures the area of the cells in pixels, converts this measurement to a cell diameter, and then calculates the cell diameter assuming the cells are circular, as described in the methods. During expansion of each cell line, cell numbers and diameters were recorded immediately prior to cryopreservation. As seen in Figure 2-4, all cell lines showed an increase in cell diameter from P3 to P7 (where applicable), and this increase in cell size is highly significant ($p<0.01$ 8F3560, $p<0.001$ for all other cell lines). The increase in cell size with increasing passage as measured by the Cellometer is consistent with findings in Figure 2-3 as measured by flow cytometry.

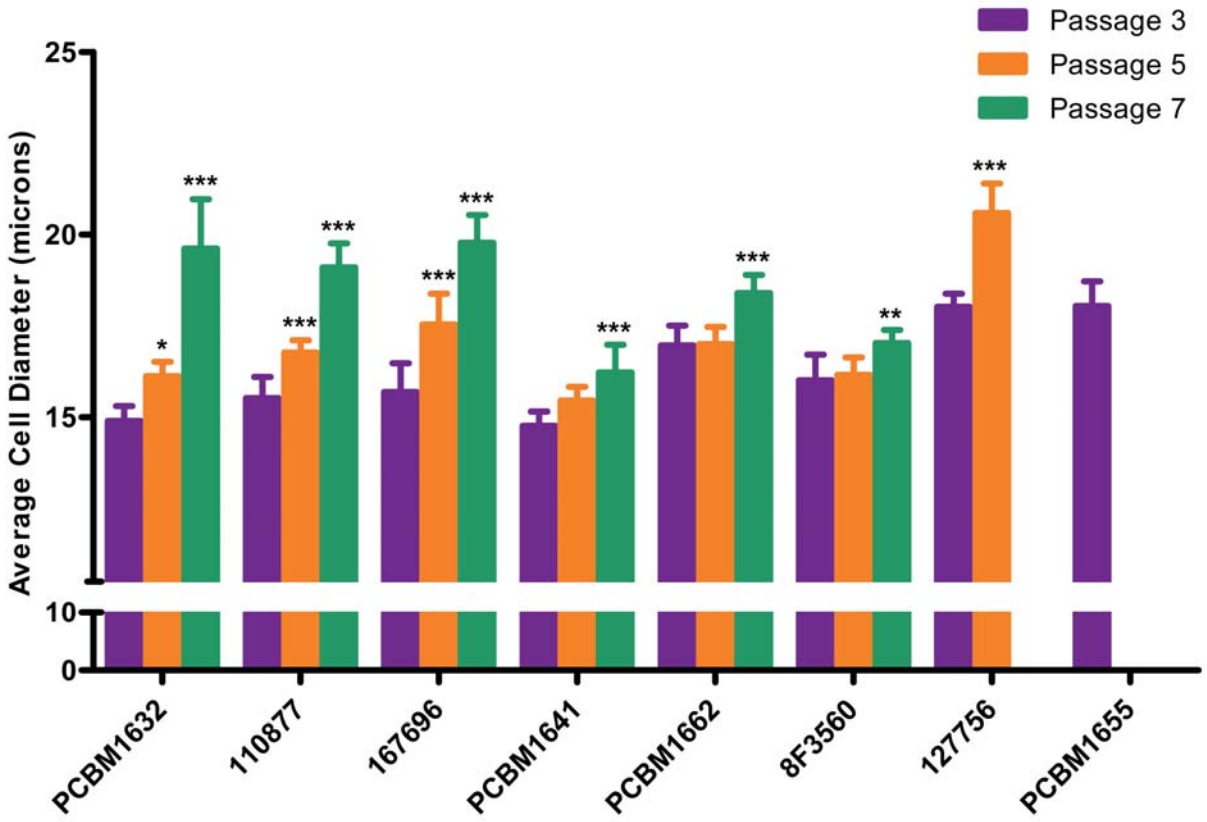

Figure 2-4. MSCs increase in cell size with increasing passage, and vary between cell lines. Bars represent average cell diameter (μm) counts of varying sample sizes ($n\geq6$), as determined by Cellometer measurements. Statistical comparisons were made within cell lines, relative to P3. Error bars represent standard error of the mean. Purple bar = P3; orange bar = P5; green bar = P7. ***$p<0.001$, **$p<0.01$, *$p<0.05$.

2.3.6 MSC CFU capacity decreases with increasing passage and varies between donors

Percent colony forming units (CFUs) are associated with stemness in populations of MSCs. Percent CFUs are highest at P3 for most cell lines, and decreased with increasing passage. Percent CFUs ranged from 10.7% (PCBM1655) to 45% (167696) at P3, and from 5.7% (PCBM1632) to 21.7% (110877) at P7. The cell lines that could not be cultured beyond P3 (PCBM1655) and P5 (127756) had the lowest CFU percentages at P3 at 10.7% and 19% respectively (Figure 2-5A). All cell lines show a significant decrease in percent CFUs from P3 to P7, with the exception of 8F3560, which remained fairly constant between passages (Figure 2-5A). Statistical analyses between cell lines at P3 revealed highly significant ($p<0.001$) differences in most donor comparisons (Figure 2-5B).

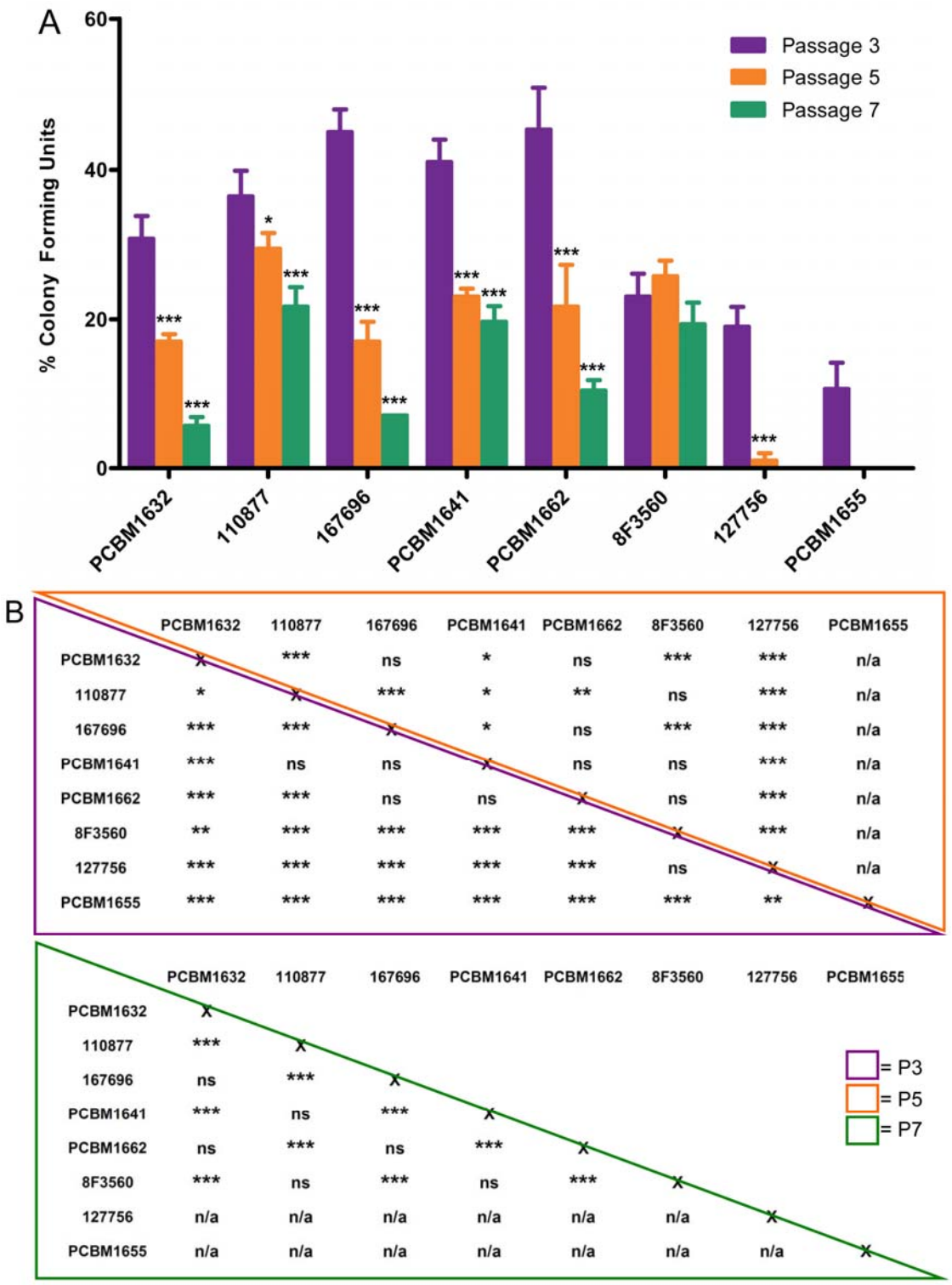

Figure 2-5. Percentage of Colony Forming Units (CFUs) tends to decrease with increasing passage, and varies between cell lines. (A) CFUs were calculated as a percentage by quantifying the number of colonies, and normalizing to the number of plated cells at Day 0. Error bars represent standard deviation; n=3. Purple bar = P3; orange bar = P5; green bar = P7. Statistical comparisons were made within cell lines, relative to P3. (B) Statistical analysis of CFU data for comparison between cell lines. Purple outline = P3, orange outline = P5, green outline = P7. For (A) and (B), ***p<0.001, **p<0.01, *p<0.05, ns = not significant, n/a = not applicable.

2.4 DISCUSSION

Between populations of MSCs, variability in cellular properties such as proliferation, morphology, and cell surface marker expression profiles have been previously observed and confirm our findings here. These differences between populations of MSCs derived from different donors, i.e. "inter-population heterogeneity", can be quantified through the use of existing population-based bioassays that have been previously used to identify and characterize MSCs (64). Further, these quantitative bioassays can be utilized to correlate with newly discovered biomarkers or other novel quantitative assays that may predict a biological function. Accordingly, in order to establish a complete assessment of the MSC cell line characteristics utilized here, cells were analyzed based on their marker expression profile and cell size, as well as their CFU and proliferative capacity. The results presented in this chapter will therefore be discussed in Chapter 3, in the context of differentiation capacity, in order to provide a more complete analysis and overview of MSC properties *in vitro.*

2.5 CONCLUSION

MSCs from eight different donors of various ages were assessed for colony forming unit capacity, proliferation, and cell surface marker phenotype at passages 3, 5 and 7. Following expansion, MSCs demonstrated a marked increase in cell size, and this was measured and confirmed by FSC/SSC analysis and a cellometer. Increases in cell size correlated with

decreased proliferative potential and CFU capacity. However, MSC phenotype assessment by flow cytometry does not reflect functional heterogeneity, which we can detect through our quantitative bioassays. Therefore, while assessment of cell surface markers is important for identifying MSCs, it does not reflect changes in function that can be detected through other quantitative bioassays discussed here, as well as differentiation assays that are discussed in the following chapter.

3.0 ESTABLISHMENT OF QUANTITATIVE BASSAYS TO MEASURE DIFFERENTIATION CAPACITY IN MSCS

3.1 INTRODUCTION

MSCs are available from adult tissues, however the percentage of MSCs in the bone marrow is low, ranging from 0.001 – 0.01% (78). In order to obtain sufficient numbers, bone marrow MSCs are typically expanded substantially in tissue culture before use. Following expansion by cell culture passaging, the biological properties of MSCs are often evaluated using qualitative assays to assess differentiation capacity. The availability of robust quantitative methods to assess differentiation capacity on a per cell basis in heterogeneous cell populations like MSCs would be of great value to assess MSC quality during and following the expansion process, and to determine if there are differences in the differentiation capacity of MSCs from different donors.

Several studies have examined the role of donor differences and cell passaging on MSC proliferation and differentiation capacity. Stenderup *et al.* studied MSCs from donors grouped by age to determine the role of donor age and cell culture expansion on bone and fat forming capacity, proliferation potential, and senescence. It was observed that an increase in senescence in older donors which was accompanied by a decrease in overall proliferative potential. However, no changes were seen in adipogenic or osteogenic capacity based on donor age. Following cell expansion, a decrease both in adipogenic and osteogenic potential was observed.

(76). Bonab *et al.* also demonstrated this decreased capacity for differentiation with cell expansion (79).

These approaches largely disregard the cellular heterogeneity within populations of MSCs (72,80). As reviewed by Pevsner-Fischer *et al.*, intra-population heterogeneities have been widely observed in MSCs, and may be in part due to the *in vivo* microenvironment or *in vitro* expansion. The heterogeneous nature of MSCs may also allow them to efficiently respond to a variety of cues seen *in vivo*, as demonstrated by their role in differentiation, tissue regeneration and immunosuppression (64). Quantitative measurements made on a per cell basis take into account this inherent heterogeneity observed in MSCs, and will allow for quantification of progenitor cells that are capable of carrying out a desired function. Further, these assays can be applied beyond measurement of donor- and passage-related differences, including use for functional analysis of populations purified by currently available cell surface markers (i.e. sorting for STRO-1 (36,81), CD271 (82,83), or other newly discovered biomarkers (84)), or various MSC sources (bone marrow, adipose tissue, muscle, placenta, umbilical cord, etc.).

Tri-lineage differentiation potential was examined for all donors and passages using quantitative bioassays, where possible. Limiting dilution was used as a technique to quantify adipogenic differentiation in MSCs. Following expansion of MSCs from 2 cell lines to passages 3, 5 and 7, it was shown that adipogenic precursors can decrease with increasing passage, and can vary between cell lines from different donors. Differentiation was successfully quantified on a per-cell basis with this simple, quantitative assay that can be utilized in almost any laboratory (74). This methodology was further expanded upon to quantify adipogenic differentiation using additional cell lines and a novel, automated technique to quantify differentiation following adipogenesis using automated microscopy. Osteogenic differentiation was quantified by

measuring threshold-based surface area staining and normalizing to nuclei. Chondrogenic differentiation was assessed qualitatively by Alcian Blue staining. Changes in gene expression for lineage-specific markers were also examined to correlate with bioassay outcomes. Our findings were correlated with previously-established quantitative assays (data shown in Chapter 2) to better understand the role of donor variability and passaging on MSC stemness and differentiation capacity.

3.2 MATERIALS AND METHODS

3.2.1 Adipogenesis

Two different methods were applied to MSCs to quantify adipogenic precursors, including limiting dilution and automated microscopy methods. Due to the labor intensive nature of the limiting dilution assay, this approach was applied to only 2 donors. Automated microscopy was applied to all donors.

3.2.1.1 Limiting dilution technique

MSCs from 2 cell lines (PCBM1632 and PCBM1641) were plated at 1000, 500, 250, 125, 63 and 32 cells/well at 48 wells/dilution in 96-well plates. After cells were allowed to adhere for 24 hours, expansion media was removed and 100ul/well adipogenic differentiation medium (NHAdipoDiff; Miltenyi Biotec) was added (day 0). Differentiation media was supplemented

every 3-5 days until day 21. At day 21, plates were removed from culture, fixed with 10% formalin, and stained with Oil Red O dye (Sigma-Aldrich).

All wells were scanned visually by eye. Wells containing at least one differentiated cell (cells containing lipid droplets stained by Oil Red O) were scored positive. Precursor frequencies were determined plotting the fraction of non-responding wells versus cell dilution on a semi-logarithmic plot. For calculating the non-responding wells, a value of 0.0001 was plotted for the lowest dell dose where all wells responded. In these instances, data for higher cell doses were not plotted. This approach was used to employ only data that generate a linear dose response. The inverse of the cell dose corresponding to 37% of the non-responding wells is the precursor frequency (85). Figure 3-1 shows an example of how data fro this technique can be used to determine the frequency of adipogenic precursors in a population of MSCs.

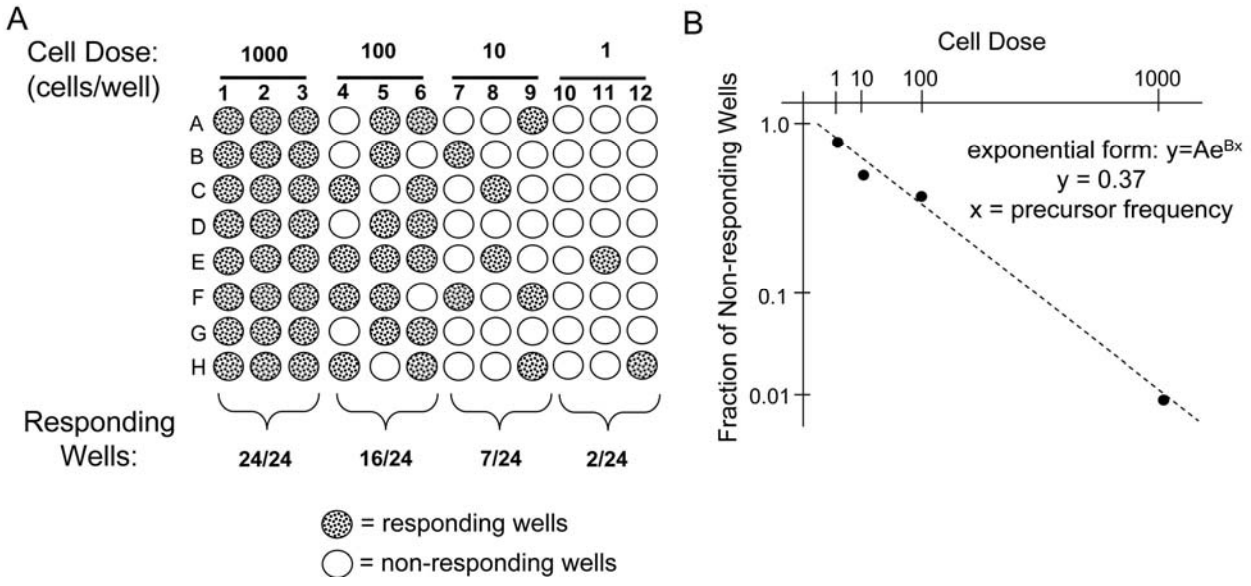

Figure 3-1. Illustration of limiting dilution methodology to calculate precursor frequency. (A) Cells are plated after serial dilution (cell dose) and are subjected to a stimulus, that is, differentiation medium. The response at each dosage is quantified and the number of responding wells is determined. (B) The number of non-responding wells at each dilution is plotted on a semi-log plot as a function of cell dose, and points are best fit to a trend line. Using the exponential form of the equation, the precursor frequency (x) can be calculated assuming y=0.37.

3.2.1.2 Automated microscopy

For automated microscopy experiments, MSCs were thawed, cultured until 80% confluence, and plated in 12-well plates at 10,000 cells/well. Following cell adherence for 24 hours, adipogenic differentiation medium (NH AdipoDiff, Miltenyi Biotec) was added to differentiation wells; undifferentiated controls were cultured in complete expansion medium. Medium was changed every 3 days and cultured until Day 21. At day 21, MSCs were fixed with 10% formalin (Sigma-Aldrich) and stained with Nile Red dissolved in DMSO (Sigma-Aldrich) at a 5μg/ml final concentration for 45 minutes at room temperature to visualize lipid droplet formation within MSCs. Cells were washed with PBS, and nuclei were stained with 1mg/ml Hoechst dissolved in water (Sigma-Aldrich) for 30 seconds.

3.2.1.3.1 Image acquisition

Widefield fluorescence microscopy was performed on a Nikon Ti-S inverted microscope with the addition of a Prior automated stage, excitation and emission filter wheels, episcopic shutter, and remote focus attachment. Acquisition of all datasets utilized a 10x, Plan Fluor objective, and Nikon Intensilight widefield illumination source. Filtering of excitation and emission wavelengths for both Hoechst and Nile Red fluorophores was accomplished using the appropriate filters of a Sedat Quad filter set from Chroma Technology (Hoechst Excitation Filter: 350nm peak, 50nm bandpass. Hoechst Emission Filter: 457nm peak, 50nm bandpass. Nile Red Excitation Filter: 490nm peak, 20nm bandpass. Nile Red Emission Filter: 617nm peak, 73nm bandpass). Acquisition of frames was accomplished with a Photometrics CoolSnap EZ, cooled, interline CCD. Multi-dimensional acquisition (intra-well, inter-well, multi-channel, and autofocus) was accomplished through NIS-Elements software. Sampling of each 12-well plate was employed by an acquisition routine such that each well would be imaged randomly in 25

locations, which excluded the outer 15% of each well (to exclude edge-effects). This randomly generated pattern was replicated (same locations with respect to each well) in the following wells to ensure that the gradient (from edge-to-center) was equally sampled in all wells and did not bias the resultant analysis. Order of acquisition proceeded to ensure the accuracy of the stage locations (with respect to channel registration) by capturing both channels before proceeding to the next location, as well as focal plane, by implementing an autofocus routine at each stage location. The autofocus routine utilized both Hoechst and Nile Red as reference channels, as the focal plane differed in each channel.

3.2.1.3.2 Image analysis

Image analysis was accomplished using NIS-Elements software, post-acquisition, by generating an analysis routine (macro) designed to automate the segmentation tools rather than performing a more manual, step-by-step analysis of each image. Once generated, the macro was run across an entire plate's dataset (300 images per plate) or further streamlined by running across multiple plates in sequence. After each plate, the data was exported to Microsoft Excel for further data sorting and analysis. The goal of the segmentation routine was to count, in an automated fashion, the number of total nuclei (per 10x field) as well as the number of those nuclei which had an associated adipocyte (positive for Nile Red). The number of those positive for Nile Red could then be normalized to the number of total nuclei per image, which varied dramatically as the sampling location moved from edge to center. The normalized value was averaged across the 25 images in each well, and then averaged across 3 wells for n=3 for each donor at each passage. Data was plotted as the percentage of Nile Red positive cells.

To ensure the accuracy of the generated macro, as well as demonstrate the variability of manually counting, an entire plate's data set was counted manually by utilizing a taxonomy

count option of NIS-Elements, whereby each of 3 separate users would click each individual nucleus, as well as those positive for Nile Red stain, as the software tallied the numbers. The manual analysis was completed for donor PCBM1632 at P3, P5 and P7.

3.2.2 Osteogenesis

MSCs from all cell lines were thawed, cultured until 80% confluence, and plated at 5000 cells per well in 24-well plates in normal expansion medium. Cells were allowed to adhere for 24 hours, then expansion medium was replaced with osteogenic differentiation medium (NH OsteoDiff, Miltenyi Biotec). Media was changed every 3-4 days, and cultured for 14 days.

3.2.2.1 ALP staining and quantification

Following 14 days of culture, differentiated MSCs were fixed in 4% paraformaldehyde for 20 minutes, and rinsed with PBS. To make the ALP staining solution, 1 pellet of Fast Blue RR salt (Sigma Aldrich) was added to 48ml of DI water, vortexed, and allowed to sit for 10 minutes. ALP Napthol (Sigma Aldrich) was brought to room temperature, and 2ml was added to the pellet/water solution. Staining solution was added to samples and incubated for 30 minutes at room temperature and washed with PBS. Following ALP staining, samples were then stained with 1mg/ml Hoechst dissolved in water (Sigma-Aldrich) for 30 seconds, and imaged using both brightfield (ALP staining) and fluorescence (Hoechst)

A 5x6 grid of images at the center of the well were acquired by automated microscopy in both fluorescence and brightfield to assess nuclei and ALP respectively. Positive ALP staining was measured via a macro designed to threshold and report pixel area of blue staining associated

with ALP. A separate macro quantified the nuclei counts for the same image locations. Binary area (μm^2) was normalized to nuclei for that image, and averaged for the 30 images acquired per well. Triplicate wells were then averaged to report binary area per nucleus.

3.2.3 Chondrogenesis

MSCs from all cell lines were thawed, and cultured until 80% confluence. Cells were trypsinized, counted, and resuspended in chondrogenic differentiation medium (NH ChondroDiff, Miltenyi Biotec) at 400,000 cells/ml. 500µl of cell suspension was added to 15ml conical tubes, centrifuged at 1200rpm for 10 minutes, and cultured in pellet culture for 21 days. Medium was changed every 3-4 days. At day 21, pellets were washed with PBS, fixed in 10% formalin for 24 hours, and submitted to American Histolabs. Samples were paraffin embedded, sectioned at 5µm, and stained with Alcian Blue to identify sulfated glycosaminoglycans. Images were acquired on an upright Nikon microscope with a DS-Ri1 camera. Images were taken at 10X and 40X for all differentiated samples and undifferentiated controls.

3.2.4 qRT-PCR

To measure changes in gene expression following adipogenesis, cell lines from all donors at P3, P5, and P7 were plated at 3.75×10^5 cells per 10cm dish, and cultured in adipogenic differentiation medium (NH AdipoDiff, Miltenyi Biotec) for 14 days. At day 14, differentiated cells were washed with PBS, and 600µl of RLT lysis buffer (Qiagen) was added to each plate. Cell lysates were collected, snap frozen in liquid nitrogen and stored at -80°C for future RNA isolation. For osteogenesis, cells were plated at 1.5×10^5 cells per 10cm dish, and cultured in

osteogenic differentiation medium (NH OsteoDiff, Miltenyi Biotec) for 14 days. To measure changes in gene expression following chondrogenesis, cell pellets were cultured as described in section 3.2.3 for 15 days. At day 15, pellets were washed with PBS, and 4-5 pellets were combined per sample set in 600µl RLT buffer. Cells were homogenized at 20,000g for 15-20 seconds using a Brinkmann Polytron PT 3000 homogenizer. Homogenized cell lysates were snap frozen and stored at -80°C for later processing. Lastly, for controls, MSCs from all cell lines and passages were thawed, cultured in expansion medium in a T175 flask until 80% confluence. Cells were trypsinized, pelleted and snap frozen for later RNA preparation. RNA was made using RNeasy columns following manufacturer's instructions (Qiagen). Total RNA quantity was determined using a NanoDrop (Thermo Scientific) and RNA quality was assessed using a Bioanalyzer (Agilent).

cDNA was synthesized using the Quantiscript Reverse Transcription Kit according to manufacturer's instructions (Qiagen) at 42°C for 15 minutes, followed by inactivation at 95°C for 3 minutes. qRT-PCR was preformed using the Taqman Gene Expression Master Mix (Applied Biosystems) per the manufacturer's instructions with primer targets outlined below. 15ng of cDNA-equivalents was added to each reaction. The primers used were based on genes known to be involved in adipogenesis, osteogenesis or chondrogenesis (Table 3-1). PCR was performed using an Applied Biosystems 7900: 50°C for 2 minutes; 95°C for 10 minutes; 40 cycles of 95°C for 15 seconds and 60°C for 1 minute per cycle. All conditions were repeated in triplicate with 20µl per well. Data was analyzed using SDS 2.3 software (Applied Biosystems). All target genes were normalized to GUSB (based on an assessment of appropriate housekeeping genes following differentiation).

Table 3-1. List of ABI primer/probe sets used in qRT-PCR.

Gene Symbol	Gene Name	Assay ID
PPARG	peroxisome proliferator-activated receptor gamma	Hs01115513_m1
CEBPA	CCAAT/enhancer binding protein (C/EBP), alpha	Hs00269972_s1
FABP4	fatty acid binding protein 4	Hs01086177_m1
RUNX2	run related transcription factor 2	Hs00231692_m1
ALPL	alkaline phosphatase	Hs01029144_m1
SPP1	osteopontin	Hs00959010_m1
SOX9	SRY (sex determining region &)-box9	Hs01001343_g1
ACAN	aggrecan	Hs00153936_m1
COL2A1	collagen type II alpha I	Hs00264051_m1
GAPDH	glyceraldehyde-3-phosphate dehydrogenase	Hs03929097_g1
18S	18S ribosomal RNA	Hs03928990_g1
HPRT1	hypoxanthine phosphoribosyltransferase 1	Hs01003267_m1
GUSB	glucuronidase, beta	Hs00939627_m1
TBP	TATA box binding protein	Hs00427620_m1
YWHAZ	tyrosine 3-monooxygenase/tryptophan 5-monooxygenase activation protein, zeta polypeptide	Hs03044281_g1

3.2.5 Statistical analyses

Statistical analyses for limiting dilution were carried out using Microsoft Excel; data was analyzed using two-tailed and unpaired t-tests. Statistical analyses for percent Nile Red positive data and ALP quantification were completed using GraphPad Prism 5. Data was grouped for

comparisons between cell lines and between passages. For adipogenesis and osteogenesis quantification (n=3), two-way ANOVA was preformed with a Bonferroni post-hoc analysis. Percent positive Nile Red data and ALP area/nucleus data is expressed as the mean ± standard deviation. For all analyses, P-values < 0.05 were considered significant. Analyses for changes in gene expression relative to passage were also completed in GraphPad Prism 5 (n=3) using a one-way ANOVA with a Bonferroni post-hoc analysis to measure differences relative to passage 3.

3.3 RESULTS

3.3.1 Adipogenic precursors decrease with increasing passage and vary between donors

3.3.1.1 Limiting dilution

Limiting dilution has traditionally been used in immunology to determine the frequency of cells that have a particular function in a mixed population (85-88). This method was applied to stem cell differentiation to quantify the adipocyte precursor frequency in cell lines PCBM1632 and PCBM1641. PCBM1641 responded similarly within each cell dose at P3, P5 and P7, while the fraction of responding wells at P7 in PCBM1632 drops greatly at all cell dilutions (Figure 3-2A). As noted in the methods, a value of 0.0001 was plotted for the lowest cell dose where all wells responded. For example, in Figure 3-2A, P3 cell doses greater than 500 cells per well were not plotted in Figure 3-2B.

The adipocyte precursor frequency for PCBM1641 was maintained at 1 in 76, 1 in 69 and 1 in 59 cells at P3, P5 and P7 respectively (Figure 3-2B). PCBM1632 precursor frequencies

were similar at P3 and P5 at 1 in 121 and 1 in 123 respectively. However, the precursor frequency for PCBM1632 dropped drastically by P7, where only 1 in 2,035 cells were capable of differentiating into an adipocyte ($P < 0.0002$, P7 compared to P3 and P5).

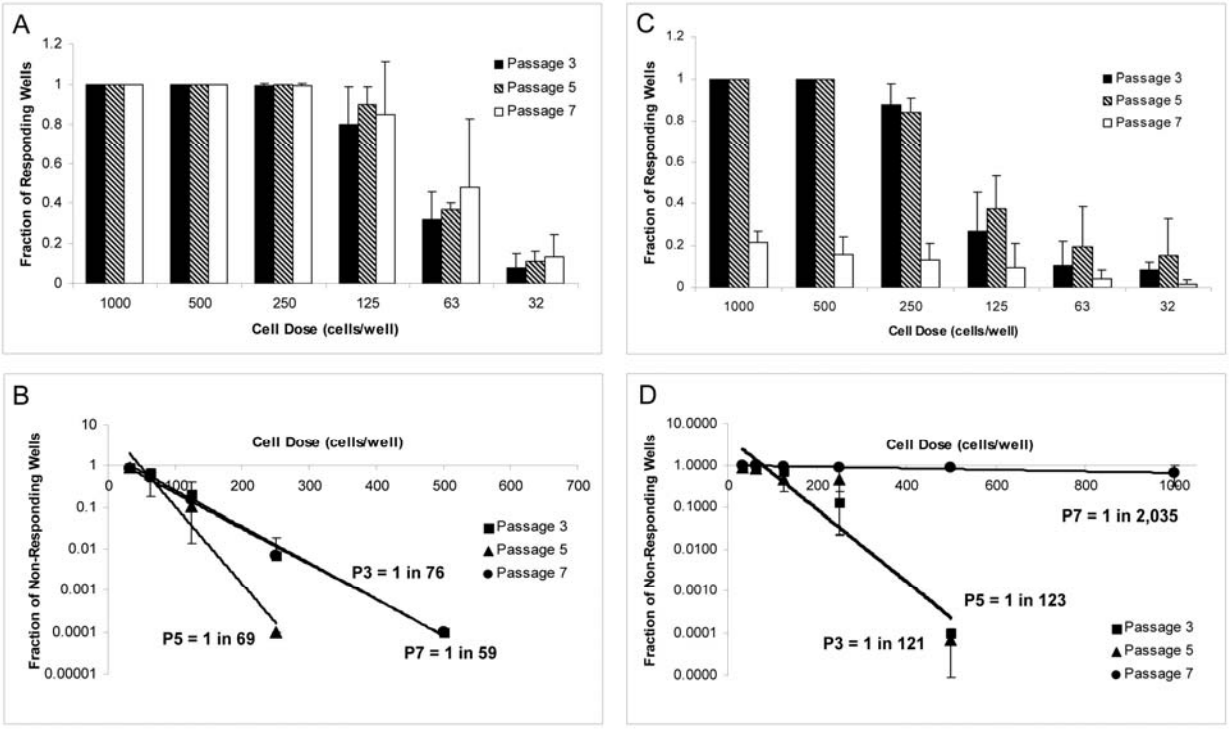

Figure 3-2. Adipogenic precursor frequency can differ between cell lines and with passaging. The fraction of responding wells is represented as a function of dose for PCBM1641 (A) or PCBM1632 (C) at P3, P5 and P7. (B) and (D) show plots of the fraction of the non-responding wells as a function of cell dose on a semi-log plot for PCBM1641 (B) or PCBM1632 (D) at P3, P5 and P7. The trend line equations were used to calculate the frequency of adipogenic precursors. Error bars represent standard deviation; n=3. R^2 values were >0.96 for PCBM1641 and >0.85 for PCBM1632 at all passages.

3.3.1.2 Automated microscopy

3.3.1.3.1 Percent adipogenesis

The application of automated microscopy as a high-throughput tool to quantify differentiation in MSCs is a novel approach in the field. This technology was applied to measure changes in adipogenic differentiation potential in all cell lines and passages in MSCs. Following staining for differentiated adipocytes, images were acquired for all cell lines and passages using automated image capture techniques. Image acquisition for each plate (1 donor per 12-well

plate, 300 images total) required approximately 2 hours of imaging time. Once image sets were acquired for all cell lines, the macro analysis was run to quantify Nile Red positive and nuclei counts for each image. Figure 3-3 shows an example of Nile Red staining (A) and the same image following macro detection of differentiated adipocytes in a field of undifferentiated cells (B).

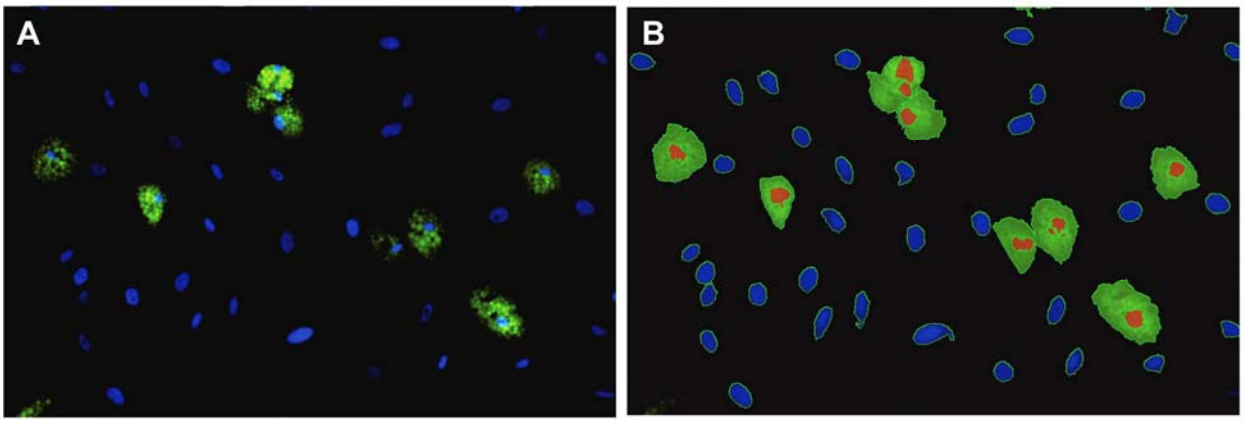

Figure 3-3. **Example of Nile Red staining and adipocyte quantification.** (A) Image of differentiated adipocytes following 21 days induction. Nile Red positive staining (green) visualized as lipid vesicles indicating a differentiated adipocyte; nuclei staining with Hoechst (blue). Image taken during automated imaging at 10X magnification. (B) Following analysis by the macro, Nile Red positive cells were indicated with a green transparent overlay plus associated nuclei (orange). Nuclei not associated with Nile Red staining are shown as blue areas. As an example, the software detected 9 adipocytes in this image. Further analysis would include normalization of this value to total number of nuclei in this image to determine a percent of differentiated cells.

Nile Red counts were normalized to nuclei counts in that image, averaged within one well and subsequently across three wells, and reported as a percentage of Nile Red positive cells. As seen in Figure 3-4A, adipogenic potential varies greatly between cell lines and consistently decreases as a result of passaging. 13.6% of MSCs from cell line PCBM1632 were capable of adipogenic differentiation at P3. This is in contrast to its 2.7% Nile Red positive cells at P7, indicating a 5-fold drop in adipogenic potential from P3 to P7, the largest drop in potential among all cell lines tested. Cell lines 127756 and PCBM1655, the cell lines that senesced by P5 and P3 respectively, demonstrated the 2nd and 3rd highest P3 adipogenic potential at 10.3% and

6.8% respectively. Donor 8F3560 had the lowest levels of percent positive Nile Red cells, where at all passages MSCs showed less than 1% adipogenic potential. Except for 8F3560, all cell lines showed a decrease in adipogenesis with an increase in passage, when cells were available to analyze, which was highly significant with $p \leq 0.001$ when comparing P3 v. P7 (Figure 3-4B). The extent of variability between cell lines within a particular passage is seen in Figure 3-4B. While most donor comparisons at P3 are significant ($p < 0.05$), MSCs converge to a low level of adipogenic potential by P7, as indicated by non-significant donor differences at P7 between most cell lines.

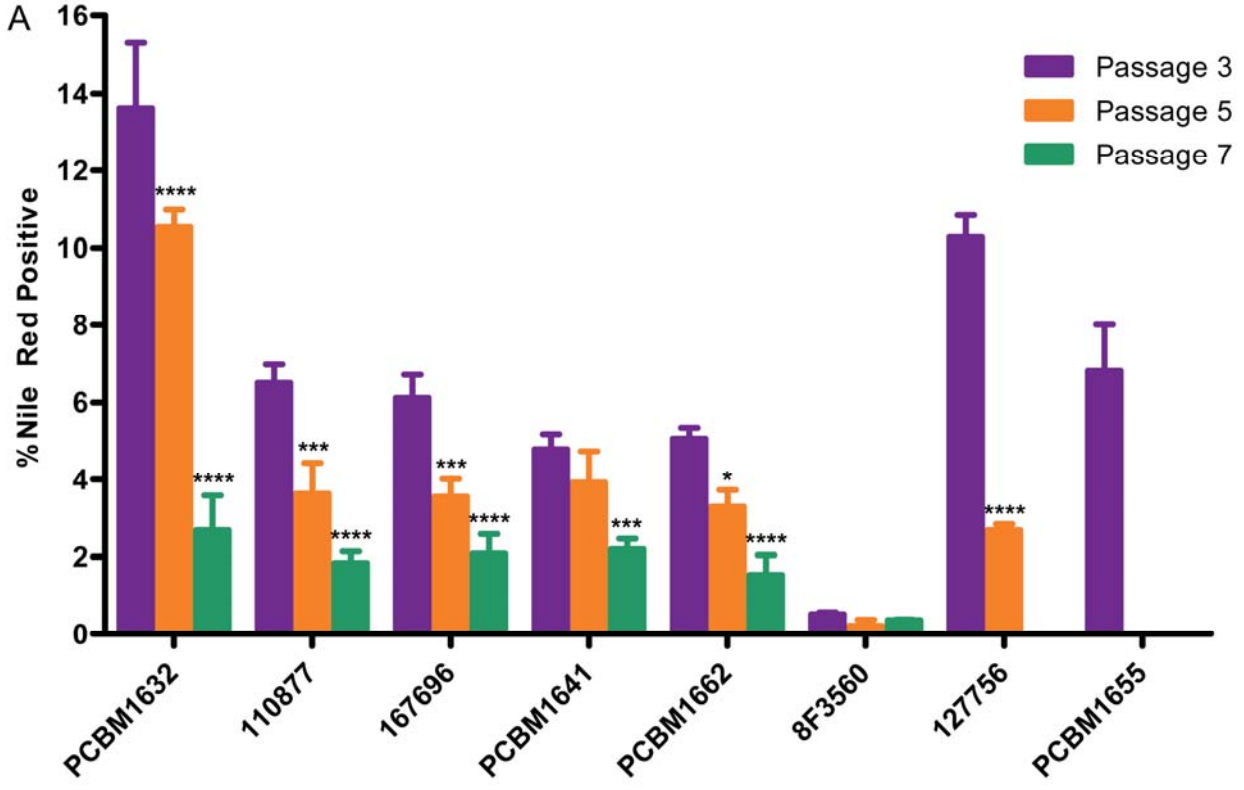

Figure 3-4. Legend on following page.

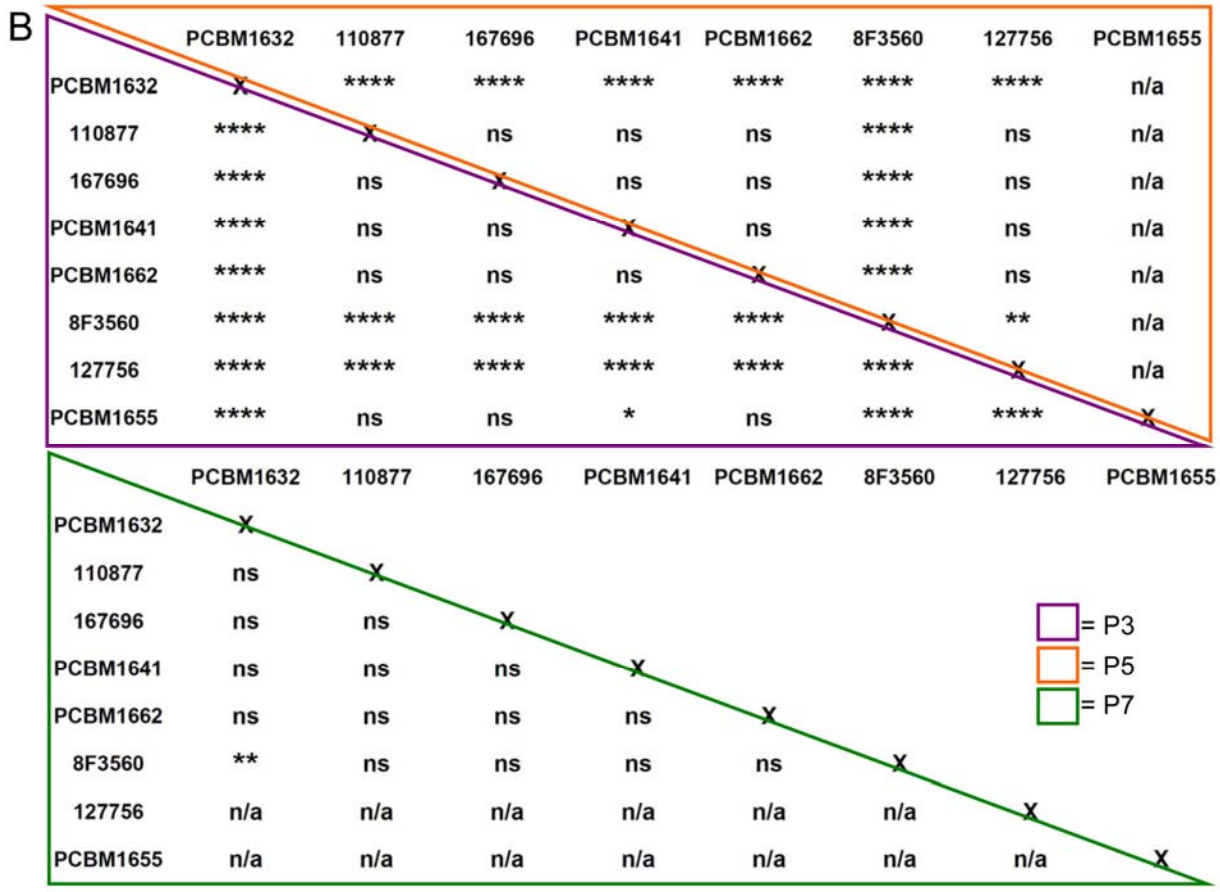

Figure 3-4. Adipogenesis can be quantified by automated microscopy, and demonstrates both donor variability and decreased adipogenic potential with increasing passage. (A) Nuclei plus Nile Red objects were normalized by the total nuclei count per image to report a percentage of differentiated cells (% Nile Red positive) as a function of passage and cell line. Purple bar = P3; orange bar = P5; green bar = P7. Error bars represent standard deviation; n=3. Statistical comparisons were made within cell lines, relative to P3. (B) Statistical analysis of percent adipogenesis data for comparison between cell lines. Purple outline = P3, orange outline = P5, green outline = P7. For (A) and (B), ****p<0.0001, ***p<0.001, **p<0.01, *p<0.05, ns = not significant, n/a = not applicable.

3.3.1.3.2 Automated versus manual analysis

To examine the accuracy of the macro in detecting Nile Red positive cells, three individual users manually counted the same image set used for automated quantification for cell line PCBM1632. Average Nile Red positive cells at each passage were averaged across the three counters, indicated as the manual count (n=3), and plotted with the automated count (n=1) (Figure 3-5). With the assumption that the manual count is the accurate representation of the data, the automated counts by the macro come very close at P5 (10.52% manual v. 10.53% automated)

and P7 (2.89% manual v. 2.68% automated), while the automated measurement at P3 is slightly higher in comparison to the manual count (12.55% manual v. 13.62% automatic). These results indicate that the macro automated count is an accurate representation of what a user would identify as a differentiated adipocyte. In addition, when considering computation time, each user spent, on average, greater than 8 hours of counting time to count a single plate of 300 images. The software's macro required less than 4 minutes on the analysis macro employed to count a single plate with 92 % or greater accuracy.

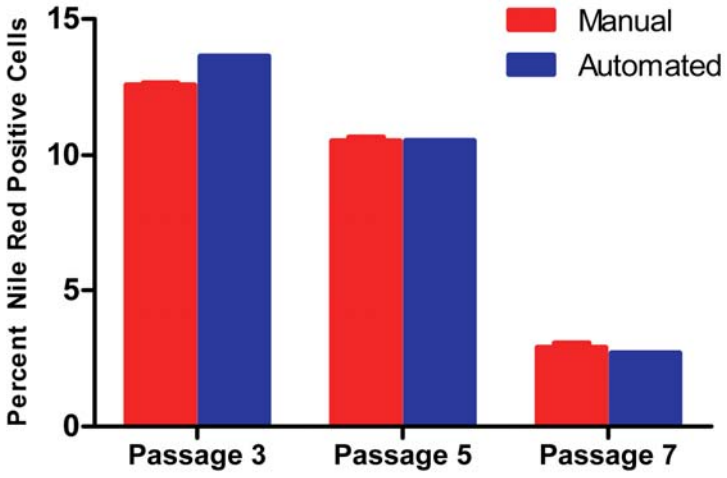

Figure 3-5. Manual quantification of percent positive Nile Red cells is in line with automated measurements in cell line PCBM1632. The number of nuclei and Nile Red positive cells were quantified manually in cell line PCBM1632 by 3 different users (n=3). The same image set was used to quantify manually as was used in the automated macro count. The red bars indicate the manual counts (n=3) and the blue bars indicate automated counts (n=1). Data reported as mean ± standard deviation for the manual count; n=3.

3.3.1.3.3 Nuclei counts

While the objective of this work was to quantify adipogenesis, the total nuclei counts harvested from the data sets also provide useful information when considering the overall proliferative capacity in complete medium vs. expansion medium, but also as a comparison between cell lines and passages. As seen in Figure 3-6, following the addition of adipogenic differentiation media

for 21 days, there is a decrease in proliferation compared to the corresponding passage controls within a particular donor, as indicated by the average nuclei count per image. This trend is seen in all cell lines and passages, and indicates MSCs decrease in proliferation following adipogenic stimulation. Further, this also demonstrates the decrease in the overall proliferative capacity with increasing passage, both following culture in normal expansion medium as well as in adipogenic differentiation medium.

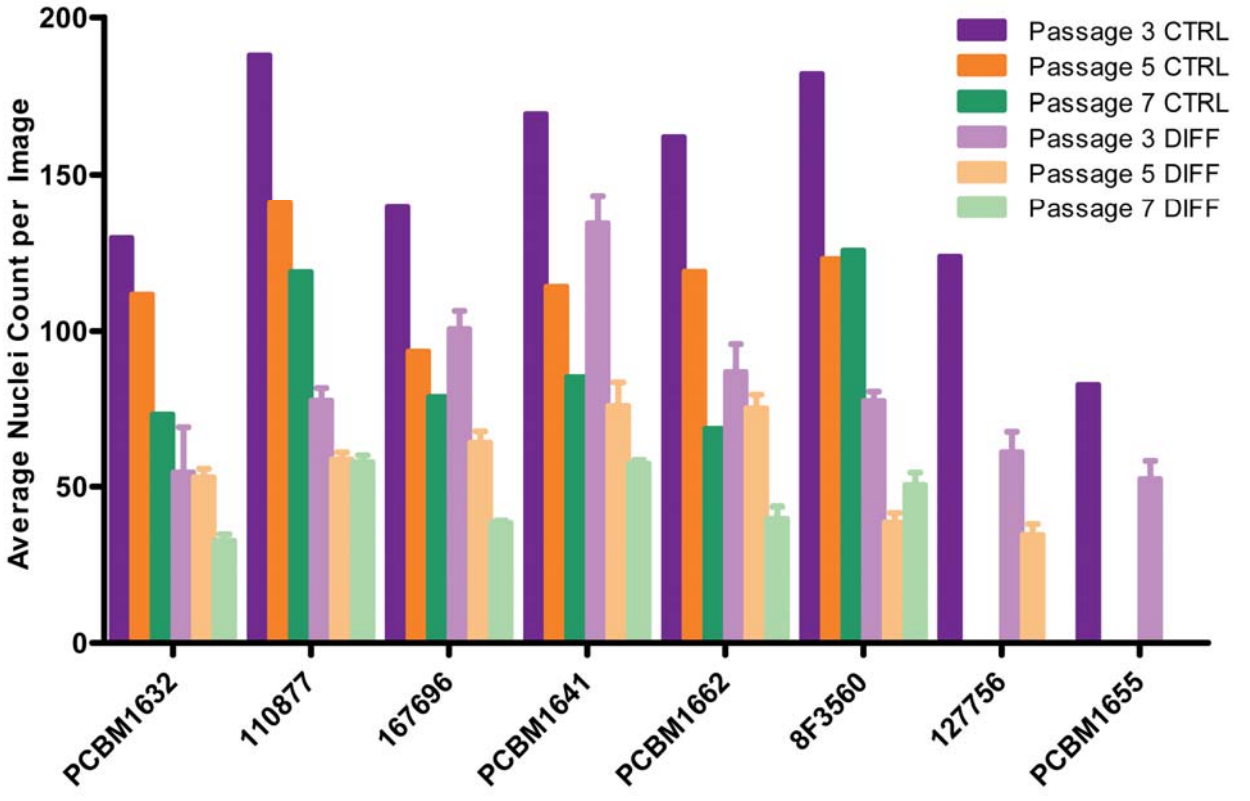

Figure 3-6. Proliferative potential decreases with increasing passage, and decreases upon adipogenic stimulation. The number of nuclei were quantified for each image, averaged across 25 images per well, then and averaged across 3 wells (n=3) following adipogenic stimulation. Nuclei were averaged in 1 well (25 images/well) following expansion in complete medium (n=1). The purple, orange, and green bars to the left within a cell line grouping indicate unstimulated controls for P3, P5 and P7 respectively, n=1. The light purple, orange and green bars to the right indicate adipogenic stimulation for P3, P5 and P7 respectively. Error bars on differentiated data points indicate standard deviation, n=3.

3.3.2 Osteogenic potential decreases with increasing passage and varies between donors

Automated microscopy methods were applied to assess osteogenic differentiation potential in MSCs. MSCs from all donors were differentiated toward the osteogenic lineage for 14 days, and changes in osteogenic potential were quantified by using a macro following ALP and nuclei staining.

3.3.2.1 Quantification of ALP

ALP-positive cells were quantified by thresholding during analysis by a macro, and normalized to the number of nuclei to report an area per nucleus, as shown in Figure 3-7.

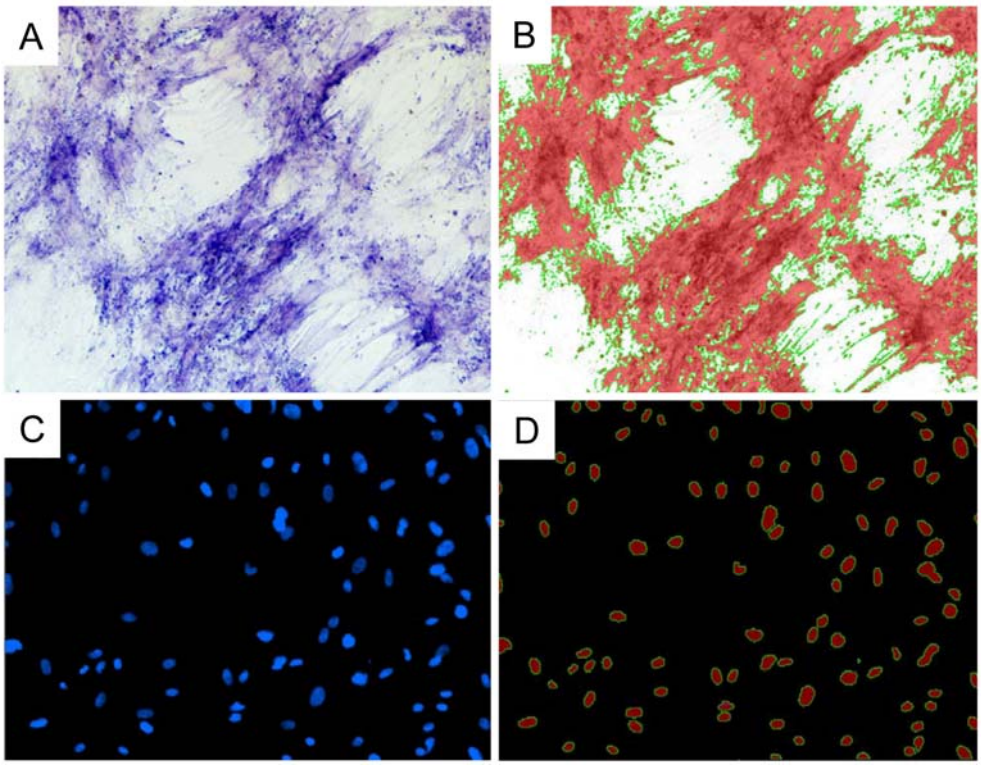

Figure 3-7. Measurement of ALP thresholded area and nucleus counts by automated microscopy. Osteogenesis-induced MSCs were stained with ALP at day 14, and imaged by automated microscopy. (A) Example of ALP staining (B) Threshold analysis completed on same image in panel A using a macro designed to report binary area in μm^2. Thresholded area to be included in analysis is shown in red and outlined in green (C) Example of Hoecshst staining for nuclei (D) Nuclei count completed by macro. Counted nuclei seen in red and outlined in green.

Using automated microscopy to quantify thresholded area on a per cell basis, osteogenic differentiation was successfully measured by ALP staining from different cell lines. As shown in Figure 3-8A, cell lines from different donors vary in their osteogenic differentiation potential. Cell line PCBM1632 and 127756 both demonstrate the highest level of osteogenic differentiation potential at P3 when compared to other cell lines. Cell line PCBM1632 demonstrated significantly more ALP staining ($p<0.01$) than other donors, except for 127756 (Figure 3-8B). Cell line PCBM1655 revealed approximately 230 μm^2/nucleus of positive ALP, which was the least positive area staining of all cell lines at P3. Further, due to *in vitro* culture, MSCs show a decrease in osteogenesis. Four out of six cell lines capable of expansion to P7 show a significant decrease in osteogenic potential from P3 to P7 ($p<0.0001$, Figure 3-8A). Comparisons made between cell lines at P7 suggest MSCs become more homogeneous between donors with a diminished ability to respond to osteogenic stimulation, as evidenced by mostly non-statistical differences (Figure 3-8B).

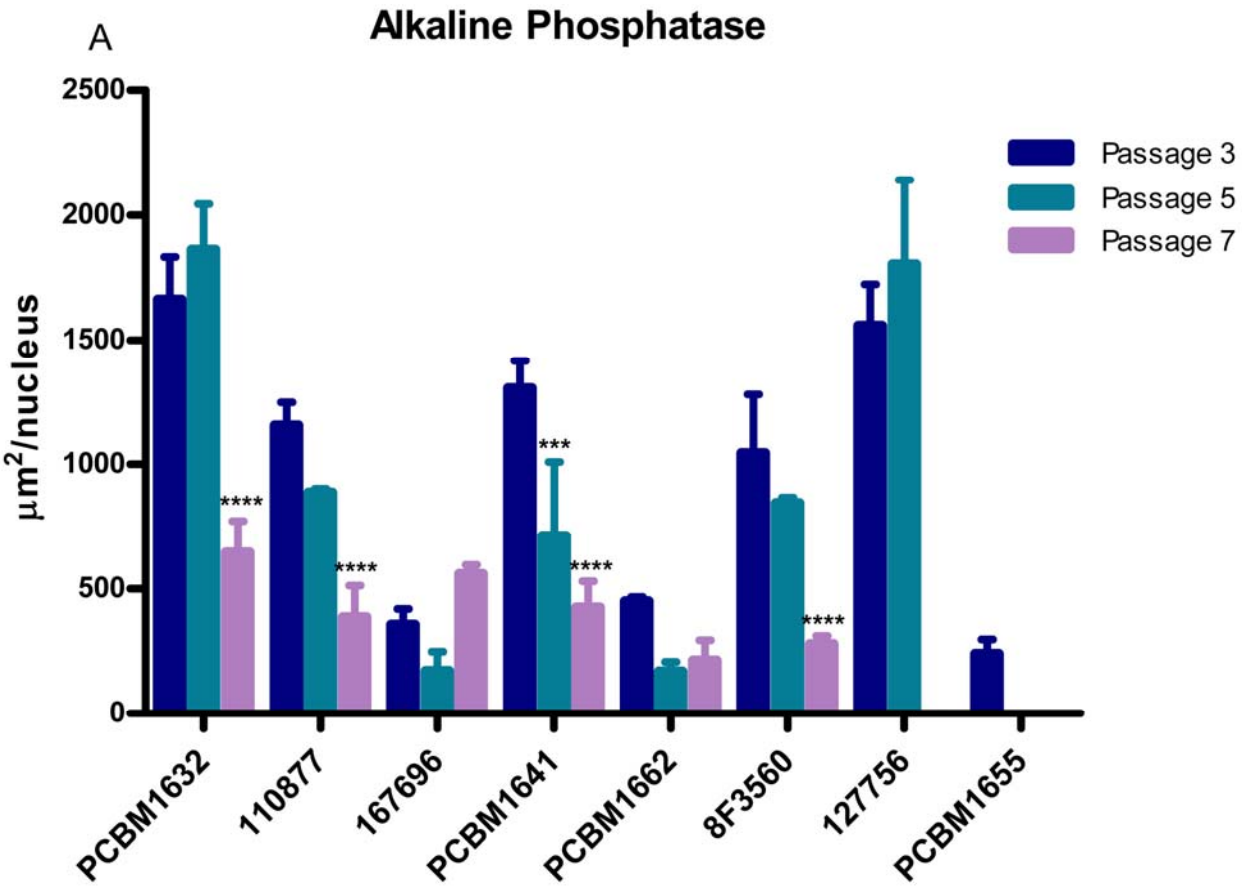

Figure 3-8. Legend on the following page.

B

	PCBM1632	110877	167696	PCBM1641	PCBM1662	8F3560	127756	PCBM1655
PCBM1632	X	****	****	****	****	****	ns	n/a
110877	**	X	****	ns	****	ns	****	n/a
167696	****	****	X	***	ns	****	****	n/a
PCBM1641	****	ns	****	X	***	ns	****	n/a
PCBM1662	****	****	ns	****	X	****	****	n/a
8F3560	****	ns	****	ns	***	X	****	n/a
127756	ns	*	****	ns	****	**	X	n/a
PCBM1655	****	****	ns	*	ns	****	****	X

	PCBM1632	110877	167696	PCBM1641	PCBM1662	8F3560	127756	PCBM1655
PCBM1632	X							
110877	ns	X						
167696	ns	ns	X					
PCBM1641	ns	ns	ns	X				
PCBM1662	*	ns	ns	ns	X			
8F3560	ns	ns	ns	ns	ns	X		
127756	n/a	n/a	n/a	n/a	n/a	n/a	X	
PCBM1655	n/a	n/a	n/a	n/a	n/a	n/a	n/a	X

= P3
= P5
= P7

Figure 3-8. Osteogenesis can be quantified by automated microscopy, and demonstrates both donor variability and decreased osteogenic potential with increasing passage. MSCs were stimulated with osteogenic differentiation media for 14 days, stained for ALP, and quantified based on thresholded area and nuclei count normalization. (A) Thresholded area was normalized to total nuclei count per image to report area of ALP staining per nucleus (μm^2/nucleus) as a function of passage and cell line. Blue bar = P3; turquoise bar = P5; purple bar = P7. Error bars represent standard deviation; n=3. Statistical comparisons were made within cell lines, relative to P3. (B) Statistical analysis of osteogenesis data for comparison between cell lines. Blue outline = P3, turquoise outline = P5, purple outline = P7. For (A) and (B), ****$p<0.0001$, ***$p<0.001$, **$p<0.01$, *$p<0.05$, ns = not significant, n/a = not applicable.

3.3.2.2 Positive ALP staining correlates with increased proliferative potential

As shown in Figure 3-8, measured area of positive ALP staining was normalized to nuclei to obtain a quantitative measurement of osteogenic differentiation on a per cell basis. While data shows osteogenic differentiation capacity decreases with passage, we wanted to determine if decreased osteogenic potential was associated with decreased proliferative potential with

passage, as demonstrated in Chapter 2. To correlate these data, the binary area fraction, a measure of the thresholded area relative to the total area, was plotted against the corresponding nuclei count. Cell lines capable of *in vitro* expansion to P7 were analyzed. As seen in Figure 3-9, there is a high degree of correlation between the measured binary area fraction and nuclei count, suggesting a role of proliferative capacity *in vitro* in the ability to undergo osteogenic differentiation.

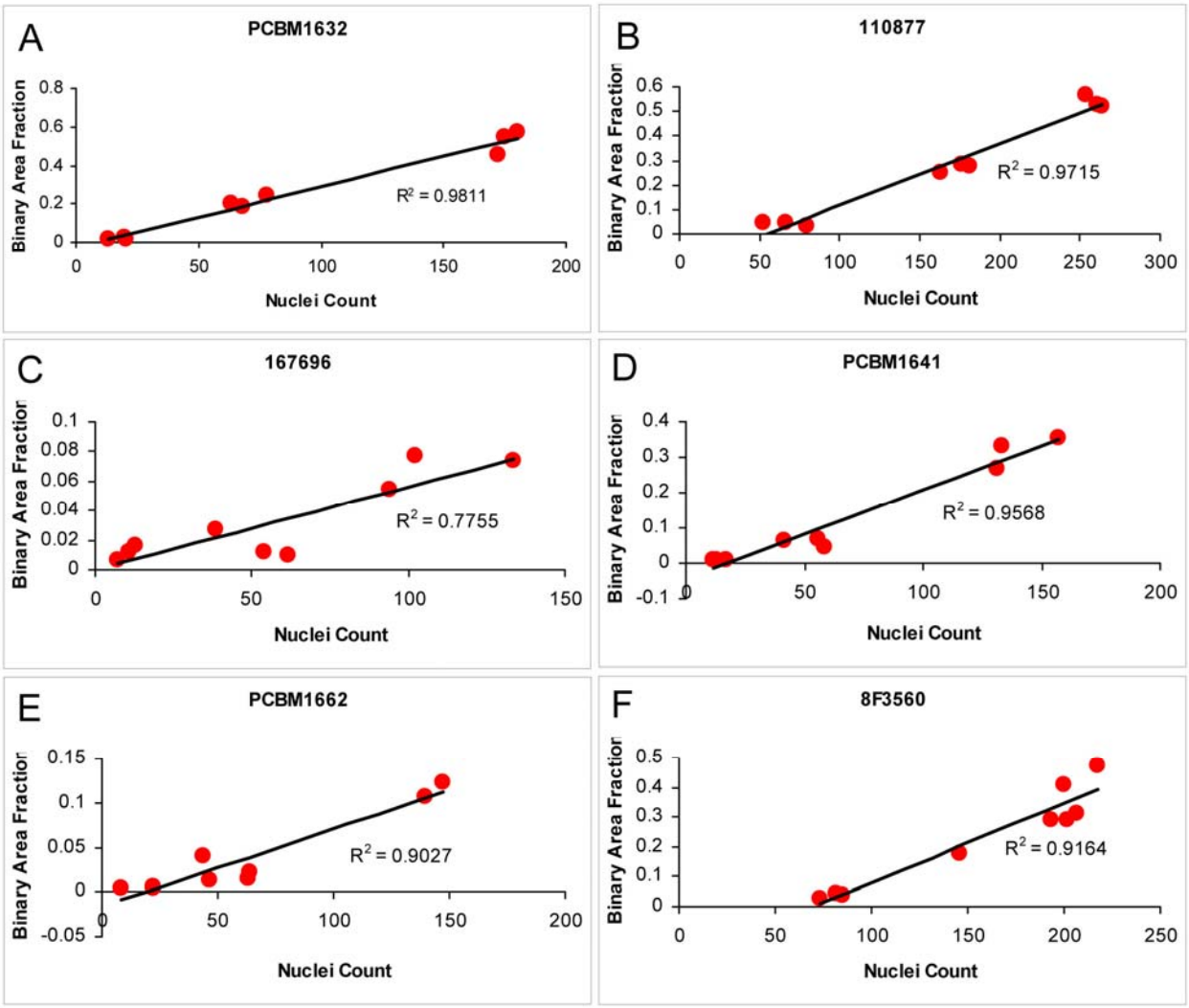

Figure 3-9. ALP expression correlates with cell number. The fraction of positive ALP staining (binary area fraction) and corresponding nuclei count is reported at all passages for the following cell lines: (A) PCBM1632 (B) 110877 (C) 167696 (D) PCBM1641 (E) PCBM1662 and (F) 8F3560.

3.3.2.3 Proliferative potential following osteogenic stimulation decreases with increasing passage

Osteogenic stimulation typically induces proliferation in MSCs *in vitro* (89). Here, proliferative potential was assessed following osteogenic stimulation by nuclei quantification via automated microscopy. Following osteogenesis, *in vitro* culture still results in decreased proliferative potential due to passaging, as shown in Figure 3-10. Passage 7 cells, where applicable, all show a highly significant decrease in proliferative potential ($p<0.0001$, Figure 3-10) with respect to passage 3.

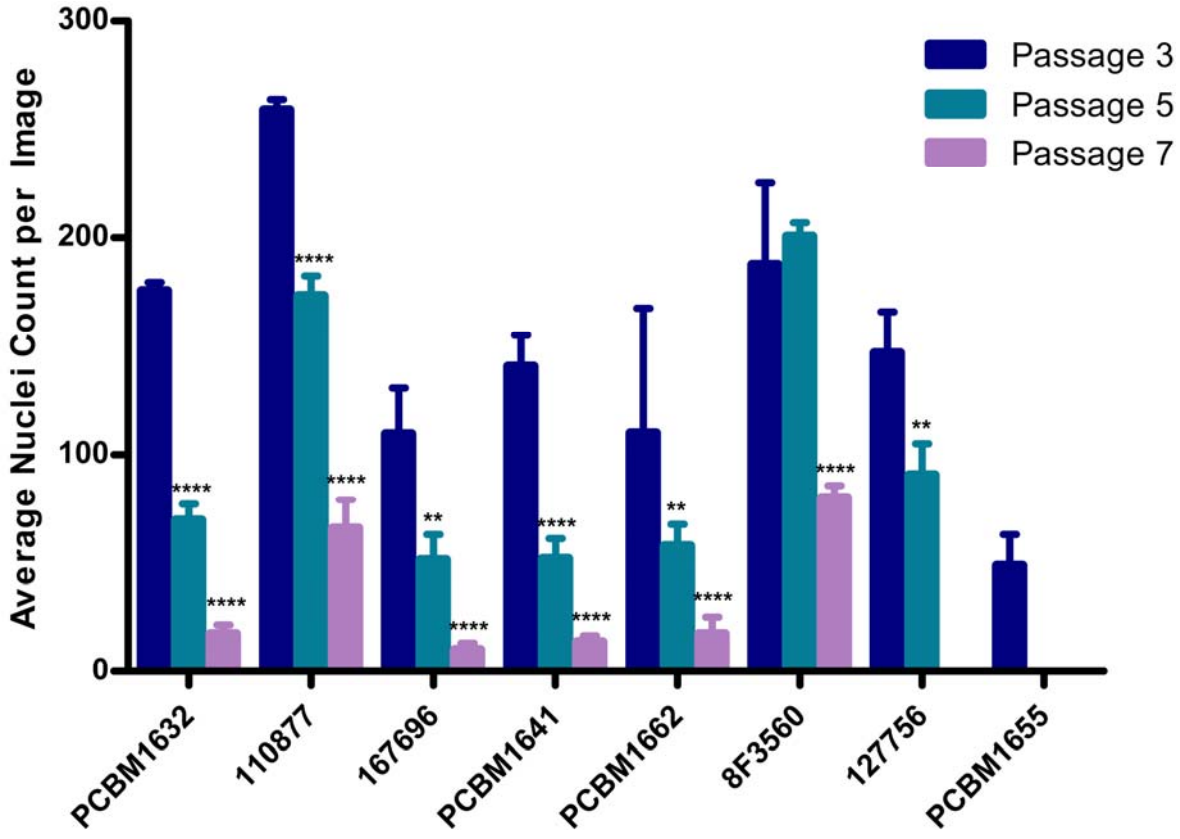

Figure 3-10. Proliferative potential decreases with increasing passage following osteogenic stimulation. Average nuclei count per image was quantified by automated microscopy following osteogenic differentiation for 14 days. Blue bar = P3; turquoise bar = P5; purple bar = P7. Statistical comparisons were made within cell lines, relative to P3. Error bars represent standard deviation; n=3. ****$p<0.0001$, ***$p<0.001$, **$p<0.01$, *$p<0.05$.

3.3.3 Chondrogenic potential decreases with increasing passage and varies between donors

Changes in chondrogenic differentiation capacity were assessed qualitatively by Alcian Blue staining following pellet culture for 21 days (Figures 3-11 to 3-18). Most cell lines appear to have a greater degree of positive Alcian Blue staining at passage 3 when compared to other passages. Cell lines PCBM1641 (Figure 3-14) and PCBM1655 (Figure 3-18) demonstrated increased levels of positive Alcian Blue staining at passage 3 compared to other cell lines, while 167696 (Figure 3-13) and 8F3560 (Figure 3-16) appeared to have the least degree of staining. All undifferentiated control cell pellets stained negative for Alcian Blue.

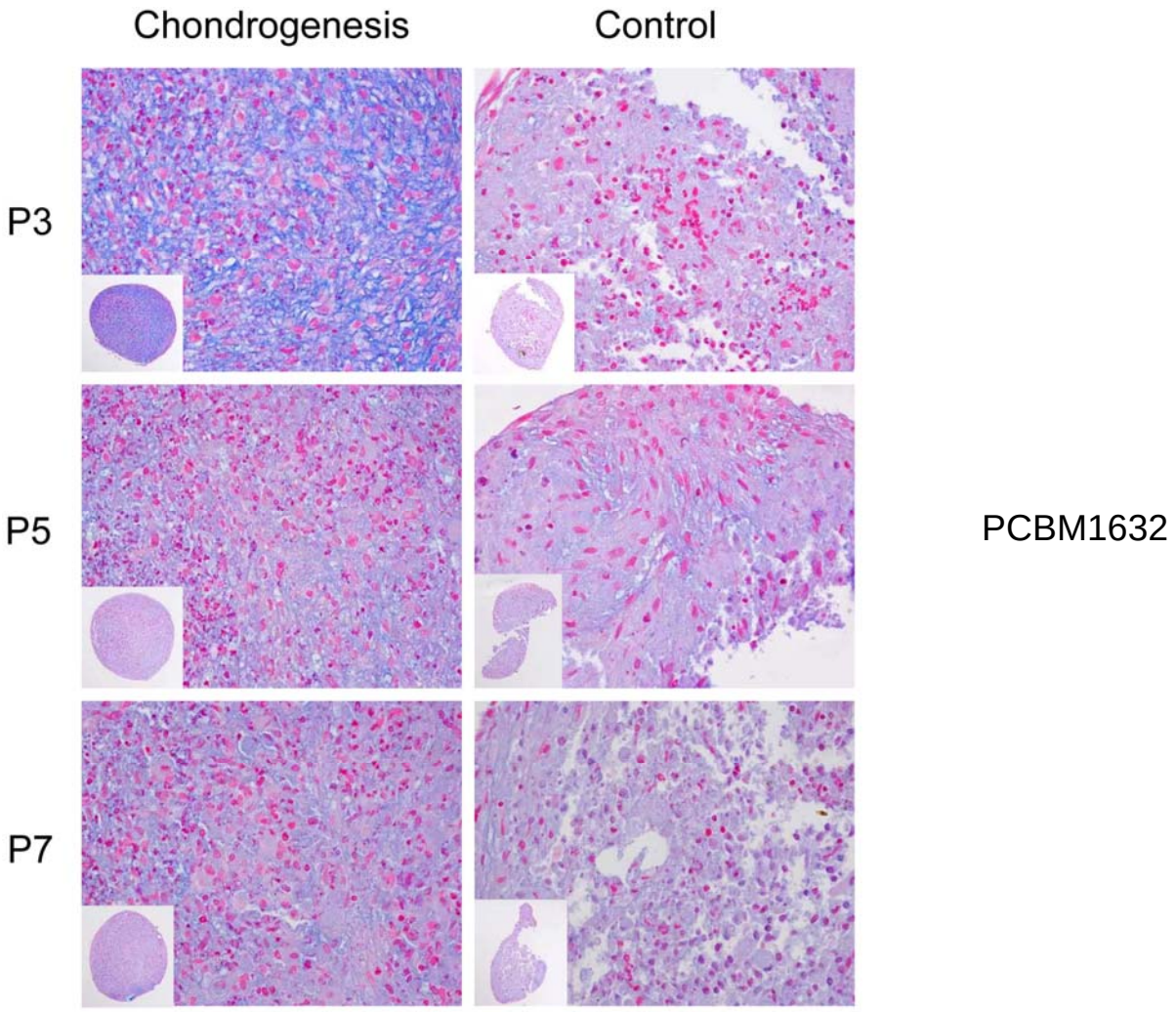

Figure 3-11. Alcian Blue staining in cell line PCBM1632 following chondrogenic differentiation. MSCs from cell line PCBM1632 P3 (top), P5 (middle), and P7 (bottom) were cultured in pellet culture for 21 days in either chondrogenic differentiation medium (chondrogenesis) or normal expansion medium (control). Blue indicates positive staining for sulfated glycosaminoglycans, pink indicates nuclei. Larger images taken at 40X; insets taken at 10X.

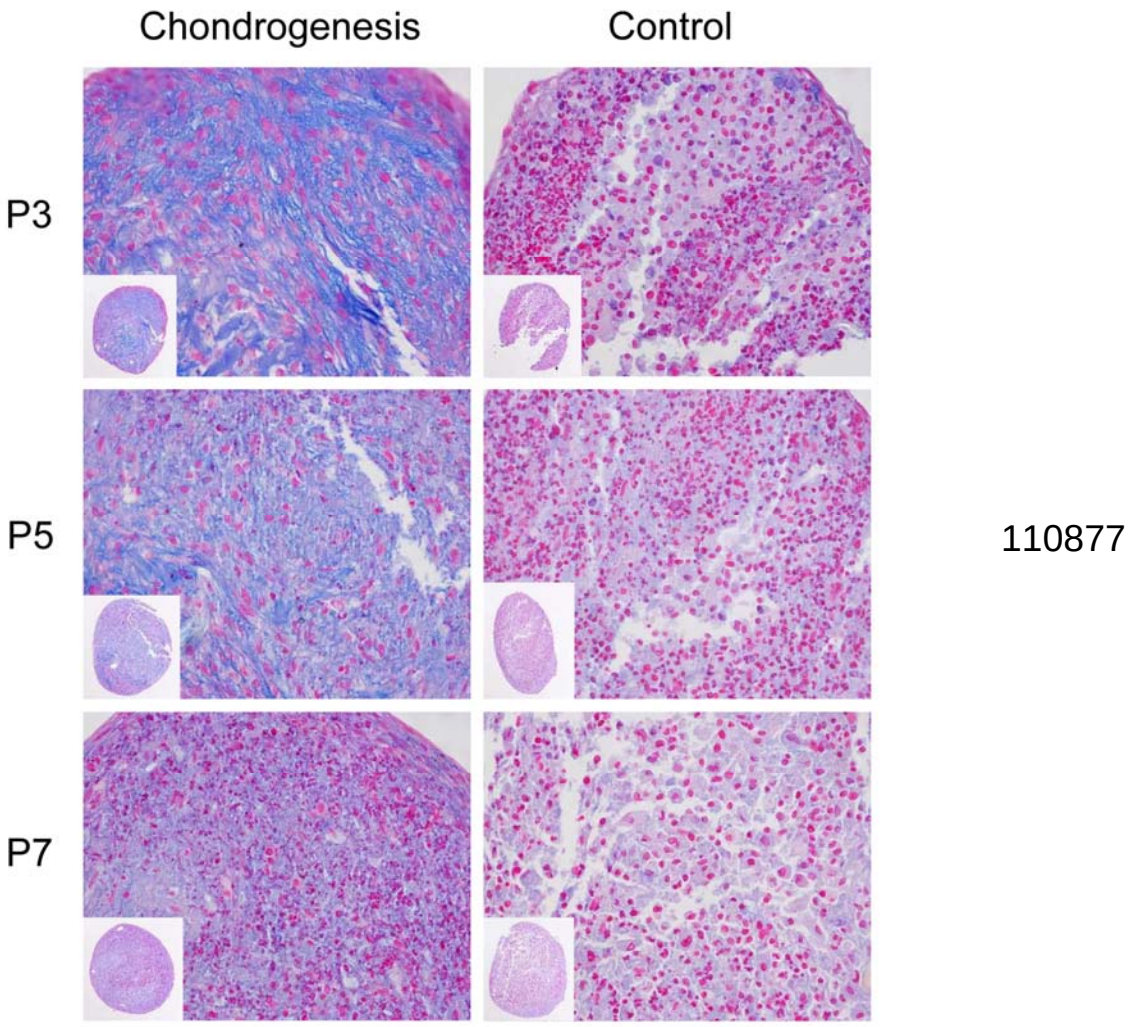

Figure 3-12. Alcian Blue staining in cell line 110877 following chondrogenic differentiation. MSCs from cell line 110877 P3 (top), P5 (middle), and P7 (bottom) were cultured in pellet culture for 21 days in either chondrogenic differentiation medium (chondrogenesis) or normal expansion medium (control). Blue indicates positive staining for sulfated glycosaminoglycans, pink indicates nuclei. Larger images taken at 40X; insets taken at 10X.

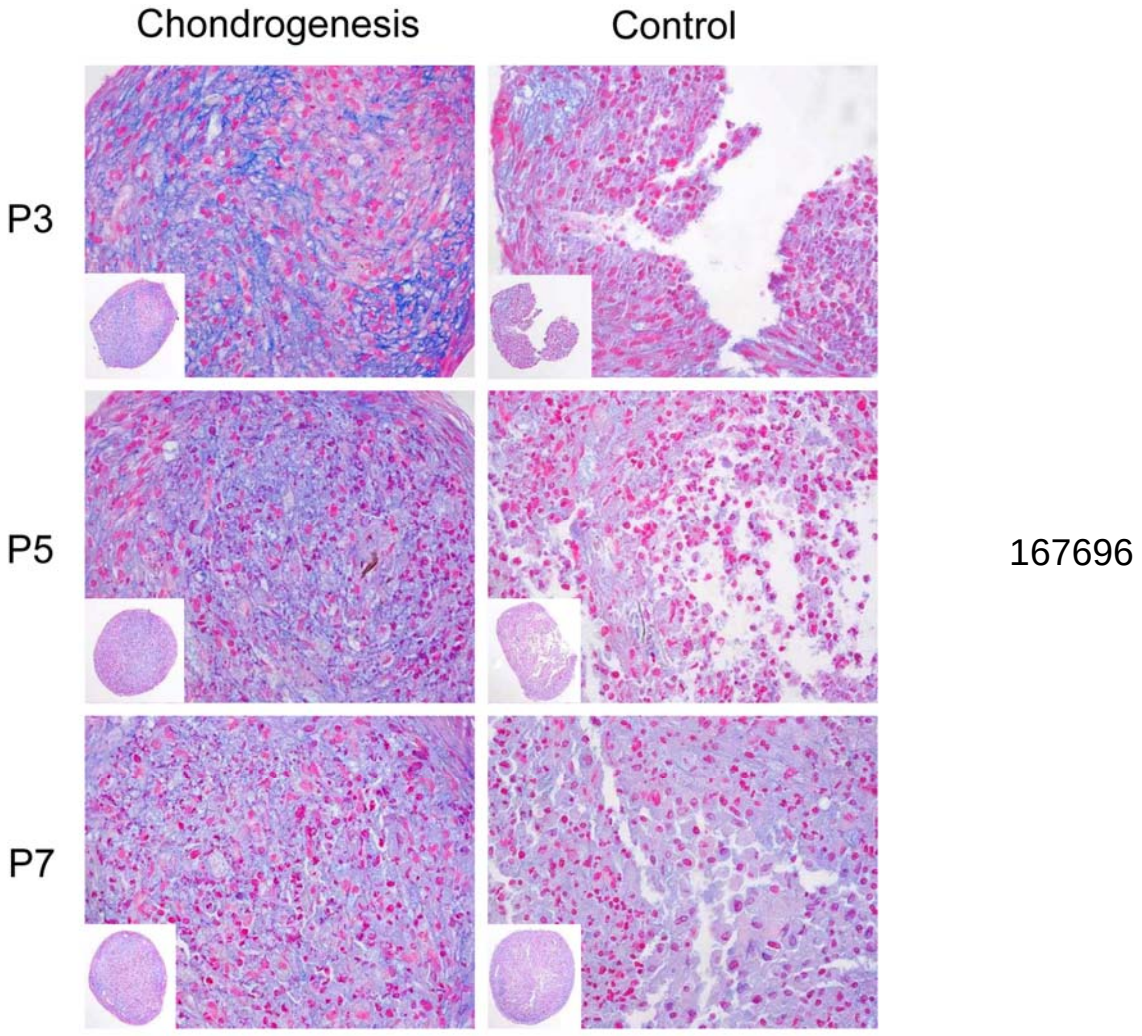

Figure 3-13. Alcian Blue staining in cell line 167696 following chondrogenic differentiation. MSCs from cell line 167696 P3 (top), P5 (middle), and P7 (bottom) were cultured in pellet culture for 21 days in either chondrogenic differentiation medium (chondrogenesis) or normal expansion medium (control). Blue indicates positive staining for sulfated glycosaminoglycans, pink indicates nuclei. Larger images taken at 40X; insets taken at 10X.

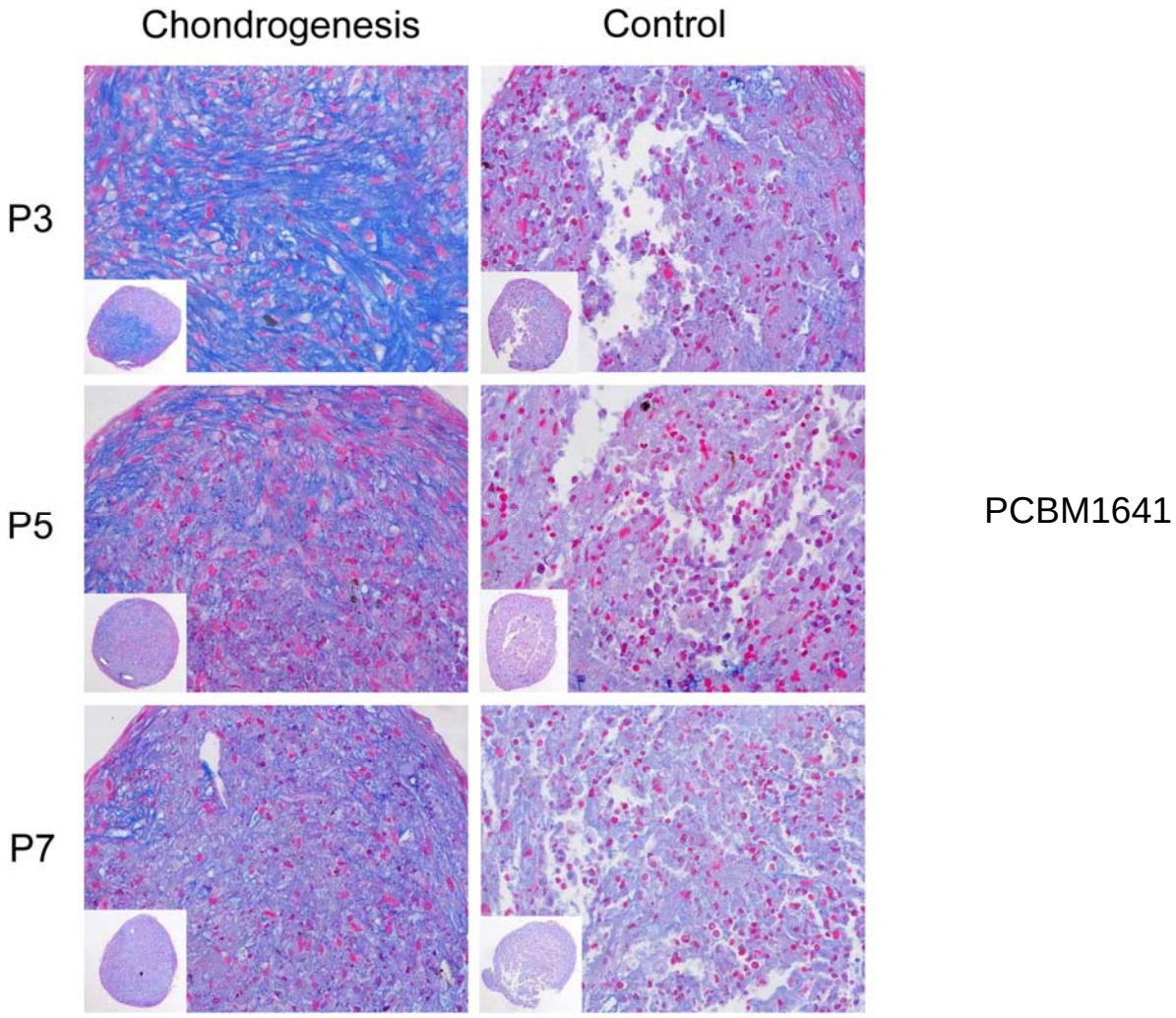

Figure 3-14. Alcian Blue staining in cell line PCBM1641 following chondrogenic differentiation. MSCs from cell line PCBM1641 P3 (top), P5 (middle), and P7 (bottom) were cultured in pellet culture for 21 days in either chondrogenic differentiation medium (chondrogenesis) or normal expansion medium (control). Blue indicates positive staining for sulfated glycosaminoglycans, pink indicates nuclei. Larger images taken at 40X; insets taken at 10X.

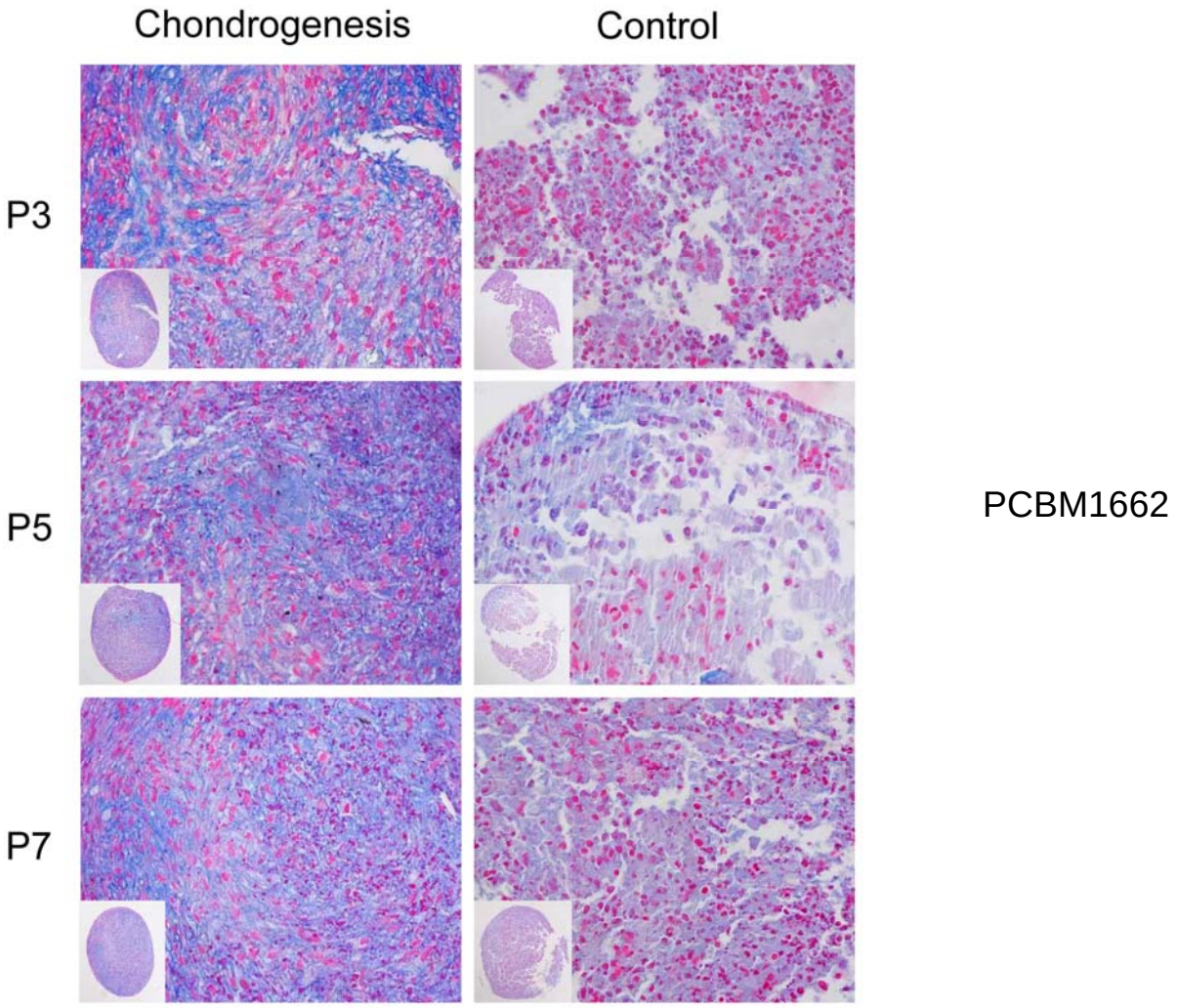

Figure 3-15. Alcian Blue staining in cell line PCBM1662 following chondrogenic differentiation. MSCs from cell line PCBM1662 P3 (top), P5 (middle), and P7 (bottom) were cultured in pellet culture for 21 days in either chondrogenic differentiation medium (chondrogenesis) or normal expansion medium (control). Blue indicates positive staining for sulfated glycosaminoglycans, pink indicates nuclei. Larger images taken at 40X; insets taken at 10X.

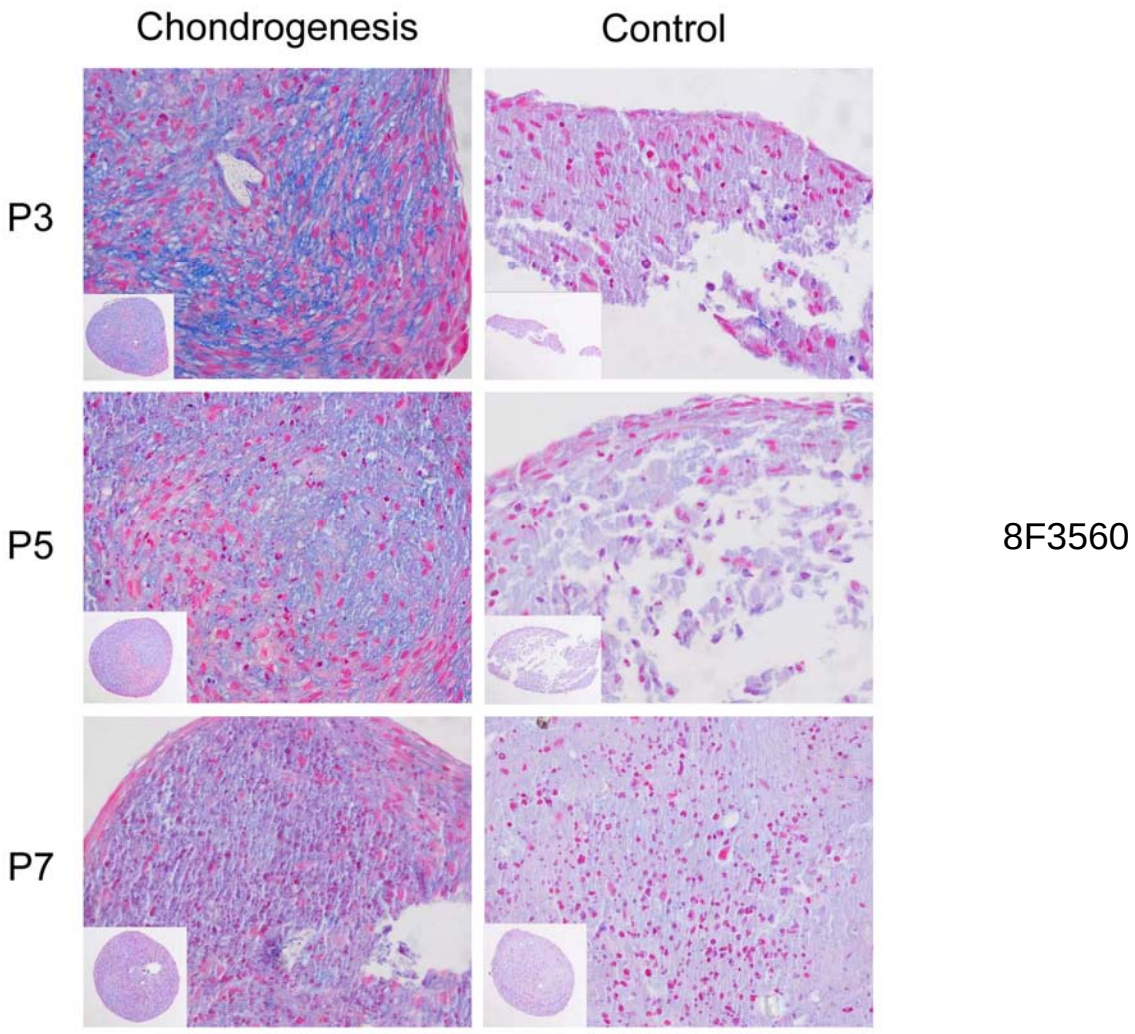

Figure 3-16. Alcian Blue staining in cell line 8F3560 following chondrogenic differentiation. MSCs from cell line 8F3560 P3 (top), P5 (middle), and P7 (bottom) were cultured in pellet culture for 21 days in either chondrogenic differentiation medium (chondrogenesis) or normal expansion medium (control). Blue indicates positive staining for sulfated glycosaminoglycans, pink indicates nuclei. Larger images taken at 40X; insets taken at 10X.

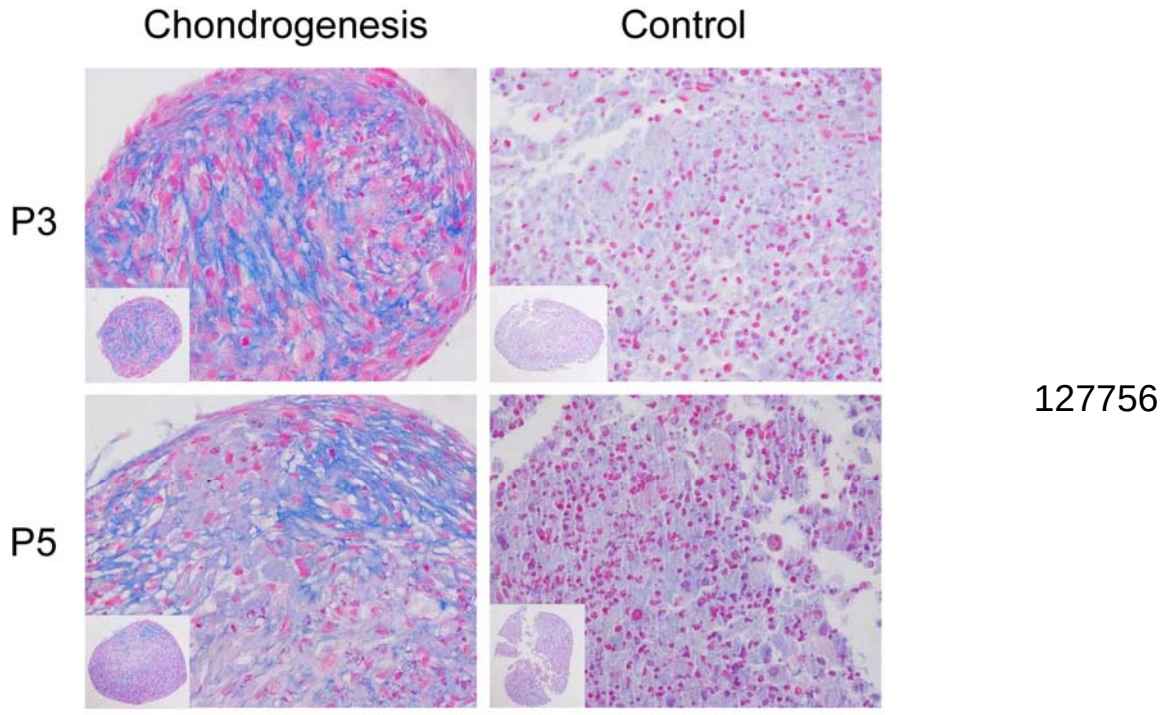

Figure 3-17. Alcian Blue staining in cell line 127756 following chondrogenic differentiation. MSCs from cell line 127756 P3 (top), and P5 (bottom) were cultured in pellet culture for 21 days in either chondrogenic differentiation medium (chondrogenesis) or normal expansion medium (control). Blue indicates positive staining for sulfated glycosaminoglycans, pink indicates nuclei. Larger images taken at 40X; insets taken at 10X.

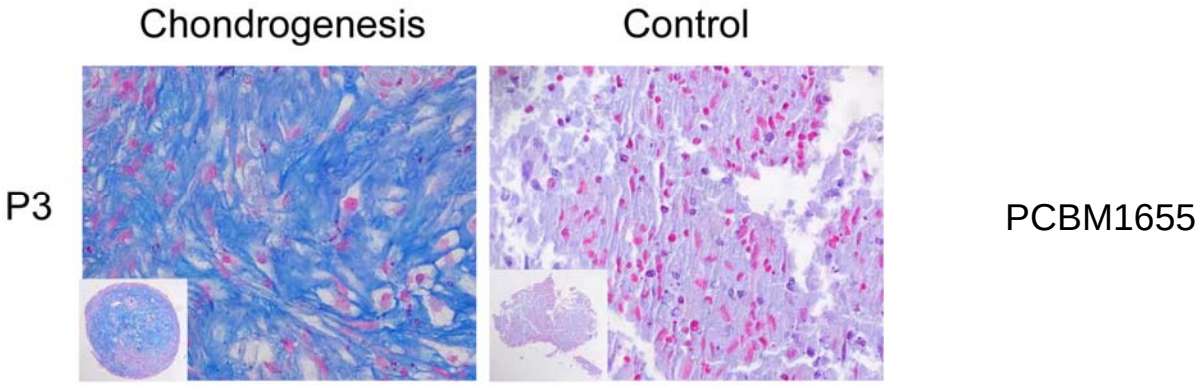

Figure 3-18. Alcian Blue staining in cell line PCBM1655 following chondrogenic differentiation. MSCs from cell line PCBM1655 P3 was cultured in pellet culture for 21 days in either chondrogenic differentiation medium (chondrogenesis) or normal expansion medium (control). Blue indicates positive staining for sulfated glycosaminoglycans, pink indicates nuclei. Larger images taken at 40X; insets taken at 10X.

3.3.4 MSCs differ in gene expression of lineage-specific markers following differentiation

To better understand the molecular response to differentiation in different cell lines and passages, changes in gene expression were assessed following adipogenic, osteogenic, and chondrogenic differentiation using common lineage-specific markers.

3.3.4.1 Determination of an appropriate housekeeping gene

Many common reference genes are unsuitable for use by qRT-PCR due to their altered expression in varying growth and differentiation conditions, as a stable house-keeping gene is a requisite to obtain reliable results. We found that commonly used glyceraldehyde-3-phosphate dehydrogenase (GAPDH) and 18S ribosomal RNA (18S) demonstrate a large degree of altered expression following adipogenic differentiation, making them unusable for our differentiation studies. The stability of additional house-keeping genes was therefore assessed, including TATA-binding protein (TBP), tyrosine 3-monooxygenase/tryptophan 5-monooxygenase activation protein, zeta polypeptide (YWHAZ), glucuronidase beta (GUSB) and hypoxanthine phosphoribosyltransferase 1 (HPRT1) (90).

Levels of mRNA transcript levels of the above-mentioned house keeping genes were assessed by reporting a raw Ct value following amplification. Cell line PCBM1632 at P3 and P7 was assessed in both undifferentiated and adipogenic-differentiated conditions (Figure 3-19). TBP (Ct values ranging from 30.3 to 31.8) and GUSB (29.0 – 30.1) showed the least variability between sample groups, while YWHAZ (23.4 – 25.2) and HPRT1 (28.7 – 30.7) varied to a slightly greater extent (Figure 3-19). Because GUSB demonstrated the least variability between sample groups, this house-keeping gene was utilized in all qRT-PCR human MSC studies.

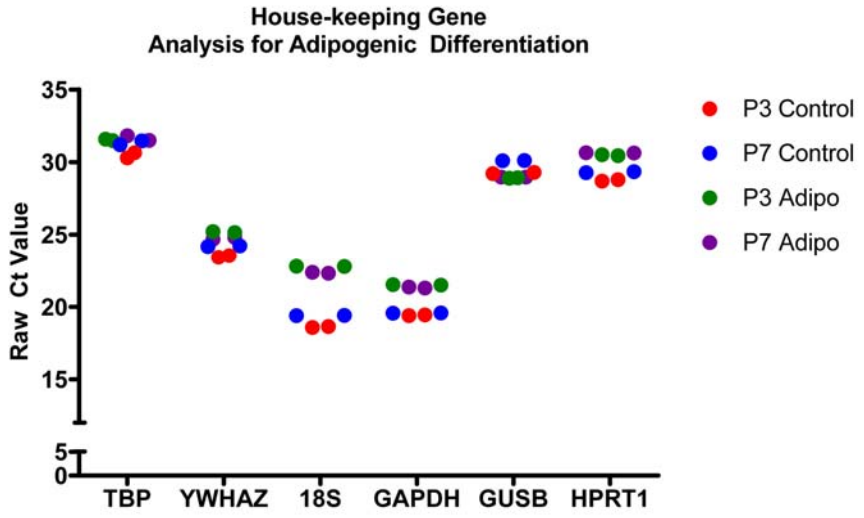

Figure 3-19. House-keeping genes show variable expression in response to differentiation. MSCs from cell line PCBM1632 P3 and P7, undifferentiated (control) and adipogenic lineage-differentiated were analyzed for changes in expression of house keeping genes as a result of passaging or following differentiation. Raw Ct values following qRT-PCR are reported.

3.3.4.2 Adipogenesis

Changes in adipogenic gene expression were evaluated to correlate with our *in vitro* quantitative assays, as well as to assess the response of different donors and passages to adipogenic stimuli. Changes in adipogenesis-related genes tend toward decreasing with passage in most cell lines, which is in line with the automated microscopy results as shown in Figure 3-4. Cell lines PCBM1632, PCBM1641, and 8F3560 show an increase in expression of C/EBPα from P3 to P5 (Figures 3-20A, 3-20D, and 3-20F respectively). All cell lines except PCBM1641 show a statistically significant decrease from P3 to P7 in FABP4 expression following adipogenic differentiation ($p<0.01$, Figure 3-21). Changes in gene expression patterns in PPARγ also concurs with other adipogenic gene markers, showing most cell lines significantly decrease in expression from P3 to P7 ($p<0.01$, Figure 3-22) with the exception of PCBM1641 (Figure 3-22D) and 8F3560 (Figure 3-22F). Overall fold change in cell line 8F3560 was the smallest in all adipogenic markers. A re-representation of the data as a donor comparison for all adipogenesis-

related genes can be seen in Appendix A, Figures A-1-1 (C/EBPα), A-1-2 (FABP4) and A-1-3 (PPARγ).

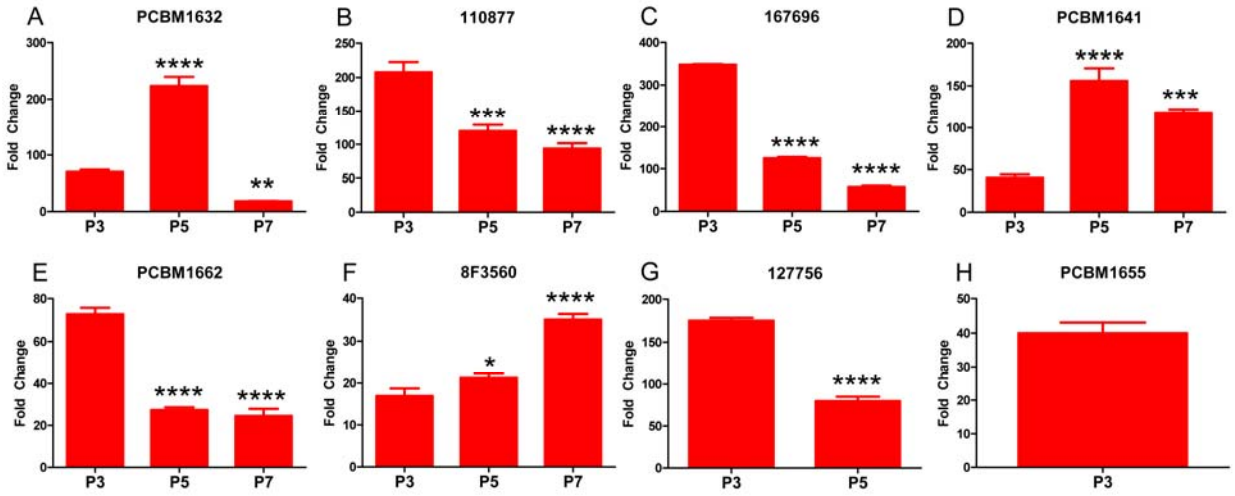

Figure 3-20. Change in C/EBPα expression following adipogenic stimulation is donor- and passage-dependent. MSCs from all cell lines were cultured for 14 days in adipogenic differentiation medium, and assessed for expression of C/EBPα by qRT-PCR. Data is expressed as mean ± standard deviation; $p<0.05$ relative to P3. (A) PCBM1632 (B) 110877 (C) 167696 (D) PCBM1641 (E) PCBM1662 (F) 8F3560 (G) 127756 (H) PCBM1655. *p<0.05, **p<0.01, ***p<0.001, ****p<0.0001.

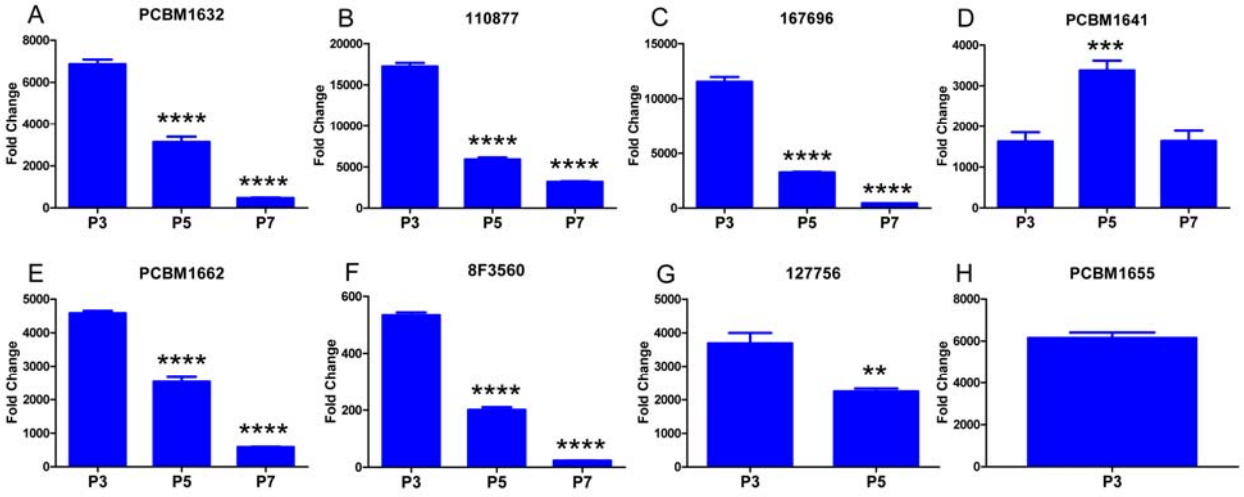

Figure 3-21. Change in FABP4 expression following adipogenic stimulation is donor- and passage-dependent. MSCs from all cell lines were cultured for 14 days in adipogenic differentiation medium, and assessed for expression of FABP4 by qRT-PCR. Data is expressed as mean ± standard deviation; $p<0.05$ relative to P3. (A) PCBM1632 (B) 110877 (C) 167696 (D) PCBM1641 (E) PCBM1662 (F) 8F3560 (G) 127756 (H) PCBM1655. *p<0.05, **p<0.01, ***p<0.001, ****p<0.0001.

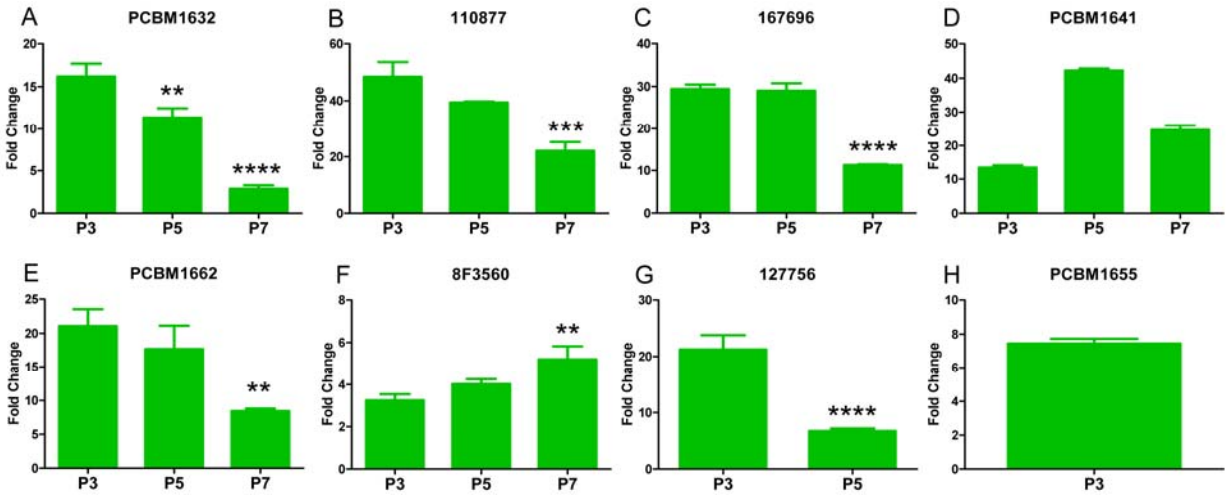

Figure 3-22. Change in PPARγ expression following adipogenic stimulation is donor- and passage-dependent. MSCs from all cell lines were cultured for 14 days in adipogenic differentiation medium, and assessed for expression of PPARγ by qRT-PCR. Data is expressed as mean ± standard deviation; $p<0.05$ relative to P3. (A) PCBM1632 (B) 110877 (C) 167696 (D) PCBM1641 (E) PCBM1662 (F) 8F3560 (G) 127756 (H) PCBM1655. *$p<0.05$, **$p<0.01$, ***$p<0.001$, ****$p<0.0001$.

3.3.4.3 Osteogenesis

Changes in gene expression of osteogenic-specific markers are variable between donors and passages. Cell lines PCBM1632, 110877, PCBM1641 and 127756 show a significant increase in RUNX2 expression with increasing passage (Figures 3-23A, 3-23B, 3-23D, and 3-23G respectively). Changes in gene expression of ALPL and SPP1 are more variable due to passaging. Cell lines PCBM1632, 167696, PCBM1662 and 127756 trends toward decreasing expression of ALPL with increasing passage (Figures 3-24A, 3-24C, 3-24E, and 3-24G respectively). SPP1 expression decreases from P3 to P7 in cell lines 110877, 167696, PCBM1641, and PCBM1662 ($p<0.0001$, Figures 3-25B, 3-25C, 3-25D, and 3-25E respectively). A re-representation of the data as a donor comparison for all osteogenesis-related genes can be seen in Appendix A, Figures A-2-1 (ALPL), A-2-2 (RUNX2), and A-2-3 (SPP1).

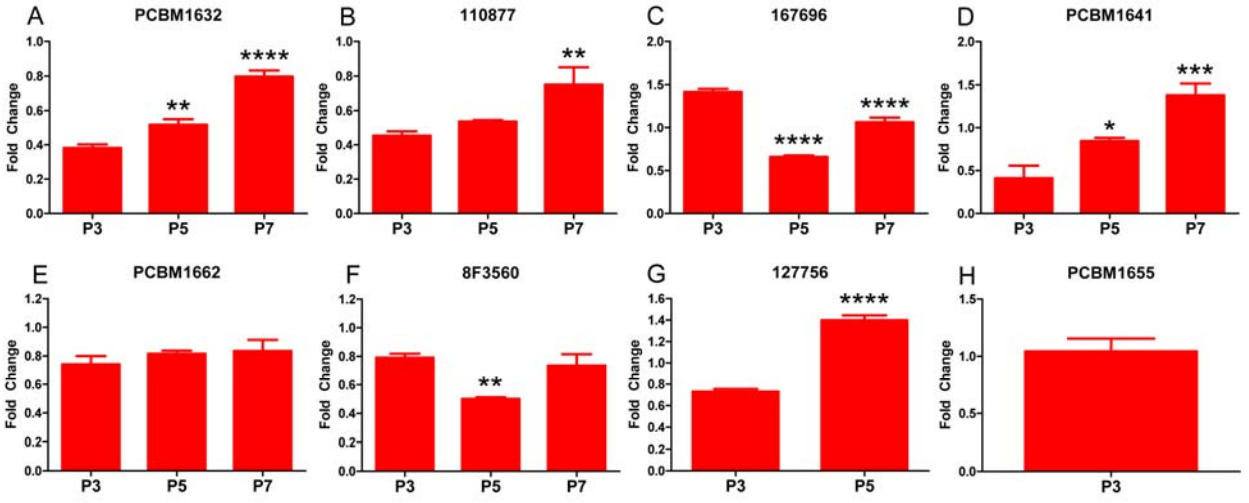

Figure 3-23. Change in RUNX2 expression following osteogenic stimulation is donor- and passage-dependent. MSCs from all cell lines were cultured for 14 days in osteogenic differentiation medium, and assessed for expression of RUNX2 by qRT-PCR. Data is expressed as mean ± standard deviation; $p<0.05$ relative to P3. (A) PCBM1632 (B) 110877 (C) 167696 (D) PCBM1641 (E) PCBM1662 (F) 8F3560 (G) 127756 (H) PCBM1655. *p<0.05, **p<0.01, ***p<0.001, ****p<0.0001.

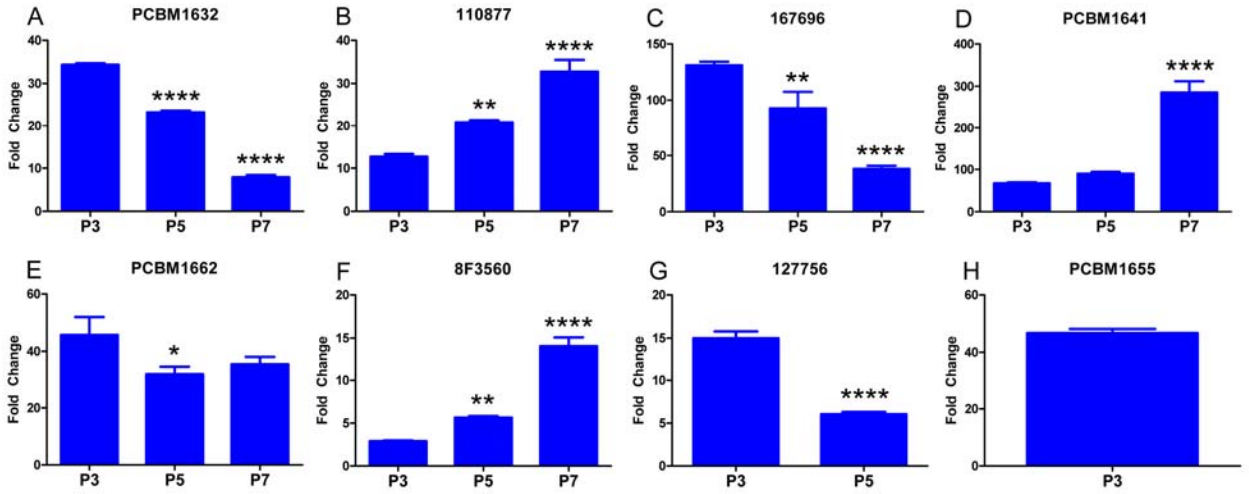

Figure 3-24. Change in ALPL expression following osteogenic stimulation is donor- and passage-dependent. MSCs from all cell lines were cultured for 14 days in osteogenic differentiation medium, and assessed for expression of ALPL (Alkaline Phosphatase) by qRT-PCR. Data is expressed as mean ± standard deviation; $p<0.05$ relative to P3. (A) PCBM1632 (B) 110877 (C) 167696 (D) PCBM1641 (E) PCBM1662 (F) 8F3560 (G) 127756 (H) PCBM1655. *p<0.05, **p<0.01, ***p<0.001, ****p<0.0001.

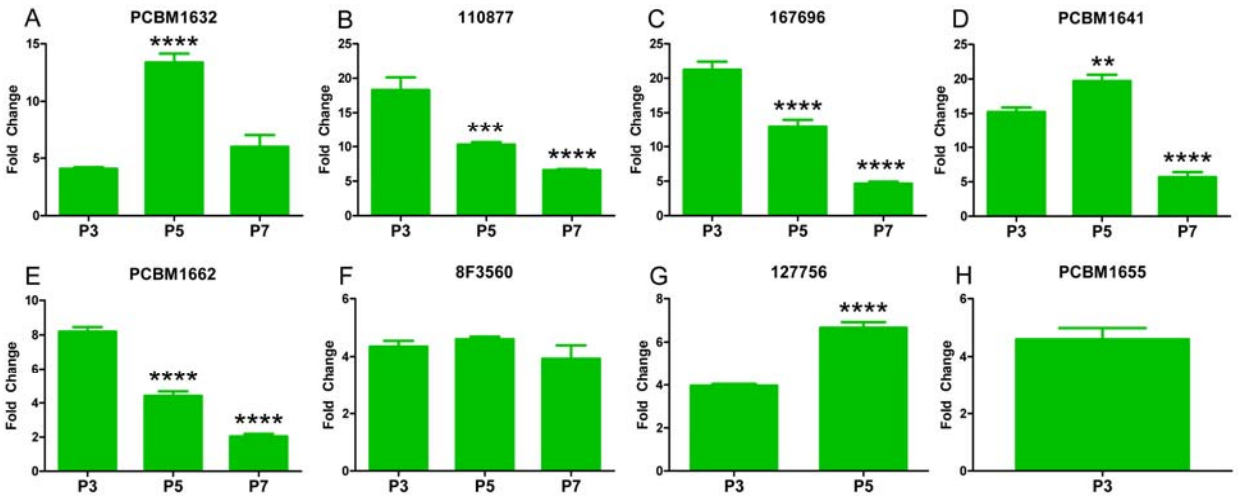

Figure 3-25. Change in SPP1 expression following osteogenic stimulation is donor- and passage-dependent. MSCs from all cell lines were cultured for 14 days in osteogenic differentiation medium, and assessed for expression of SPP1 (osteopontin) by qRT-PCR. Data is expressed as mean ± standard deviation; $p<0.05$ relative to P3. (A) PCBM1632 (B) 110877 (C) 167696 (D) PCBM1641 (E) PCBM1662 (F) 8F3560 (G) 127756 (H) PCBM1655. *$p<0.05$, **$p<0.01$, ***$p<0.001$, ****$p<0.0001$.

3.3.4.4 Chondrogenesis

Following chondrogenic differentiation, expression in Sox9 decreased in most cell lines due to *in vitro* culturing from P3 to P7 ($p<0.01$, Figure 3-26). Conversely, cell line 8F3560 increased in Sox9 expression with passaging ($p<0.05$, Figure 3-26F). Aggrecan expression also decreased at P3 to P7 in most cell lines, which was statistically significant ($p<0.0001$, Figure 3-27). Cell lines 167696 and 127756 increased with passage, however only cell line 167696 was significant ($p<0.0001$, Figure 3-27). Col2A1 expression was assessed, however only cell lines PCBM1641 and 110877 at P3 showed a fold change in expression at approximately 2.5 and 3.9 respectively (data not shown). A re-representation of the data as a donor comparison for all chondrogenesis-related genes can be seen in Appendix A, Figures A-3-1 (Sox9) and A-3-2 (ACAN).

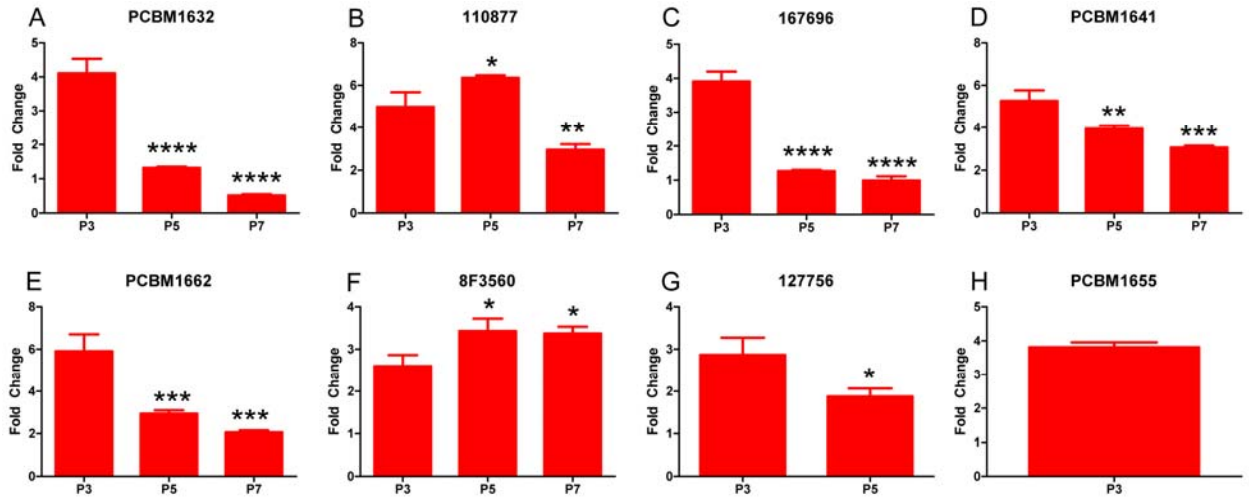

Figure 3-26. Change in Sox9 expression following chondrogenic stimulation is donor- and passage-dependent. MSCs from all cell lines were cultured for 15 days in chondrogenic differentiation medium, and assessed for expression of SOX9 (SRY (sex determining region Y)-box 9) by qRT-PCR. Data is expressed as mean ± standard deviation; $p<0.05$ relative to P3. (A) PCBM1632 (B) 110877 (C) 167696 (D) PCBM1641 (E) PCBM1662 (F) 8F3560 (G) 127756 (H) PCBM1655. *$p<0.05$, **$p<0.01$, ***$p<0.001$, ****$p<0.0001$.

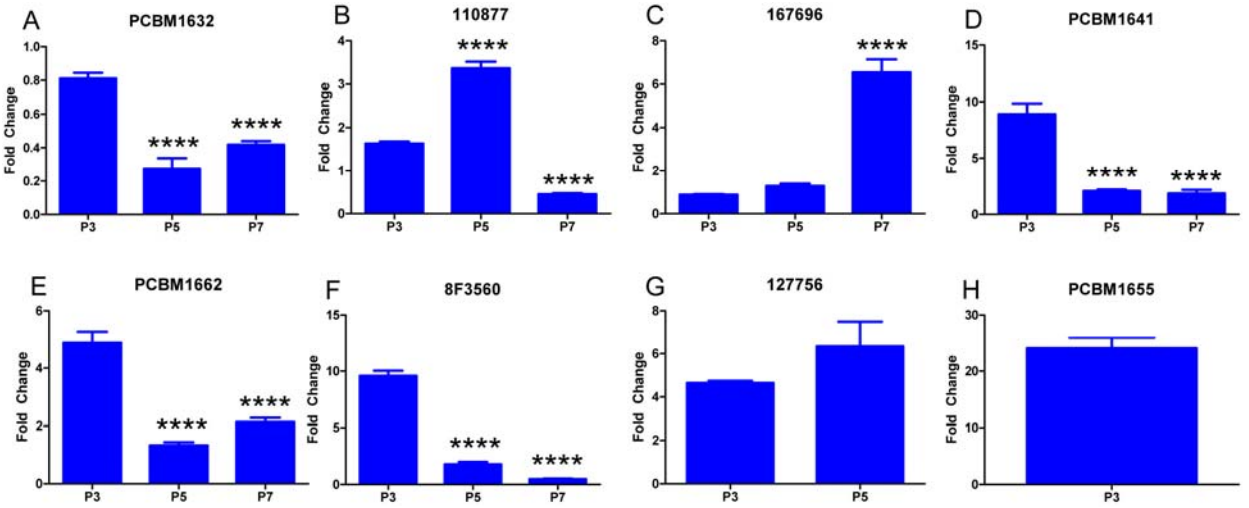

Figure 3-27. Change in ACAN expression following chondrogenic stimulation is donor- and passage-dependent. MSCs from all cell lines were cultured for 15 days in chondrogenic differentiation medium, and assessed for expression of ACAN (Aggrecan) by qRT-PCR. Data is expressed as mean ± standard deviation; $p<0.05$ relative to P3. (A) PCBM1632 (B) 110877 (C) 167696 (D) PCBM1641 (E) PCBM1662 (F) 8F3560 (G) 127756 (H) PCBM1655. *$p<0.05$, **$p<0.01$, ***$p<0.001$, ****$p<0.0001$.

3.4 DISCUSSION

MSCs are of great interest because of their potential clinical application in treating many diseases due to both their immunosuppressive properties as well as application in tissue regeneration (91). Because MSCs exist at low levels in the bone marrow (0.001 – 0.01%) (78), extensive expansion from multiple donors will be required to achieve numbers necessary for desired applications. Therefore, establishing the role of passaging and donor differences through the use of quantitative bioassays will be necessary to measure these changes. Here, it was demonstrated that limiting dilution was used successfully to detect changes in adipogenic potential following differentiation between 2 cell lines at P3, P5, and P7 (74). The simplicity of the limiting dilution assay also allows for its use in almost any laboratory. However, this assay is subjective due to its reliance on an individual to discern between an adipocyte and an undifferentiated MSC. Further, because limiting dilution requires a dilution of MSCs as part of the assay setup and analysis, it may inherently ignore community effects (cell-cell and cell-environment interactions), as Schinkothe *et al.* have demonstrated cytokine secretion profiles of MSCs include factors involved in proliferation and differentiation (92). Lastly, the time required for an individual to scan each well of 3, 96-well plates for each experiment is significant. Automated microscopy addresses these concerns with limiting dilution, as MSCs are plated at an identical cell density, while also introducing an efficient, automated measurement that eliminates any subjectivity in the analysis. We have taken advantage of these desirable features of automated microscopy to quantify both adipogenic and osteogenic differentiation potential as a function of cell line and passage.

Automated microscopy is inherently precise, as identical parameters are used during each analysis to quantify differentiated MSCs using the same automated procedure (macro).

Automated microscopy was applied to 8 cell lines following differentiation to quantify adipogenic and osteogenic potential at P3, P5 and P7 where applicable. To determine the accuracy of the macro in quantifying true differentiated cells, differentiated adipocytes were manually counted following adipogenic induction on the identical image set acquired for PCBM1632. As seen in Figure 3-5, the macro is an accurate representation of the number of differentiated cells, based on very similar measurements at P5 and P7 between the automated and manual counts, while still close at P3. Taken together, this demonstrates both the precision and accuracy of automated microscopy in quantifying differentiated MSCs following adipogenic differentiation. Further, when considering computation time, the macro closely predicts actual values in close to 1% of the time it takes to manually count an image set. This result points to the utility of automated microscopy as a high-throughput tool to quantify differentiation in MSCs.

Following automated analysis of all cell lines at P3, P5, and P7, we have successfully demonstrated that adipogenic differentiation can be quantified on a per cell basis, allowing us to determine the percentage of cells capable of adipogenic differentiation. As seen in Figure 3-4, this percentage is highly variable between cell lines, ranging from 0.51% in cell line 8F3560 to 13.62% in cell line PCBM1632 at P3. The effect of donor variability becomes less significant by P7, where percent differentiation converges to a level of around 2% differentiation in most cell lines. All cell lines except 8F3560 show a highly significant ($p<0.001$) drop in adipogenic potential when comparing P3 v. P7. Because automated microscopy provides a quantitative readout of differentiation capacity, we were able to measure differences between cell lines and passages on a per cell basis. As there has been little effort in the field to quantify differentiation in MSCs, many researchers utilize qualitative (i.e. Oil Red O staining (93-95)) or semi-

quantitative (pixel quantitation or spectrophotometry following isopropanol extraction of Oil Red O-stained adipocytes (72,80) measurements to demonstrate differentiation capacity. However, without a quantitative bioassay that measures differentiation on a per cell basis, these differences cannot be truly measured to determine changes in varying populations of MSCs as a result of donor variability or passaging.

A similar methodology was utilized to quantify osteogenic differentiation by automated microscopy. Because of the morphological differences in the osteogenesis-differentiated phenotype, quantitative analyses had to be based on thresholding and subsequent surface area quantification, as there was no all-or-none response to osteogenic stimulation. Therefore, ALP staining was utilized to represent positive osteogenic differentiation, and ALP-positive area was normalized to nuclei counts. Interestingly, our data suggests osteogenic potential correlates with proliferative capacity in MSCs, as shown in Figure 3-9. However, normalization to nuclei counts still demonstrates that osteogenic differentiation capacity decreases as a result of passaging. Further, a high degree of donor variability at P3 was demonstrated based on the ability to form bone *in vitro,* as shown in Figure 3-8. Similar to adipogenic potential, P7 osteogenic-differentiated cells show more homogeneity between donors as demonstrated by an overall decreased potential.

Although not genetically identical as in a mouse-model system, it is interesting to point out the differences in osteogenic potential based on gender. The cell lines demonstrating the largest degree of osteogenic differentiation potential are those derived from male donors (PCBM1632 and 127756), while those showing the least amount of osteogenic differentiation are derived from females (PCBM1655, PCBM1662, and 167696). The role of gender differences in the ability to form bone in MSCs (96) and other cell types (97,98) has been documented, and it is

of note that our *in vitro* quantitative bioassay to measure osteogenic capacity can detect these differences. In regards to bone formation, male murine muscle-derived stem cells (MDSCs) show enhanced bone forming capacity based on ectopic bone formation in a cranial defect wound healing model (98). Others have demonstrated this in adipose-derived stem cells (ASCs) derived from male rabbits via an increase ALP-positive staining following osteogenic differentiation (99). Conversely, ASCs derived from female mice show increased expression of PPARγ, a major transcriptional factor involved in adipogenesis (100). Interestingly, female bone marrow-derived MSCs have demonstrated improved response to activation by hypoxia via increases in VEGF secretion and decreases in secretion of pro-inflammatory cytokine TNF-α when compared to male bone marrow-derived MSCs (101). Taken together, these studies suggest a potential role of gender that is lineage-specific, and therefore may be considered as a potential factor in clinical applications (102).

To substantiate our quantitative measurements of adipogenic and osteogenic differentiation potential, we investigated changes in lineage-specific differentiation markers on the molecular level by qRT-PCR. In regards to adipogenesis, changes in gene expression appear to be in line with automated measurement results, showing a general trend toward decreasing in expression with increasing passage. While cell line 8F3560 appears to be the most variable in regards to expression of adipogenic-specific markers, the overall change in gene expression of this cell line is low relative to other cell lines, and therefore the level of detection may allow contribution of noise. Changes in osteogenic gene expression are more variable. Interestingly, expression of RUNX2 uniformly increases in all cell lines, however it has been shown that expression of RUNX2 in late stages of differentiation inhibits maturation of osteoblasts, which correlates with the decreased ALP as quantified by automated microscopy. With the exception

of cell line 8F3560, the hallmark transcription factor involved in chondrogenesis Sox9 shows a decrease in expression with passage, which correlates with our qualitative assessment of chondrogenesis by Alcian Blue staining. While Col2A1 expression was not detected, it is likely due to the time point in which chondrogenic differentiation was assessed by qRT-PCR. In general, while some of these patterns behave as would be predicted by biological outcomes based on quantitative assessments, others do not. Changes in gene expression are temporal, and variability between donors may be due to the kinetics of specific gene responses. Therefore, gene expression may be a poor substitute to assess differentiation capacity compared to quantitative bioassay assessments.

Because the macro quantifies differentiated cells, the total nuclei count per image is also recorded. When plotting this data alone in differentiated and in undifferentiated controls, the overall proliferative potential of each cell line at varying passages can be inferred. As seen in Figure 3-6, this data demonstrates that upon adipogenic stimulation, the overall proliferative potential decreases in MSCs when compared to corresponding undifferentiated controls. Further, this data also suggests that the overall proliferation decreases with increasing passage in both differentiated and undifferentiated samples, and this can also vary between cell lines. Similar trends in decreased proliferative potential with passage was also seen in osteogenic-induced MSCs (Figure 3-10)

This decrease in proliferation and adipogenic/osteogenic capacity with passage, as demonstrated by automated microscopy, also correlates with the decrease in percent CFUs with passage, as seen in Figure 2-5 and discussed in Chapter 2.0. As outlined by Prockop *et al.*, MSCs capable of clonal expansion are more proliferative and have a greater capacity to differentiate (75). Interestingly, cells from the 2 oldest donors (127756 and PCBM1655), which

were not capable of expansion beyond P5 and P3 respectively, both had the lowest CFU percentage at P3 (Figure 2-5), and also had the lowest proliferation potential as shown in Figure 2-1). In addition, both of these cell lines had the largest average cell diameters (Figure 2-4) which also correlated their respective FSC/SSC size data (Figure 2-3). This suggests donor age may play a role in growth potential and CFU capacity, which in turn correlates with cell size. Others have shown the function of cell size as well, as Colter *et al.* demonstrated a high correlation with recycling stem cells (a subpopulation of small, agranular, rapidly proliferating cells) and CFU capacity compared to the large, granular mature MSCs that are a slow growing subpopulation (103). Stenderup *et al.* also showed MSCs from younger donors had improved proliferative capacity over older donors based on higher cumulative population doublings and a lower percentage of senescence-associated beta-galactosidase (76). However, despite the decrease in percent CFUs and increase in cell size seen in both of these cell lines at P3, both cell lines 127756 and PCBM1655 had the 2nd and 3rd highest percent adipogenic differentiation when compared to cells from other younger donors at P3. While this finding goes against our hypothesis that those MSCs with the lowest CFU capacity and largest cell diameters would be less likely to differentiate, there may be multiple factors at play. Many have hypothesized a shift from high osteogenic and low adipogenic capacity in young donor MSCs to a low osteogenic and high adipogenic capacity in older donor MSCs due to the downregulation of osteogenesis-associated genes with age (104,105). In many cases, aging leads to a decrease in bone mass, as seen in osteoporosis, while typically accompanied by larger number of adipocytes in the bone marrow (73). This proposed inverse relationship between adipogenesis and osteogenesis has been reviewed extensively by Kim *et al* (106). Almeida *et al.* have suggested that this shift may be in part due to oxidative stress during aging, through the involvement of FoxO transcription

factors that are cellular mediators of oxidative stress (107). Taken together, this paradigm describing the shift from osteogenesis to adipogenesis in the bone marrow as we age, may partially explain our findings described here. Overall, however, decreased differentiation potential with passage is consistent amongst adipogenic and osteogenic lineages.

Others describe this osteogenic to adipogenic shift in MSCs to correlate with *in vitro* age, or passaging. Kim *et al.* demonstrated that after culturing MSCs up to passage 15 in both adipogenic and osteogenic-inducing media, there is a decrease in Von Kossa staining, while an increase in adipogenesis was shown by Oil Red O staining with increasing passage. Further, they correlated this shift in potential with increasing passage with an increase in senescence-associated beta-galactosidase staining, suggesting senescent MSCs are still capable of adipogenic differentiation (106). Unlike other published literature which relies only on cell population staining to demonstrate differentiation, adipogenic and osteogenic differentiation was quantified on a per cell basis in MSCs using automated microscopy. With a quantitative readout on differentiation, automated microscopy (in conjunction with other previously established quantitative bioassays) allows us to measure both the role of passaging and donor variability on MSC differentiation capacity, and therefore in turn correlate differentiation capacity with other cell properties.

MSCs are also partially defined by their ability to undergo chondrogenesis. Due to the nature of the *in vitro* differentiation assay by pellet culture, we have not yet quantified chondrogenic differentiation on a per cell basis. Nonetheless, to obtain a full overview of the differentiation potential of the cell lines used in this study, we wanted to assess chondrogenic differentiation potential as it relates to donor and passage differences. Based on a qualitative assessment, we do see slight differences in chondrogenic potential between donors, as some

donors appear to have more positive staining for sulfated GAGs by Alcian Blue than other donors (Figures 3-11 to 3-18). Further, it appears that most donors have more positive Alcian Blue staining at P3 than at P7, indicating *in vitro* culture may decrease chondrogenic potential with passage. Decreased expression in Sox9 and Aggrecan due to passaging in most donors (Figures 3-26 and 3-27) also supports our qualitative assessment.

Both researchers and manufacturers of MSCs use cell surface markers to characterize MSCs. As outlined in a white paper published by the ISCT, it is accepted in the field that MSCs should be plastic-adherent cells that are positive for CD73, CD90 and CD105, negative for CD14, CD34, CD45, CD79a, and HLA-DR, and capable of tri-lineage differentiation (29). Our findings demonstrate that while MSCs maintain positive expression for CD73, CD90, CD105, and other relevant MSC markers (Figure 2-2), this maintenance of positive expression does not correlate with their decreased functionality/differentiation capacity as demonstrated by automated microscopy. In other words, expression of these cell surface markers does not correlate with maintenance of adipogenic or osteogenic precursors through passaging. Further, it is widely accepted that trilineage differentiation is a required characteristic of MSCs, but quantitative assessments of this capacity are not often reported. To date, it has been acceptable in the literature to show differentiation by simple staining techniques, or by semi-quantitative methods that do not take into account the inherent heterogeneity of MSCs by quantifying on a per cell basis. Here, an efficient method to quantify adipo- and osteogenesis was developed, while also assessing the effects of passaging and donor variability on differentiation capacity *in vitro.* By quantifying differentiation capacity, we are also able to correlate these findings with other quantitative bioassay readouts to provide an overview of donor variability while also assessing the effects of culturing on MSC stemness and potency.

3.5 CONCLUSION

Quantitative assessments of the biological characteristics of MSCs will allow for the detection of donor and passage-specific differences and may be of great utility in discovery of molecular markers that correlate with differentiation and proliferation capacity of MSCs. Further, these quantitative measurements may also help assess various growth conditions (serum v. serum free), the addition of exogenous growth factors, the role of oxygen conditions, etc. to better understand the role of these parameters in a quantitative readout. In this chapter, limiting dilution was shown to be capable of determining a precursor frequency that provides a quantitative measure of the adipogenic differentiation capacity in populations of MSCs. Further, automated microscopy was also shown to be a technique that can quantify adipogenic and osteogenic differentiation on a per cell basis. Future work will focus on quantitative assays to assess chondrogenic differentiation *in vitro.* Lastly, it was shown that differentiation capacity varies between MSCs from different donors and passages, and that mean cell size increases with cell passage. The next chapter will focus on cell size and assessing MSC characteristics and differentiation capacity in sorted small and large cells, as well as determining a mechanism of action as it relates to differentiation capacity and senescence in MSCs while utilizing quantitative bioassays discussed in Chapters 2 and 3.

4.0 DETERMINATION OF THE ROLE OF CELL SIZE AND WNT SIGNALING IN DIFFERENTIATION AND SENESCENCE OF MSCS USING QUANTITATIVE BIOASSAYS

4.1 INTRODUCTION

4.1.1 MSCs and cell size

The role of cell size in MSC behavior has been previously described in earlier literature, where Mets and Verdonk showed MSCs in early passages were heterogeneous containing both small, rapidly-dividing spindle-shaped cells, and large, slowly-dividing cells (108). At later passages, cultures became more homogeneous, predominantly containing the large, slow dividing cells that are closer to senescence. This shift in heterogeneity was also associated with decreased potency and proliferation capacity. Colter *et al*. later identified the small, agranular cells as "recycling stem cells" (RS cells) and the large, granular cells as mature MSCs (mMSCs). The number of RS cells also highly correlated with the percent CFUs, indicating early progenitors reside in the RS population of MSCs, and are responsible for the rapid expansion of MSCs *in vitro* (13,103).

Many others have documented changes in cell size in response to *in vitro* culture. More recent studies have reported these changes using flow cytometry to measure FSC (size) and SSC (granularity). Larson *et al.* have shown that the percentage of cells in the high FSC/SSC

quadrant increases with time in culture, while the percentage of cells in the low FSC/SSC quadrant decreases with time in culture. Further, they also document that this may be a result of cell density, as replated cells after confluence at a lower density will revert back to the 'RS' cells described above (84).

In our own work, as seen in Chapter 2, we have also documented an increase in cell size and granularity with increasing passage by flow cytometry. We have also validated this by quantifying cell diameter using a cell counter, which has the capability of measuring cell diameter when counting cells. While many have correlated this increase in cell size with decreased stemness and potency, few have separated small and large cell populations to study purified cell populations. In this chapter, we have taken advantage of the cell size heterogeneity seen in MSCs to directly evaluate the role of cell size on potency and stemness through two different methods. Enrichment of small cell progenitors in MSCs may allow for the identity of novel stemness markers that correlate with improved MSC function *in vitro* and *in vivo*, and an improved understanding of signaling pathways involved in stem cell maintenance in the small cell subpopulation.

4.1.2 Wnt Signaling in MSCs

In regards to differentiation, inhibition of Wnt signaling has been shown to be necessary for adipogenic differentiation (109). Canonical Wnt signaling in MSCs inhibits expression of adipogenesis-related transcription factor PPARγ in MSCs (110). In line with this, it has been suggested that downstream targets of Wnt signaling, namely cyclin D1 and c-myc, regulate adipogenesis through the respective inactivation of PPARγ and C/EBPα (111,112). The role of Wnt signaling in osteogenesis is less clear, as differential effects have been reported. Exogenous

addition of Wnt3a, a Wnt agonist, has been shown to both enhance (113-115), and inhibit (11,71), osteogenesis. Further, Wnt signaling may improve differentiation in osteogenic lineage-committed MSCs, while terminal differentiation was inhibited in mature osteoblasts (116-118). Further, β-catenin may be a functional positive and negative regulator of chondrogenesis. Lithium ion-induced β-catenin accumulation decreased chondrogenesis as shown by decreases in Alcian Blue-positive staining for collagen type II in chick embryo wing chondroprogenitors (119). However, siRNA knockdown of β-catenin has also been shown to decrease expression of collagen type II and aggrecan by RT-PCR (119).

The canonical Wnt signaling pathway can be modulated by various methods. Secreted frizzled-related proteins (sFRPs) act as Wnt antagonists and inhibit Wnt signaling through binding of Wnt ligands (120) or frizzled protein receptors (121). sFRP has been shown to positively regulate proliferation and wound repair. Specifically, sFRP enhances the proliferative capacity of human MSCs (122), while Mirotsou *et al.* demonstrated sFRP is involved in myocardial repair in MSCs (123). In this chapter, we will utilize a sFRP inhibitor to block Wnt signaling to better understand the role of Wnt signaling in proliferation and differentiation.

4.2 MATERIALS AND METHODS

4.2.1 FACS based on cell size

Cell line PCBM1641 P7 cells were thawed, expanded and sterilely sorted into populations of small and large cells based on forward scatter (FSC) properties using the FACS Aria (BD Biosciences). FSC correlates with cell size, therefore separate sorting gates were applied to approximately the upper (large cells) and lower (small cells) thirds of an FSC histogram plot. For example, for one experiment with PCBM1641 P7 cells, this corresponded to a gate from 45 to 105 FSC units (small cells) and from 170 to 258 FSC units (large cells). Cells in the middle third were not analyzed. Sorted populations were then counted and plated for limiting dilution analysis as described in Chapter 2.

4.2.2 Cell size separation via filtration

6 x 6cm nitex meshes of 10, 15 and 20μm in diameter were purchased from SEFAR. Mesh holders were made from Lexan (a polycarbonate), and designed to fit in standard 50ml conical tubes. Holders are comprised of 2 separate components, an inner and outer ring, designed to allow the nitex mesh square fit tightly in between. Mesh holders were fabricated by Mechanical Instrumentation Design and Fabrication Branch at the National Institutes of Health. Figure 4-1 shows a schematic of the filter rings and corresponding dimensions.

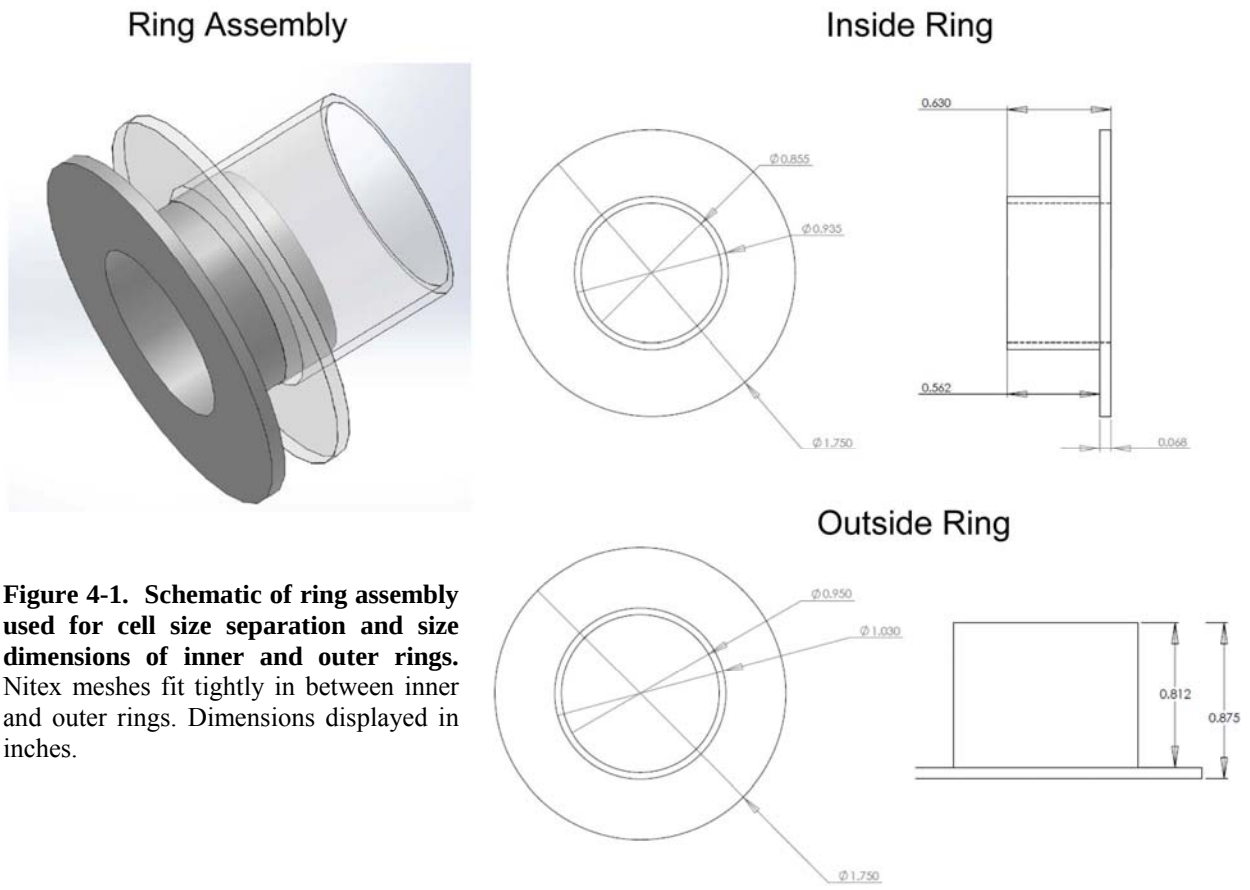

Figure 4-1. Schematic of ring assembly used for cell size separation and size dimensions of inner and outer rings. Nitex meshes fit tightly in between inner and outer rings. Dimensions displayed in inches.

P5 cells from cell line PCBM1632 were thawed and expanded until 80% confluent. Cells were trypsinized, counted, and resuspended in expansion medium at 100,000 cells/ml. The cell suspension was first applied to the 20µm mesh and allowed to passively drip through the column, leaving cells greater than 20µm on top. Flow through < 20µm in diameter was collected and passed through the 15µm mesh. To collect the cells >20µm, the filter rings were separated, and the top of the mesh was rinsed with 500µl of expansion medium and collected. This procedure was repeated to collect cells in the following cell size ranges: >20µm, 15-20µm, 10-15µm, and <10µm. Cells from each size range were spun down and counted for various endpoints. Large cells were considered to be cells that did not pass through the 20µm filter, and

small cells were considered to be cells the cells that passed through the 10μm filter. These numbers varied slightly between replicate experiments. The workflow for cell size separation is illustrated below in Figure 4-2.

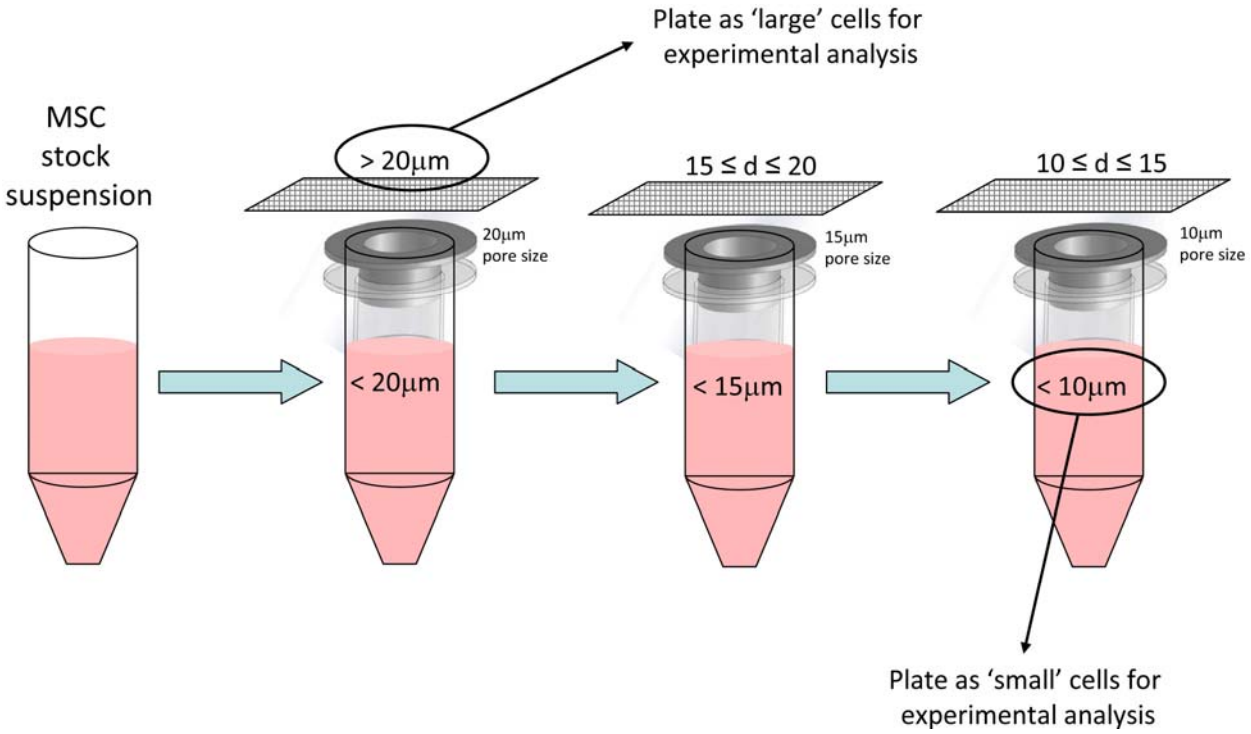

Figure 4-2. Schematic of cell size separation workflow. MSCs from PCBM1632 P5 at 100,000 cells/ml were applied to nitex meshes held by filter rings (not shown) to separate cells by cell size. Cell size ranges >20μm, 15-20μm, 10-15μm, and <10μm were collected and processed for further endpoint analysis.

4.2.3 Inhibition of Wnt signaling

Inhibition of Wnt signaling in MSC cell lines was carried out through exogenous addition of a diphenylsulfone sulfonamide derivative (Enzo Life Sciences), an sFRP-1 inhibitor and Wnt antagonist, to cell culture media at 5μM concentration. Optimal concentration was determined following a titration experiment examining proliferation potential and based on previously

published data (124). To assess proliferative capacity and response of adipo- and osteo-lineage specific genes following differentiation in the presence and absence of sFRP-1 inhibitor, cells were plated as described in Section 2.2.3 to assess proliferation, and as described in section 3.2.4 to measure changes in gene expression.

4.2.4 Senescence-associated beta-galactosidase staining

Following cell size separation, MSCs from the large (>20μm) and small (<10μm) were plated in 6-well plates at 30,000 cells/well. After cells were allowed to adhere for 24 hours, plates were processed using a senescence β-galactosidase staining kit (Cell Signaling) per instructions. Briefly, MSCs were fixed for 15 minutes with 1X fixative solution, rinsed, and incubated overnight with 1ml β-galactosidase staining solution in a non-CO_2 incubator. Plates were imaged using a Nikon Ti-S inverted microscope.

4.2.5 Quantitative functional endpoints

Following cell-size separation by filtering, MSCs were evaluated for CFU, proliferation capacity, and adipogenic and osteogenic differentiation potential as described in Chapter 3 to further elucidate the role of cell size in MSC biological function.

4.2.6 Statistical Analyses

Statistical comparisons made between small and large cells were completed using a Student's 2-tailed t-test in Microsoft Excel. Likewise, statistical analyses for qRT-PCR comparing the

addition of sFRP-1 inhibitor were also carried out in excel using the same analysis. Data is represented as an average of n=3 and $p<0.05$ was considered significant.

4.3 RESULTS

4.3.1 Wnt signaling inhibitor may improve proliferation and adipogenic capacity

Following addition of sFRP-1 inhibitor to block Wnt signaling, MSCs at P3 appear to show a slight improvement of proliferative capacity. MSCs at P7 show no response in proliferative capacity following Wnt inhibition (Figure 4-3).

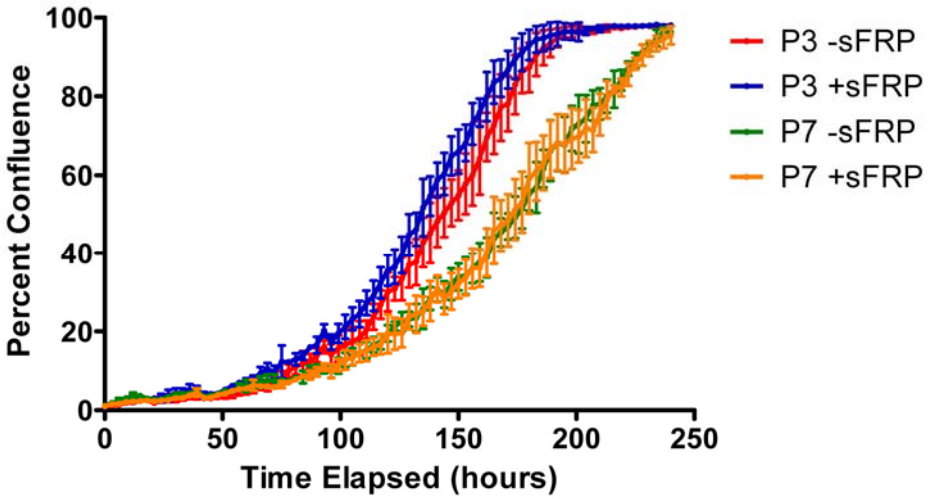

Figure 4-3. sFRP may slightly improve proliferation at early passages in MSCs. Cell line 110877 P3 and P7 was cultured with (+sFRP) or without (-sFRP) at 5μm until confluence. Percent confluence was recorded using a live cell imager.

MSCs at P3 and P7 were differentiated toward adipo- and osteogenic lineages for 7 days with or without addition of sFRP-1 inhibitor, and were examined for changes in gene expression for lineage-specific markers by qRT-PCR. Addition of sFRP-1 inhibitor increases expression of

PPARγ, C/EBPα and FABP4 at P3 ($p<0.05$), while no effect was shown at P7 (Figure 4-4). Further, addition of sFRP-1 inhibitor appears to have little to no effect on osteogenic differentiation at either P3 or P7 (Figure 4-5).

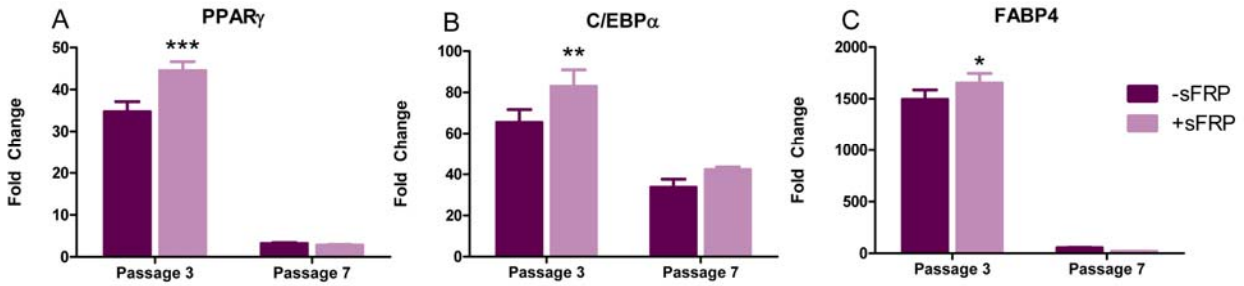

Figure 4-4. sFRP-1 inhibitor increases expression of adipogenic-specific markers at passage 3. Cell line 110877 P3 and P7 was cultured with (+sFRP) or without (-sFRP) at 5μm for 7 days in adipogenic differentiation medium. Changes in gene expression of (A) PPARγ (B) C/EBPα and (C) FABP4 were assessed by qRT-PCR. Data is represented as mean ± standard deviation, n=3. *p<0.05, **p<0.01, ***p<0.001.

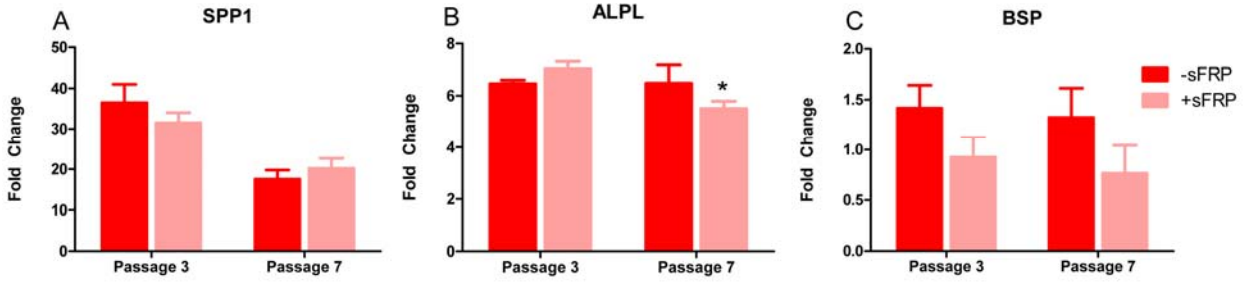

Figure 4-5. sFRP-1 inhibitor has little effect on osteogenic-specific markers. Cell line 110877 P3 and P7 was cultured with (+sFRP) or without (-sFRP) at 5μm for 7 days in osteogenic differentiation medium. Changes in gene expression of (A) SPP1 (B) ALPL and (C) BSP were assessed by qRT-PCR. Data is represented as mean ± standard deviation, n=3. *p<0.05.

4.3.2 Cell size separation by FACS

Due to the detectable changes in the FSC profile between passages, we utilized this property to sort small and large cells. We then applied the adipogenic precursor limiting dilution method to the sorted populations to determine whether cell size affects differentiation. PCBM1641 cells at P7 were sorted into high FSC ("large" cells) and low FSC ("small" cells) populations. The average cell diameter post-sort was 14.6 and 19.3μm respectively. The number of cells that were capable of differentiating into an adipocyte in the small population was 1 in 126 cells, while in the large cell population it was 1 in 296 cells, which was statistically significant ($p<0.05$, Figure 4-6)

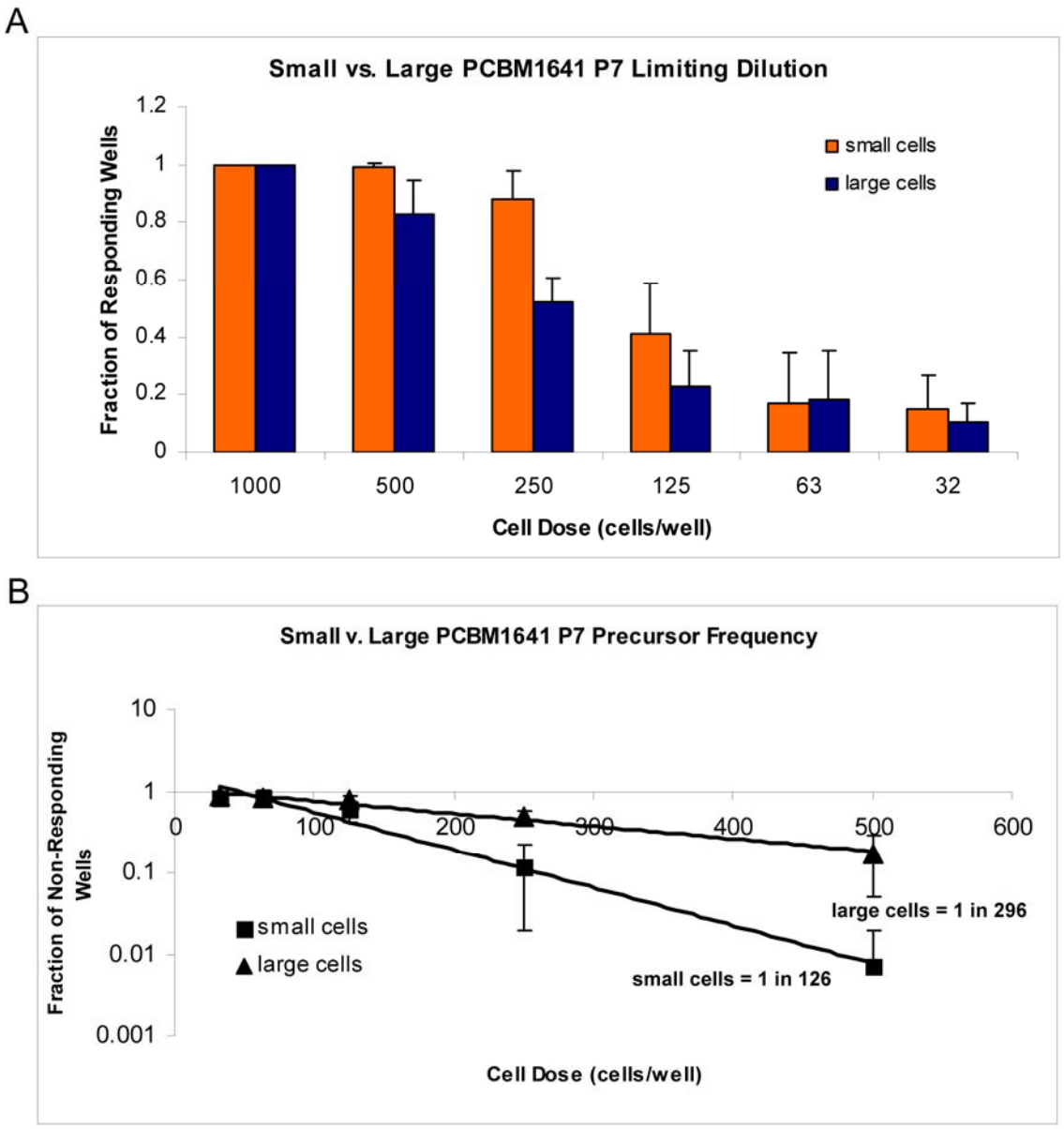

Figure 4-6. MSCs of different sizes have different adipogenic precursor frequencies. Cell size thresholds were based on separate FSC sorting gates that were applied to the upper (large cells) and lower (small cells) thirds of an FSC histogram plot. (A) The fraction of responding wells was plotted as a function of cell dose in sorted small and large cells from PCBM1641 following limiting dilution analysis. (B) A plot of non-responding wells as a function of cell dose. The trend line was used to calculate precursor frequency in populations of small and large cells. Error bars represent standard deviation; n=3 for both cell populations. R^2 values were 0.99 for both small and large cells.

4.3.3 Cell size separation by filtering

4.3.3.1 Cell Diameter

Cell diameters were recorded following cell size separation to confirm the average diameter within each cell size range, including >20μm, 15-20μm, 10-15μm, and <10μm. Due to cell deformation when passing through filters and/or cell-cell adhesions, the actual final cell size diameter was 23.9μm in the large cell population and 14.9μm in the small cell population (Figure 4-7). The frequency of cells within each size range were measured in 1μm bins as a function of cell diameter. A representative example of the cell size separation results can be seen Figure 4-7.

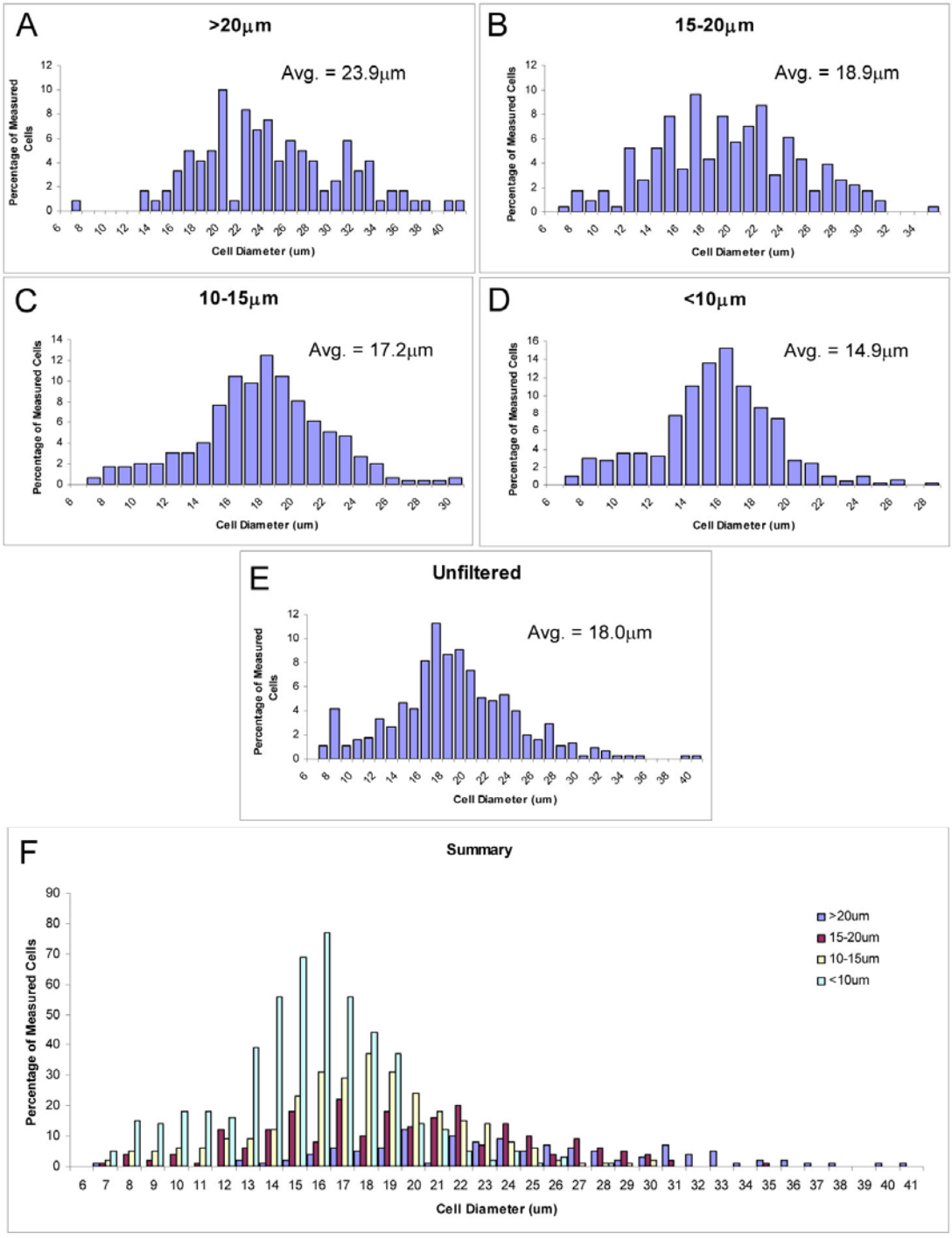

Figure 4-7. Cell size distribution summary. MSCs from PCBM1632 P5 were separated sequentially by cell size into >20µm (A), 15-20µm (B), 10-15µm (C), and <10µm (D) size ranges from the unfiltered (E) population. Cell diameters were measured using a cellometer. *Note: x-axis size ranges vary in panels A-E.

4.3.3.2 The small cell population demonstrates increased CFU capacity

CFU analysis is a simple method to quantify stem like progenitors in various populations of MSCs, as discussed in previous chapters. Enrichment for separate small and large cell populations demonstrates decreased CFU capacity in the large cell population (Figure 4-8). Average CFU in the small cell population was 14%, and decreased to 6.7% in the large cell population, which was significant ($p<0.05$).

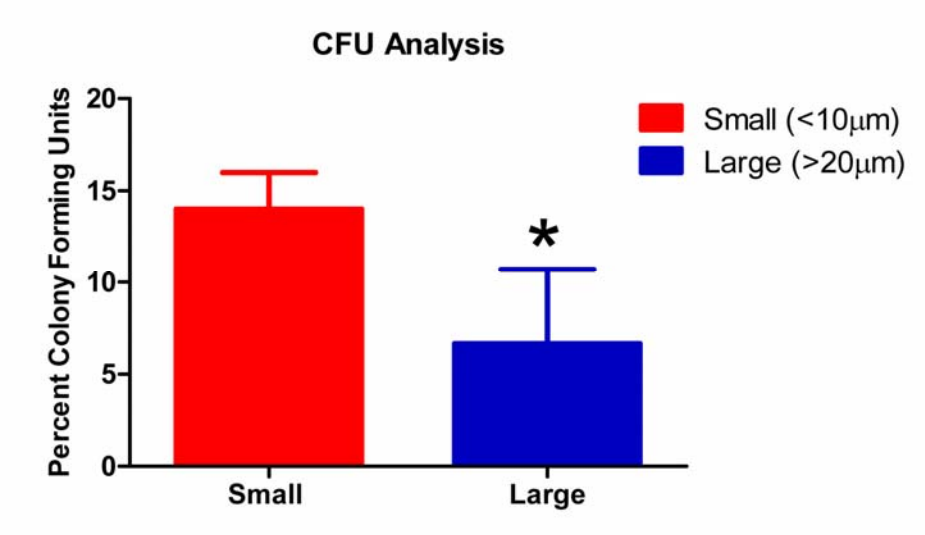

Figure 4-8. Colony forming unit capacity decreases in the large cell population. MSCs from PCBM1632 P5 were separated based on cell size, and plated for CFU analysis. Red = small cells (<10μm) and Blue = large cells (>20 μm). Data plotted as mean ± standard deviation, n=3, *p<0.05.

4.3.3.3 The small cell population demonstrates increased proliferative potential

MSCs from size-separated small and large cell populations were assessed for proliferative capacity using a live cell imager capable of measuring percent confluence over time. The small cell population shows an improved proliferation rate compared to the large cell population (Figure 4-9).

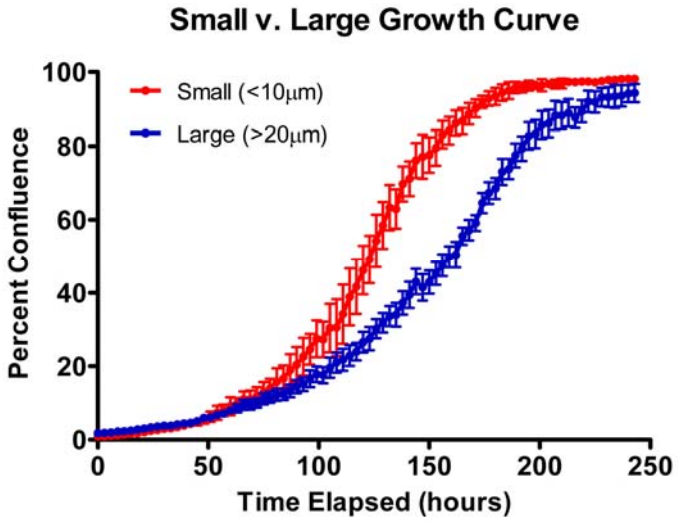

Figure 4-9. Large cell population shows decreased proliferative potential. MSCs from PCBM1632 P5 were separated based on cell size, and plated for proliferation analysis. Red = small cells (<10μm) and Blue = large cells (>20 μm). Data plotted as mean ± standard deviation, n=6.

4.3.3.4 The small cell population contains more adipogenic precursors

Following cell size separation, adipogenic differentiation capacity was assessed by automated microscopy to determine changes in the frequency of adipogenic precursors in the small and large cell population. The small cell population contained twice as many Nile Red positive cells following differentiation than the large cell population ($p<0.05$) as seen in Figure 4-10 below.

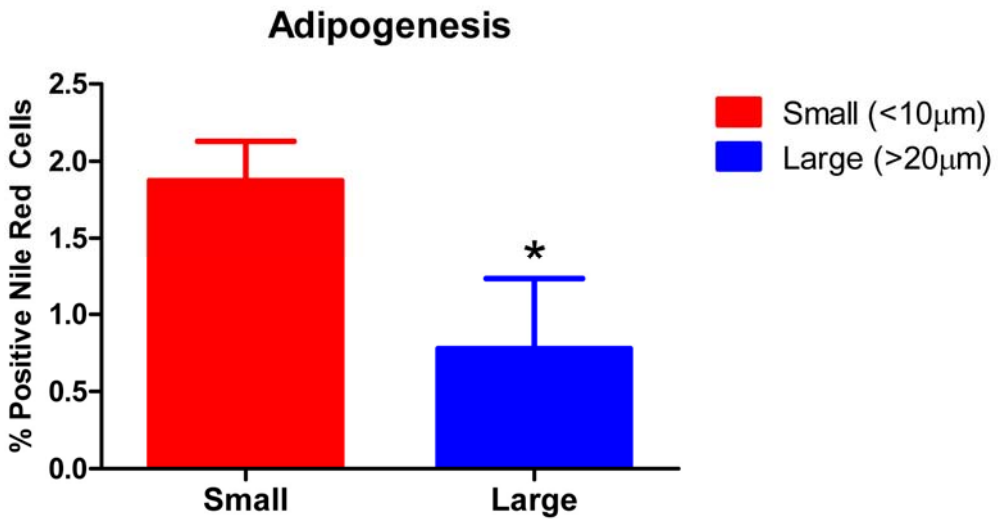

Figure 4-10. Adipogenic capacity decreases in the large cell population. MSCs from PCBM1632 P5 were separated based on cell size, and plated for adipogenesis and Nile Red quantification via automated microscopy. Red = small cells (<10μm) and Blue = large cells (>20 μm). Data plotted as mean ± standard deviation, n=3 for small cells, n=2 for large cells, *p<0.05.

4.3.3.5 The small cell population contains more osteogenic precursors

Osteogenic differentiation in size-separated populations was assessed following ALP staining and quantification via automated microscopy and surface area quantification. Figure 4-11 below demonstrates a qualitative difference in ALP expression, showing the small cell population (Figure 4-11B) has a greater degree of positive ALP staining than the large cell population (Figure 4-11A).

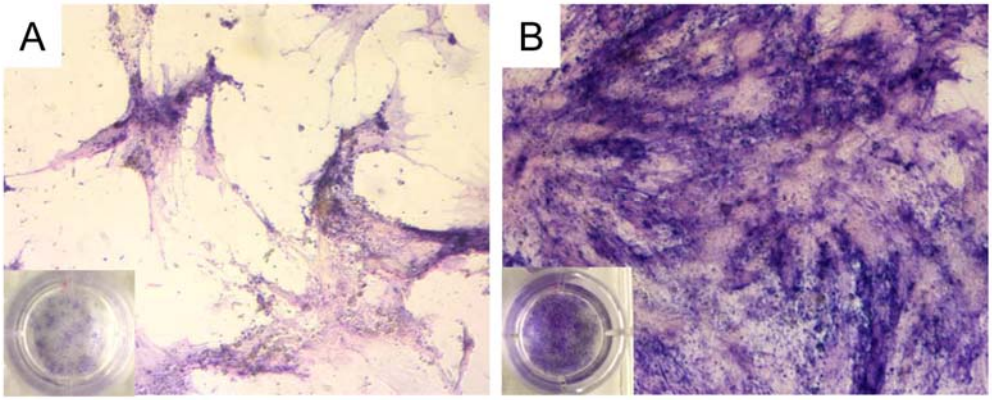

Figure 4-11. Overall osteogenic capacity decreases in the large cell population. MSCs from PCBM1632 P5 were separated based on cell size, and plated for osteogenesis and imaged for ALP expression. (A) large cells (>20 μm) and (B) small cells (<10μm).

Interestingly, following a quantitative assessment of osteogenic differentiation by automated microscopy, a cell-by-cell analysis of the osteogenic potential of the small and large cell populations show no statistical difference. Although there is an overall increase in osteogenesis based on a qualitative assessment of ALP staining as shown in Figure 4-12, normalization to nuclei counts to obtain a measurement on a per cell basis suggests there are no cell-to-cell differences based on cell size and osteogenic potential.

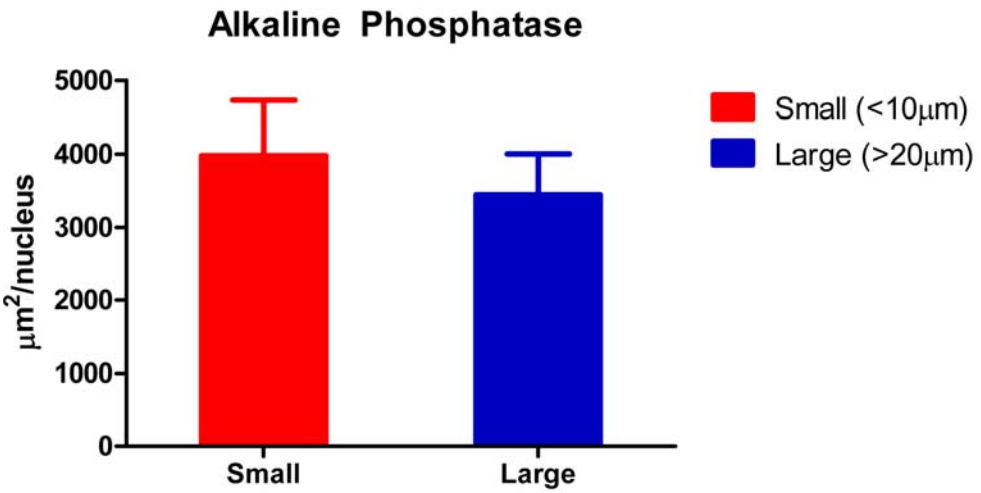

Figure 4-12. Measurement of osteogenic differentiation capacity on a per cell basis suggests there are no differences in the small and large cell size population in the ability to form bone *in vitro*. MSCs from PCBM1632 P5 were separated based on cell size, and plated for osteogenesis and imaged for ALP expression. Alkaline Phosphatase staining was quantified by thresholding (A) large cells (>20 µm) and (B) small cells (<10µm).

4.3.3.6 The large cell population contains more senescent cells

Size-separated MSCs from cell line PCBM1632 at P5 were plated and stained for β-galactosidase after cells were allowed to adhere for 24 hours. Staining as shown in blue indicates senescent MSCs reside in the large cell population as seen in Figure 4-13.

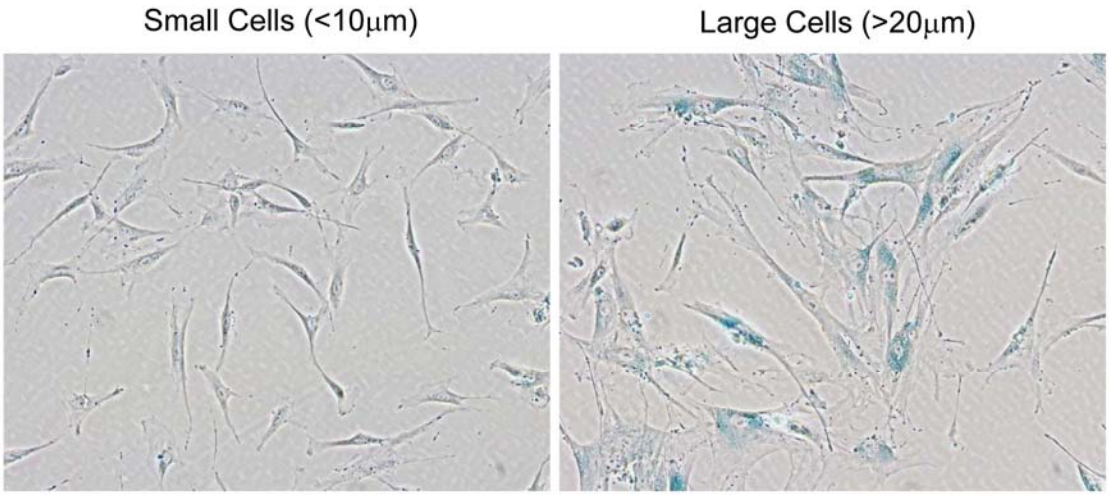

Figure 4-13. β-Galactosidase staining in sorted small and large populations. MSCs from PCBM1632 P5 were separated by cell size into small (left) and large (right) subpopulations and stained with β-galactosidase, an indicator of senescence. Images were taken at 10X, and positive β-galactosidase is seen in blue.

4.4 DISCUSSION

Due to the inherent heterogeneity of MSCs, there is a need in the field to purify and enrich MSC populations for early progenitors that are capable of improving a desired outcome. Much work is being done to identify novel biomarkers that may correlate with *in vitro* and *in vivo* potency assays that could be used to enhance stemness in MSC populations (36,39,84,125). Here, based on our observations that increased cell size with passaging correlates with decreased biological functions, we took advantage of this cell size heterogeneity to purify small and large cell subpopulations to further understand the role of cell size in MSC function and stemness. Enrichment of different cell size populations will also eventually allow us to identify markers and understand the role of various cells signaling pathways that are associated with the small and large cell phenotype.

Our first attempts to isolate small and large cell populations were based on observations of an increase in forward (FSC) and side scatter (SSC) with passage as seen by flow cytometry. By gating on low FSC/SSC MSCs to enrich for small cells, and conversely high FSC/SSC to enrich for large cells, we were able to successfully isolate enrich small and large subpopulations by FACS (74). While this was effective to show a significant increase in adipogenic potential by limiting dilution, there was likely small cell contaminants in the large cell population that may have contributed to the measured potential of the large cell population. Further, cell sorting requires cells to be out of culture for hours during a sort, which is not ideal. We therefore moved toward creating a simple filtering device to separate cells based on cell size. While standard cell filters exist, their pore sizes are too large to filter within particular cell size ranges. We therefore created a simple filter apparatus designed to fit in standard 50ml conical tubes, and capable of tightly fitting a mesh size of our choosing to separate specific cell diameters with precision. While straightforward, few investigators have enriched for MSCs based on a cell size metric to study specific cell size populations.

As seen in Figure 4-7, we demonstrated that our filtering ring apparatus successfully separates cells based on cell size. While our cell size measurements may or many not represent the filter size range indicated, cells are fluid and cells larger than the designated filter size may partially deform and passively pass through the filter. Nonetheless, we show a 9μm difference in cell size between the small and large cell populations, which was significant enough to show functional differences based on our quantitative measurements.

Our data confirms that early progenitors primarily reside in the small cell population. As seen Figure 4-9, the small cell population has greater proliferative potential than the large cell population, which correlates with increased CFU capacity ($p<0.05$, Figure 4-8) and decreased

senescence as shown by β-galactosidase staining in Figure 4-13. Further, small cells show enhanced ability to undergo adipogenic differentiation, which was statistically significant between the two cell size populations, both by limiting dilution and by Nile Red quantification ($p<0.05$, Figures 4-6 and 4-10). Based on a qualitative, population-based assessment of osteogenic differentiation by ALP staining, it appears as though the small cell population has improved capacity overall to undergo osteogenesis (Figure 4-11). However, based on our quantitative measurements of osteogenesis on a per cell basis, it appears as though there are no differences in osteogenic potential based on cell size (Figure 4-12). Based on the correlation of the binary area fraction to nuclei counts as shown in Figure 3-9 in Chapter 3, this suggests osteogenic potential may be closely tied to proliferative capacity. Because the small cell population can readily proliferate and there are therefore inherently more cells at the end of a 14-day differentiation experiment, this may explain why there is an overall increase in ALP staining in the small population, but no differences on a per-cell basis. Due to MSC heterogeneity, it is important to quantify differentiation on a cell-by-cell basis. However, it appears as though unlike adipogenic differentiation, following osteogenic differentiation there is a more homogeneous response that is not cell-size dependent. Therefore, differences may more so depend on cell source from different donors, as well as the overall proliferative potential of a particular cell line.

When considering MSC heterogeneity, it is interesting to consider the idea that these distinct cell size populations may need to co-exist. While enhanced proliferative potential was demonstrated in the small cell population as shown in Figure 4-9, one particular observation of interest is that the small cells become large cells rapidly in culture following cell size separation, suggesting a role of the large cell population in maintaining the small, stem-like population.

While it is shown here that the large cells are inactive by their decreased proliferative potential and CFU capacity, they perhaps have a contact-dependent and/or secretory role in maintaining stemness in the small cell population. Future experiments elucidating the secretome of cell size-separated MSCs may point to a paracrine role of the large cell population in maintaining the stem-like phenotype in the small cell population.

To better understand the mechanism behind decreased function with passage beyond changes in cell size, the role of Wnt signaling and its potential role in proliferation and differentiation in MSCs was evaluated. An sFRP-1 inhibitor was utilized to block Wnt signaling *in vitro* and measured changes in proliferative capacity and gene expression of adipo- and osteogenic-specific markers by qRT-PCR in cell line 110877 at P3 and P7. It has been previously documented in the literature that blocking Wnt signaling may improve adipogenesis and proliferation in MSCs. Here, the addition of a Wnt signaling inhibitor demonstrated slight improvements in proliferative potential at P3, but has no effect at P7 (Figure 4-3). Our gene expression data confirms previous findings based on the role of Wnt signaling as it relates to adipogenesis. Following adipogenic differentiation for 7 days with or without the presence of sFRP-1 inhibitor, changes in gene expression of PPARγ, C/EBPα and FABP4 were measured, and show a significant increase at P3, but no differences were detected at P7 (Figure 4-4). Interestingly, blocking Wnt signaling during osteogenic differentiation appeared to have no significant effect on regulation of osteogenic-specific markers by qRT-PCR (Figure 4-5). The literature does not suggest a clear role of Wnt signaling in osteogenic differentiation, and there are likely more relevant signaling pathways that play a role in osteogenic differentiation capacity (126,127). Future work will apply quantitative assays described in Chapters 2 and 3 to assess the

role of additional signaling pathways in size-separated MSCs to better understand the small cell phenotype.

4.5 CONCLUSION

In this chapter, we demonstrated that the small cell population contains early progenitors capable of enhanced proliferation and differentiation capacity. Small cell enrichment in MSCs may therefore be a useful tool to improve MSC function *in vitro* and *in vivo* for cellular therapies. However, more work needs to be done to understand the molecular signature of the small cell population as it relates to its enhanced stemness demonstrated here. While our data suggests Wnt signaling may play a role in regulating adipogenic differentiation and proliferative capacity in MSCs, many other signaling pathways have been demonstrated in the literature to regulate stemness and differentiation in MSCs.

5.0 QUANTIFICATION OF IMMUNOSUPPRESSIVE ACTIVITY IN MSCS

5.1 INTRODUCTION

While MSCs are known to possess a wide variety of cell surface markers and differentiate down several lineages, they possess a unique ability to home to a site of injury and suppress the local immune and inflammatory responses *in vivo* (128-132). This unique potential has been utilized by several investigators, as MSCs are currently being used in investigational clinical trials to treat Graft vs Host Disease (GvHD), a common complication associated with bone marrow transplants (128,132-134). MSCs may be particularly non-immunogenic due to the lack of MHC Class II (135,136), and their ability to release factors that suppress the host immune system (137). This makes MSCs particularly attractive for their use in an allogeneic environment. MSCs may also suppress several T cell, B cell and Natural Killer (NK) functions (138).

Aggarwal and Pittenger have previously investigated the role of human MSCs in modulating immunosuppression when co-cultured with purified sub-populations of immune cells. Naïve human T cells were activated to undergo T_H1 effector cell differentiation with or without the presence of human MSCs. The presence of MSCs during T cell differentiation significantly decreased the expression of IFN-γ, a pro-inflammatory cytokine. Similarly, this was repeated during T_H2 effector cell differentiation, where co-culture with MSCs plus T cells

led to a significant increase in IL-4 production, therefore promoting a shift toward the anti-inflammatory T_H2 cells (138).

A study by Le Blanc *et al.* investigated the alloreactivity of MSCs *in vitro* using a mixed lymphocyte culture with either allogeneic or autologous MSCs. Proliferative activity was suppressed in all cultures after the addition of higher concentrations of MSCs, regardless of the source (autologous or allogeneic), indicating the T cell responses are inhibited by MSCs regardless of the major histocompatibility complex. Further, there appeared to be a dose-dependent response in T cell reactivity as smaller doses of MSCs led to less suppression in mixed lymphocyte cultures.

It has been previously established that MSCs cultured with exogenous IFN-γ improve their immunosuppressive capacity *in vitro* (139). IFN-γ stimulation leads to upregulation of indoleamine 2,3-dioxygenase (IDO), which inhibits T cell proliferation. It has been suggested that the response to IFN-γ is variable among donors, and that MSCs sourced from low IDO inducers may be less potent immunosuppressors. There is currently no marker that predicts this responsiveness to IFN-γ stimulation, and there is therefore a need to better-predict IFN-γ responsiveness in MSCs derived from different human donors (140).

MSCs expanded *in vitro* have been shown to undergo teleomere shortening and subsequently cellular senescence (141), which may ultimately affect their immunosuppressive capacity. Extensive *in vitro* expansion of MSCs may modify their regenerative capacity and immunosuppressive function, and may limit their potency and survival *in vivo* (142). Data from late passage MSCs suggests they are less effective in survival of GvHD patients than MSCs used at earlier passages (143).

Many investigators have evaluated the immunosuppressive activity by MSCs through the use of mixed lymphocyte (MLR) assays with lymphocytes from the same species. However, the use of an *in vitro* xenogeneic system using clonal T cells specific for known peptide antigens will reduce the sources of variability that are unavoidable in traditional polyclonal MLR assays. Sources of variability arise due to heterogeneity of non-clonal allogeneic T cells and the use of pooled donors. There is currently a need for quantitative bioassays to measure differences in immunosuppressive activity by MSCs from different donors, or to measure the effect of *in vitro* expansion of MSCs on their ability to immunosuppress. In this chapter, we will evaluate the role of donor variability and passaging on immunosuppressive capacity in MSCs.

5.2 MATERIALS AND METHODS

5.2.1 Cell culture

Human MSCs were expanded as described in Section 2.2.1. Cells from all donors were thawed from P3 and P7 vials (where applicable) into T175 flasks, cultured until 80% confluence in expansion medium, and trypsinized for use in immunosuppression assays.

5.2.2 Mice

Non-obese diabetic 8.3 TCR transgenic mice (NOD 8.3) and NOD/ShiLtj mice were purchased from Jackson Laboratories (Bar Harbor, Maine). Mouse colonies were maintained in a

pathogen-free environment as per CBER's Institutional Animal Care and Use Committee (IACUC). $CD8^+$ T cells from NOD 8.3 mice specifically recognize the K^d-restricted $IGRP^{206-214}$ epitope derived from the islet antigen IGRP (islet-specific glucose-6-phosphatase catalytic subunit-related protein) (144). NOD/ShiLtj mice were used as a syngeneic source of antigen presenting cells (APCs).

5.2.3 Immunosuppression assay

Spleens and lymph nodes were isolated from NOD8.3 and NOD/ShiLtj mice, and tissues were disassociated with a syringe plunger over a 40μm filter (BD Biosciences). Cells from spleens were incubated in ACK red lysis buffer (Invitrogen). Total spleenocytes from NOD/ShiLtj mice were irradiated at 4000 rads, counted using a Cellometer (Nexcelom), and plated at 4×10^6 cells per well in 24-well plates (Corning) in RPMI (Invitrogen) containing 10% FBS and 1% Penicillin/Streptomycin (Invitrogen). IGRP peptide was added at 1μg/ml per well. Peptides were synthesized by the FDA Facility for Biotechnology Resources core facility. Cells from NOD8.3 mice were purified over MACS columns for $CD8a^+$ cells via negative selection (Miltenyi Biotec), counted, and plated at 2×10^6 cells/well. Last, MSCs from all donors at P3 and P7 were trypsinized and added to the wells at varying T cell:MSC ratios of 1:20 and 1:5. Co-cultures were kept at 37°C for 3-days. Samples from each condition were removed for RNA isolation and ddPCR analyses at 48 hours. An overview of the immunosuppression assay setup can be seen below in Figure 5-1.

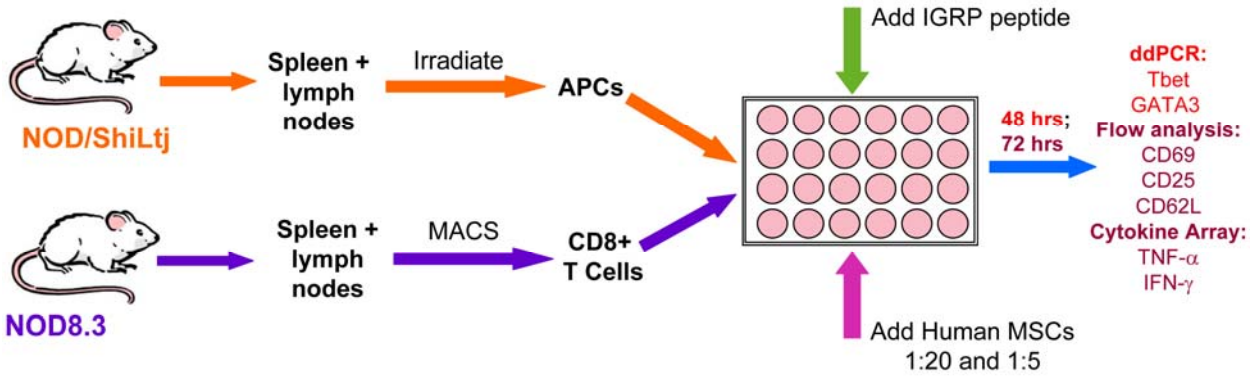

Figure 5-1. Schematic of immunosuppression assay. Human MSCs were co-cultured with mouse T cells to evaluate immunosuppressive response by ddPCR, flow cytometry and cytokine array analyses. After either 48 or 72 hours, murine T cells were processed for endpoints listed to the right.

5.2.4 Flow cytometry

After 3-days in culture, murine T cells were removed from wells and labeled with antibodies including anti-CD8a, Vβ8.1/8.2, anti-CD25, anti-CD69 and anti-CD62L with various fluorochrome conjugates (BD Biosciences). Cells were analyzed using the FACSCanto flow cytometer (BD Biosciences). For surface marker analysis in Flow Jo (Tree Star), gating analysis included cells that were double positive for CD8a and Vβ8.1/8.2.

5.2.5 Digital Droplet PCR (ddPCR)

At 48 hours, murine T cells from all conditions were removed from cell culture, pelleted, and snap frozen in liquid nitrogen for later use. For RNA preparation, pellets were thawed at 37°C, lysed with RLT buffer, and passed through a QIAshredder column. Samples were then processed for RNA cleanup per the manufacturer's instructions. Total RNA was quantified using a NanoDrop (Thermo Scientific) and purity was determined using a Bioanalyzer (Agilent).

cDNA was synthesized utilizing the Quantiscript Reverse Transcription Kit according to the manufacturers instructions (Qiagen) at 42°C for 15 minutes, followed by inactivation at 95°C for 3 minutes. Reaction mixtures were made with ddPCR 2X PCR Master Mix (BioRad) per the manufacturer's instructions, and 15ng of cDNA-equivalents was added to each reaction. Target gene sequences included Tbet and GATA3, transcription factors involved in T cell differentiation (Table 5-1). A step unique to the ddPCR system is the generation of droplets following the preparation of reaction mixtures. 20µl of sample was loaded into center cartridge wells, each cartridge containing enough for 8 samples at one time. 70µl of droplet generator oil was added to corresponding wells. Cartridges were secured with a gasket, and placed in the droplet generator. Once droplet generation was complete, 40µl of droplet/reaction mixture was added to 96-well PCR plates (Eppendorf). This process was repeated for all samples, and plates were foil-sealed in a thermal plate sealer (Eppendorf). Targets were amplified using a Touchgene Gradient thermal cycler under the following conditions: 95°C for 10 minutes; 40 cycles of 94°C for 30 seconds and 60°C for 1 minute per cycle; 95°C for 10 minutes.

Following amplification, plates were placed in a BioRad QX100 digital droplet reader for analysis using Quantasoft software (Biorad). Data was analyzed to determine total copy number based on absolute quantification. An example of the ddPCR workflow is seen below in Figure 5-2.

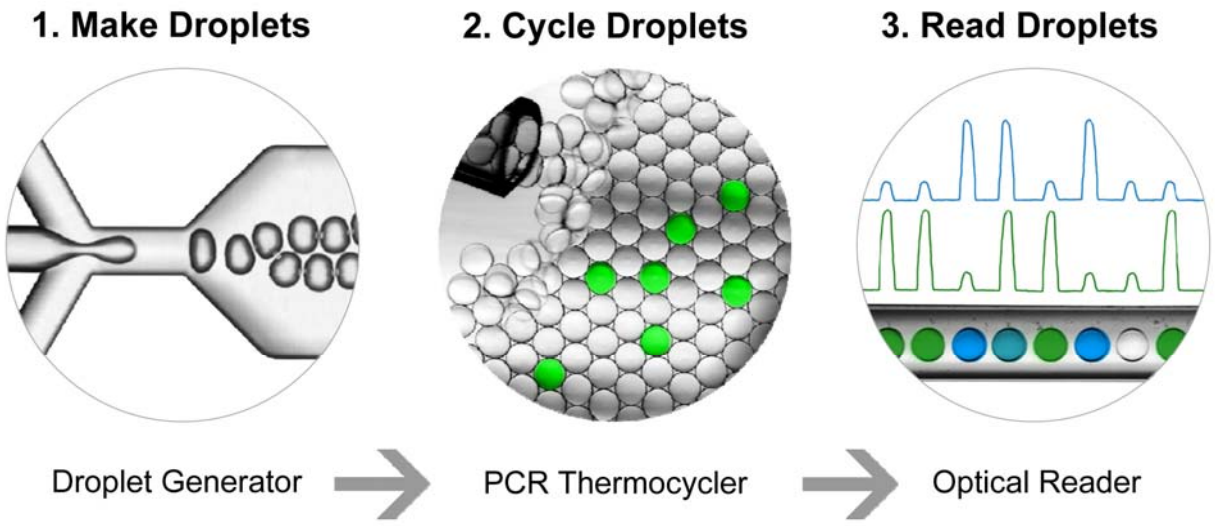

Figure 5-2. Schematic of ddPCR workflow. Reaction mixture is created as during a normal PCR reaction setup. Prior to amplification, reaction mixture is mixed with oil and placed in a droplet generator to create thousands of droplets containing reaction mixture. Droplet solution is then amplified as during normal PCR. Droplets are then read in a droplet reader to report an exact copy number based on absolute quantification.

Table 5-1. List of ABI primer/probe sets used in ddPCR.

Gene Symbol	Gene Name	Assay ID
GATA3	GATA binding protein 3	Mm00484683_m1
Tbx21	Tbet, T-box21	Mm00450960_m1
Actb	actin, beta	Mm00607939_s1
B2m	beta-2 microglobulin	Mm00437762_m1
Gusb	glucuronidase, beta	Mm01197698_m1
Hsp90ab1	heat shock protein 90 alpha	Mm00833431_g1
GAPDH	glyceraldehyde-3-phosphate dehydrogenase	Mm99999915_g1

5.2.6 Cytokine array

Following the completion of each 3-day experiment, 500µl of cell culture supernatant was collected from each experimental condition and stored at -80°C for future use. Mouse TH1/TH2 9-plex cytokine array multiplex assays were purchased from Meso Scale Discovery (MSD, Rockville, MD). Supernatants, reagents and the array plate were brought to room temperature, and the plate was blocked with 25 µl of Diluent 4 per well. The plate was sealed and incubated at room temperature for 30 minutes with vigorous shaking at 300-1000 RPM. Samples and calibrators were then added to separate wells in duplicate at 25µl/well, then sealed and incubated at room temperature for 2 hours and 300-1000 RPM shaking. The plate was washed with 25µl 0.05% Tween/PBS three times. 25µl of 1X Detection Antibody Solution was added per well, and plates were sealed and shaken for 2 hours as described above. The plate was then washed with 150µl 0.05% Tween/PBS three times, and 25µl 2X Read Buffer T was added immediately prior to reading the plate on the SECTOR imager.

5.3 RESULTS

5.3.1 Human MSCs vary in their ability to modulate expression of Tbet and GATA3 in murine T cells

To understand the immunosuppressive effect of MSCs on mouse T cells on the molecular level, transcription factors involved in T cell activation were assessed. Following 48 hours of co-culture with MSCs, murine T cells were analyzed by PCR for expression of activation markers T

bet and GATA3. First, to determine an appropriate house-keeping gene for analysis, we used qRT-PCR to assess mouse T cells under in all experimental conditions (unactivated, activated, and co-cultured with MSCs) for expression of various house-keeping genes, including B2m, GUSB, HSP90ab1, 18S, and beta-actin. Raw Ct values were plotted to assess variability between conditions, as seen in Figure 5-3. Most house-keeping genes show a high degree of variability between conditions, and therefore are not suitable as an appropriate house-keeping gene for analysis. While 18S appears to show similar values, there is a 3 Ct value difference between the lowest and highest expressers, and therefore again not ideal for analysis (Figure 5-3).

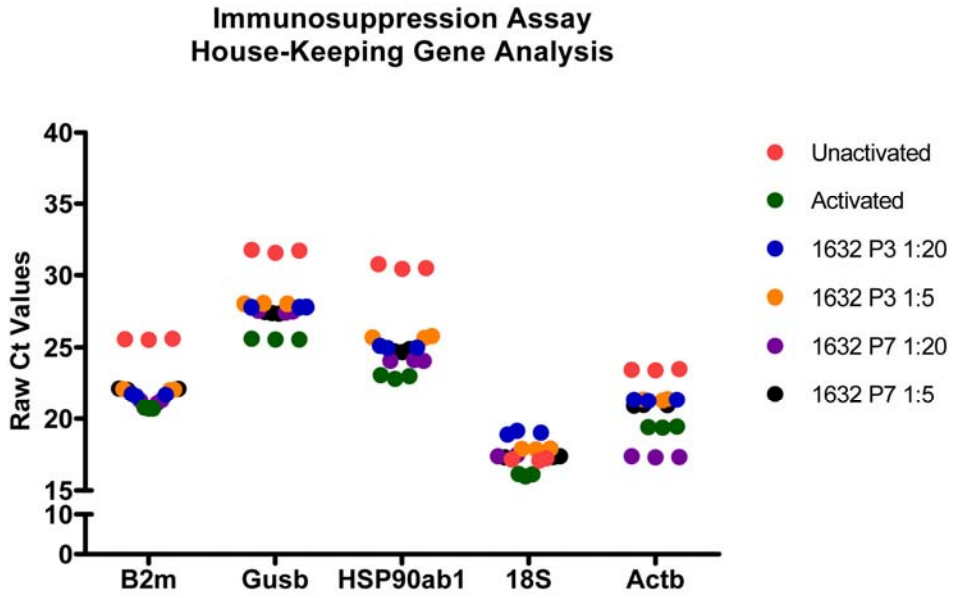

Figure 5-3. House-keeping genes vary in suitability for PCR in immunosuppression assay. Several house-keeping genes were analyzed by qRT-PCR in unactivated, activated, and co-culture samples. Raw Ct values are represented in triplicate and plotted as a function of house-keeping gene.

Due to these results outlined above in Figure 5-3, we utilized novel PCR technology to measure changes in gene expression via absolute quantification to report an exact copy number of the target of interest by ddPCR. Tbet and GATA3 expression in murine T cells was assessed

by ddPCR following 48 hours in unactivated, activated, and co-culture samples. Inhibition of T cell activation is variable between donors and passages, and is dose-dependent. Cell line PCBM1632 demonstrates the largest inhibition of Tbet expression, showing a 3.3-fold decrease when co-cultured with P3 MSCs at 1:5, and a 2.3-fold decrease in copy number in P7 MSCs at the same dilution, suggesting P3 MSCs may be better immunosuppressors (Figure 5-4A). Similar trends in GATA3 expression with T cells cultured with PCBM1632 are shown in Figure 5-5A. Other cell lines do not show the same degree of inactivation; data from cell line 110877 suggests poor immunosuppression, as co-culture with murine T cells shows increased activation and expression of Tbet upon co-culture with MSCs in both dilutions and at both passages (Figure 5-4B).

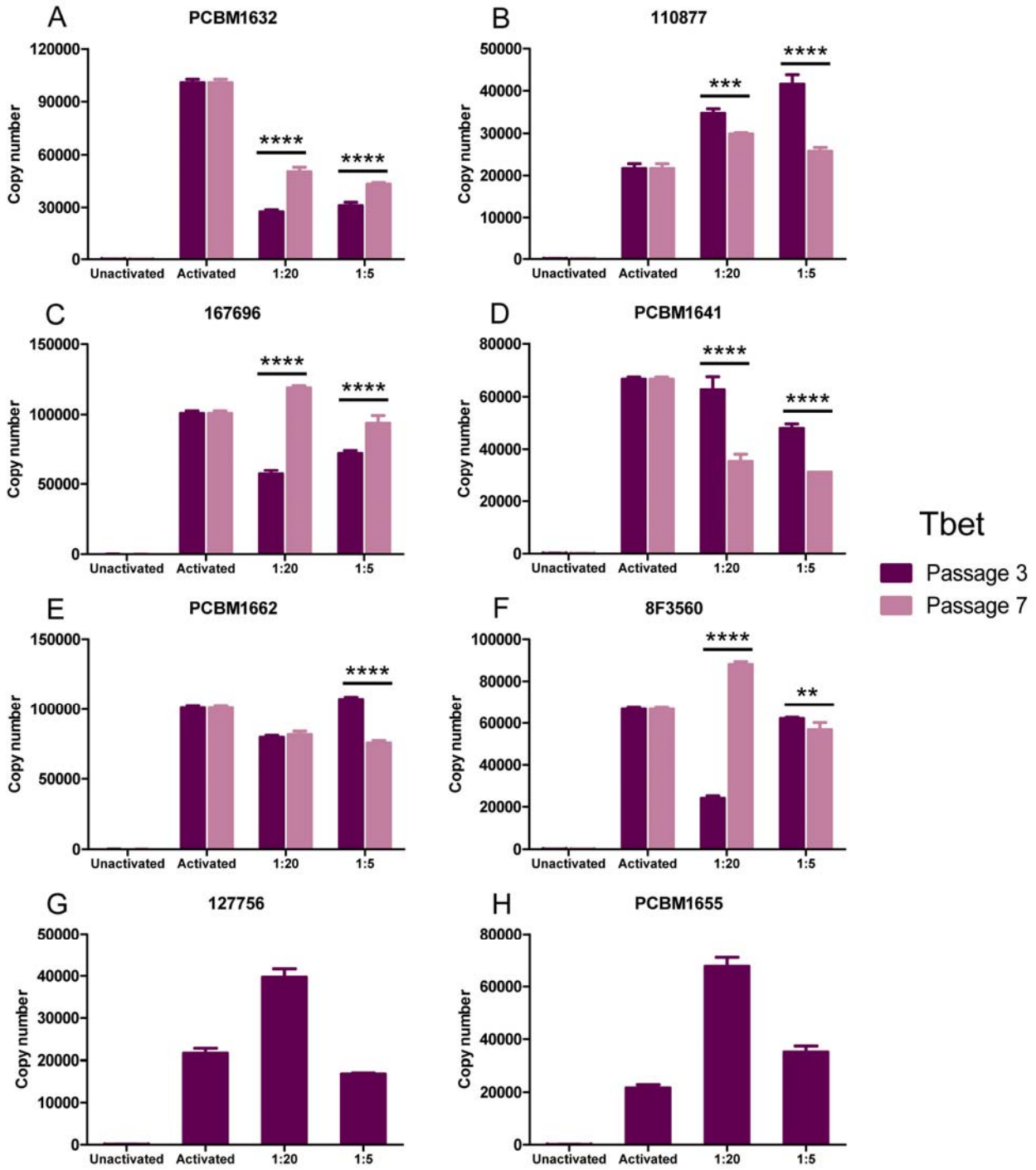

Figure 5-4. Tbet expression in mouse T cells vary and is cell line- and passage-dependent. Changes in Tbet expression in murine T cells following co-culture with human MSCs were measured using the ddPCR method. Data is expressed as mean ± standard deviation (n=1-3), *p<0.05, **p<0.01, ***p<0.001, ****p<0.0001. Ratios indicate the number of MSCs:murine T cells. (A) PCBM1632 (B) 110877 (C) 167696 (D) PCBM1641 (E) PCBM1662 (F) 8F3560 (G) 127756 (H) PCBM1655.

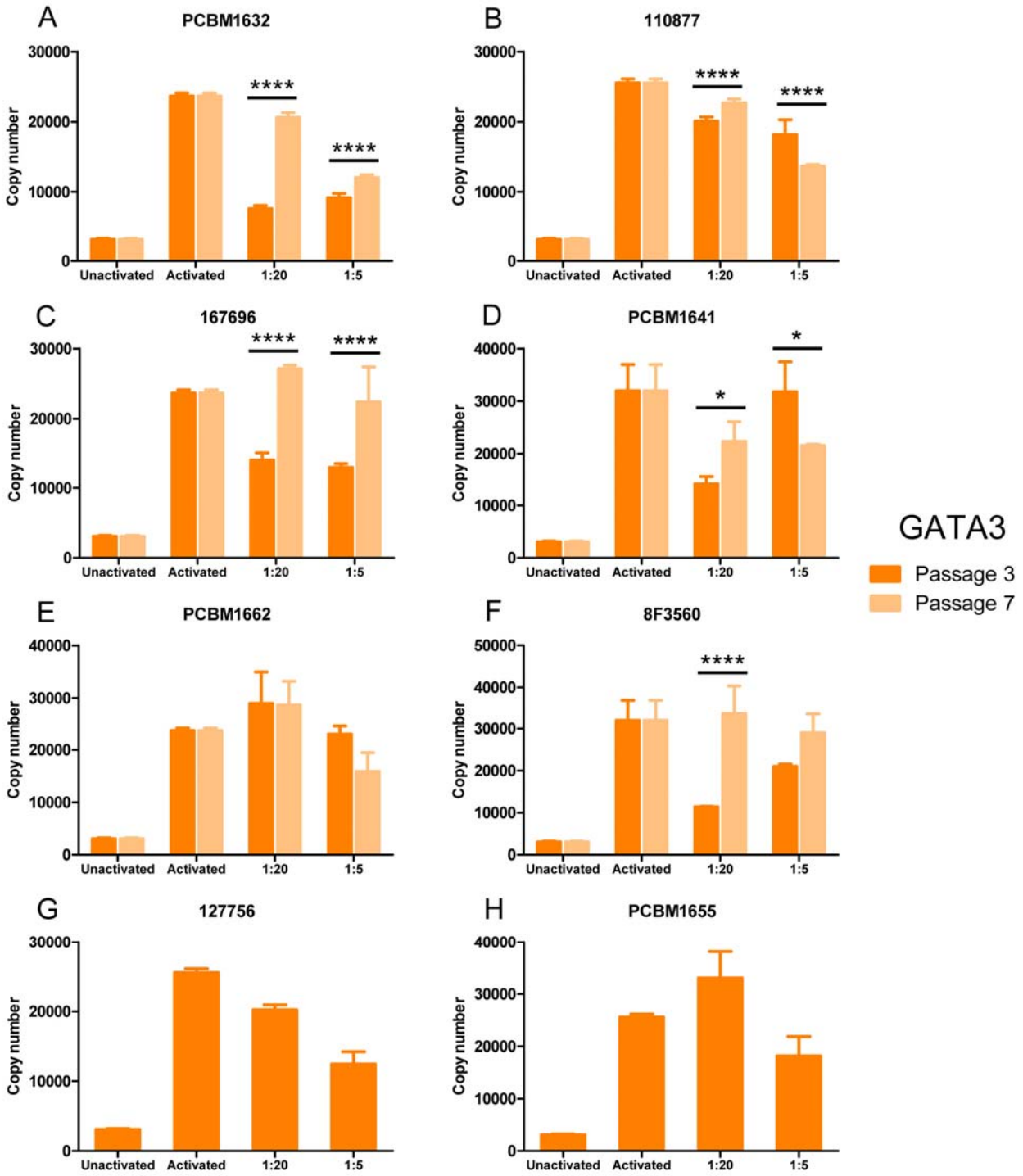

Figure 5-5. GATA3 expression in mouse T cells vary and is cell line- and passage-dependent. Changes in GATA3 expression in murine T cells following co-culture with human MSCs were measured using the ddPCR method. Data is expressed as mean ± standard deviation (n=1-3), *p<0.05, **p<0.01, ***p<0.001, ****p<0.0001. Ratios indicate the number of MSCs:murine T cells. (A) PCBM1632 (B) 110877 (C) 167696 (D) PCBM1641 (E) PCBM1662 (F) 8F3560 (G) 127756 (H) PCBM1655.

5.3.2 MSCs inhibit murine T cell proliferation

Following 72 hours in co-culture, unactivated and activated T cells, and T cells + MSCs were examined for any changes in morphology. Activated samples (Figure 5-6B) show distinct formation of clusters that are unique to the activated phenotype. The clustering also correlates with a high degree of proliferation. Upon addition of MSCs (Figures 5-6C and 5-6D), there is little detection of cluster formation, indicating MSCs are inhibiting this response.

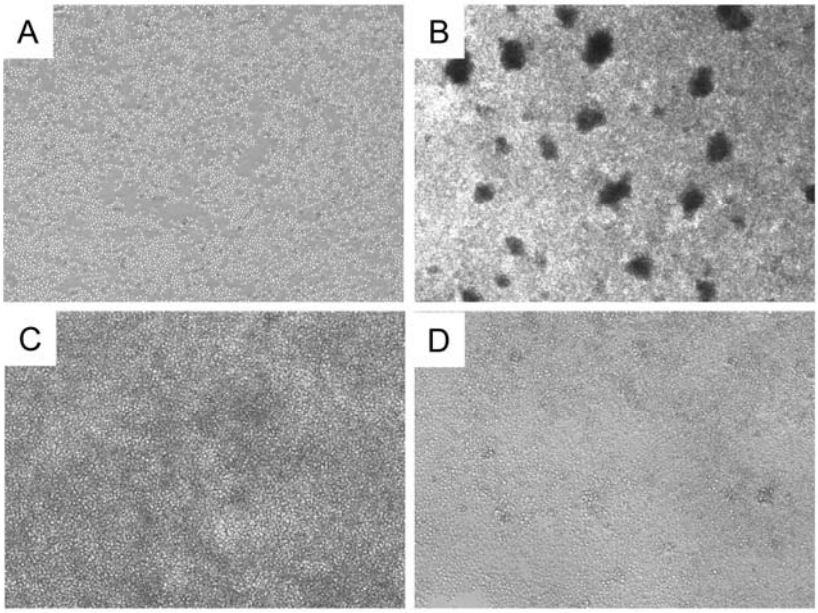

Figure 5-6. MSCs modulate T cell morphology and inhibit proliferation. MSCs were co-cultured with murine T cells and imaged using brightfield microscopy after 72 hours. (A) unstimulated T cells (B) Activated T cells – T cells + peptide (C) T cells + peptide + MSCs 1:10 (D) T cells + peptide + MSCs 1 :5. Image from panel B was taken at 4X ; images from panels A, C, and D taken at 10X.

5.3.3 Human MSCs downregulate expression of activation markers CD25, CD62L and CD69 upon co-culture with murine T cells

Following 72 hours in culture, T cells were assessed for expression of activation markers CD25, CD62L and CD69 by flow cytometry. The mean fluorescence intensity (MFI) values were plotted for ease of comparison between experimental groups. All experimental groups were normalized to unactivated samples by subtracting the unactivated MFI value, and therefore appears as zero. MSCs from most cell lines downregulate expression of CD25, CD62L and CD69 at P3 and P7 in a dose-dependent manner (Figures 5-7, 5-8 and 5-9). This decreased expression may be passage-dependent, as most donors show a slightly improved inhibition in P7 samples compared to P3. Further, this downregulation of activation markers may be donor-dependent. Cell line 110877 shows consistently higher MFIs upon co-culture at both 1:20 and 1:5 dilutions, indicating decreased immunosuppressive activity in all activation markers (Figures 5-7B, 5-8B, and 5-9B). At P7 1:20, cell line 110877 demonstrates a 4.6, 1.2 and 2.3-fold decrease in expression of CD25, CD62L and CD69 respectively. Conversely, cell line PCBM1632 induces the largest decrease in MFI across all activation markers, showing an approximately 10, 37, and 5-fold decrease at P7 1:5 in CD25, CD62L, and CD69 respectively (Figures 5-7A, 5-8A, and 5-9A).

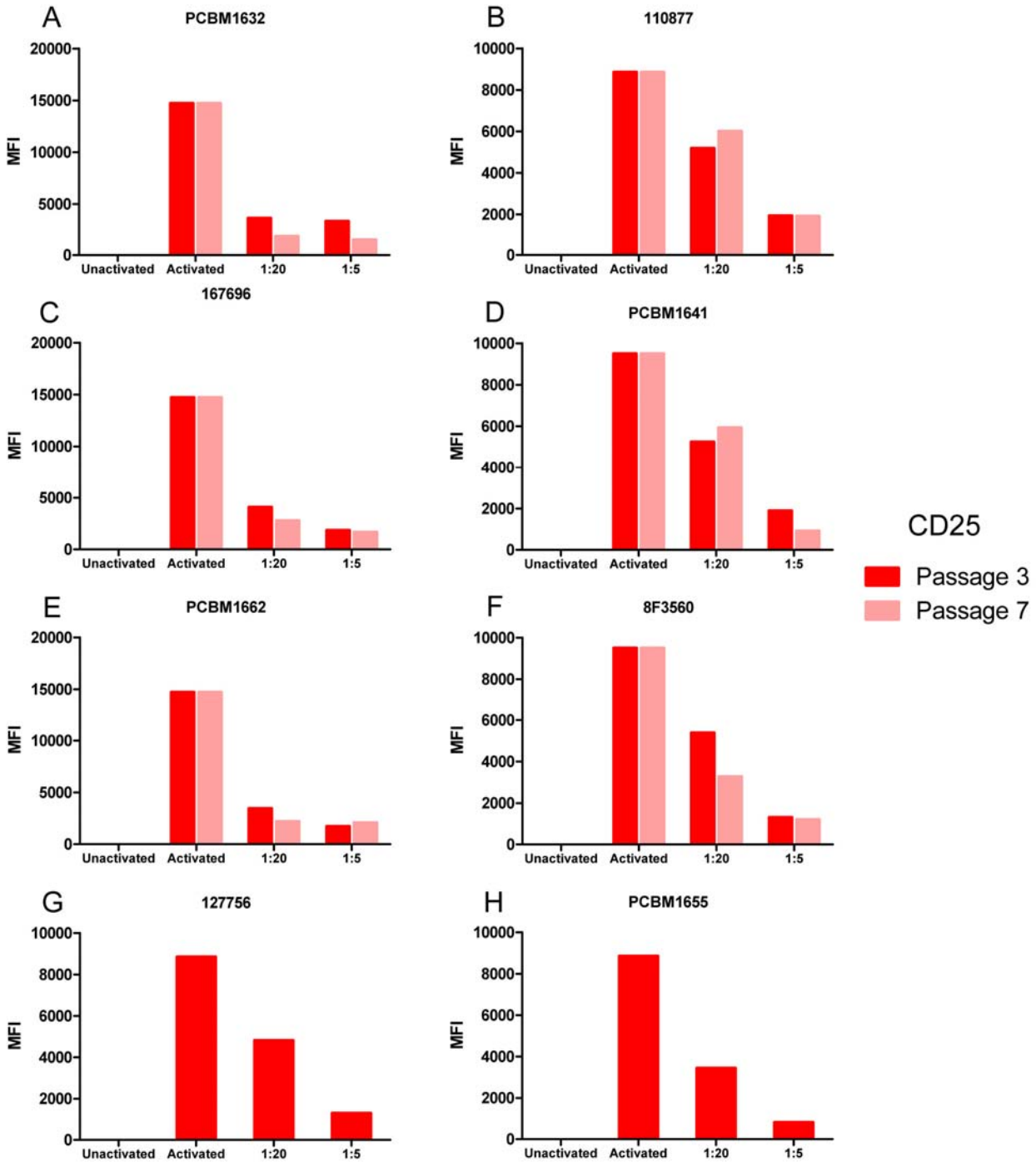

Figure 5-7. Co-culture of human MSCs with mouse T cells downregulates expression of CD25, and varies between passages. Changes in surface marker expression of CD25 in murine T cells following co-culture with human MSCs were measured by flow cytometry. Data is expressed as mean fluorescence intensity (MFI), n=1. Ratios indicate the number of MSCs:murine T cells. (A) PCBM1632 (B) 110877 (C) 167696 (D) PCBM1641 (E) PCBM1662 (F) 8F3560 (G) 127756 (H) PCBM1655.

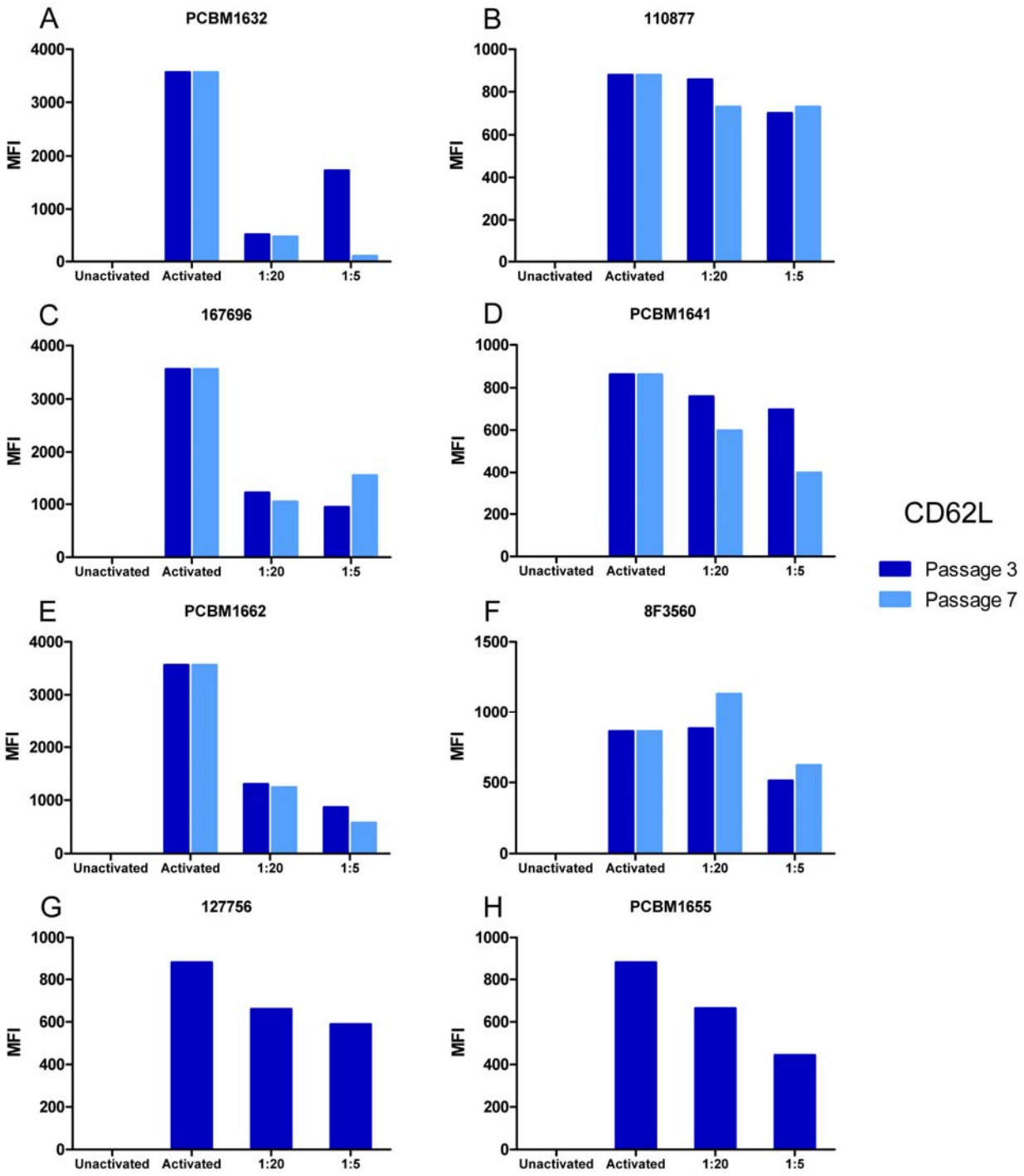

Figure 5-8. Co-culture of human MSCs with mouse T cells downregulates expression of CD62L, and varies between passages. Changes in surface marker expression of CD62L in murine T cells following co-culture with human MSCs were measured by flow cytometry. Data is expressed as mean fluorescence intensity (MFI), n=1. Ratios indicate the number of MSCs:murine T cells. (A) PCBM1632 (B) 110877 (C) 167696 (D) PCBM1641 (E) PCBM1662 (F) 8F3560 (G) 127756 (H) PCBM1655.

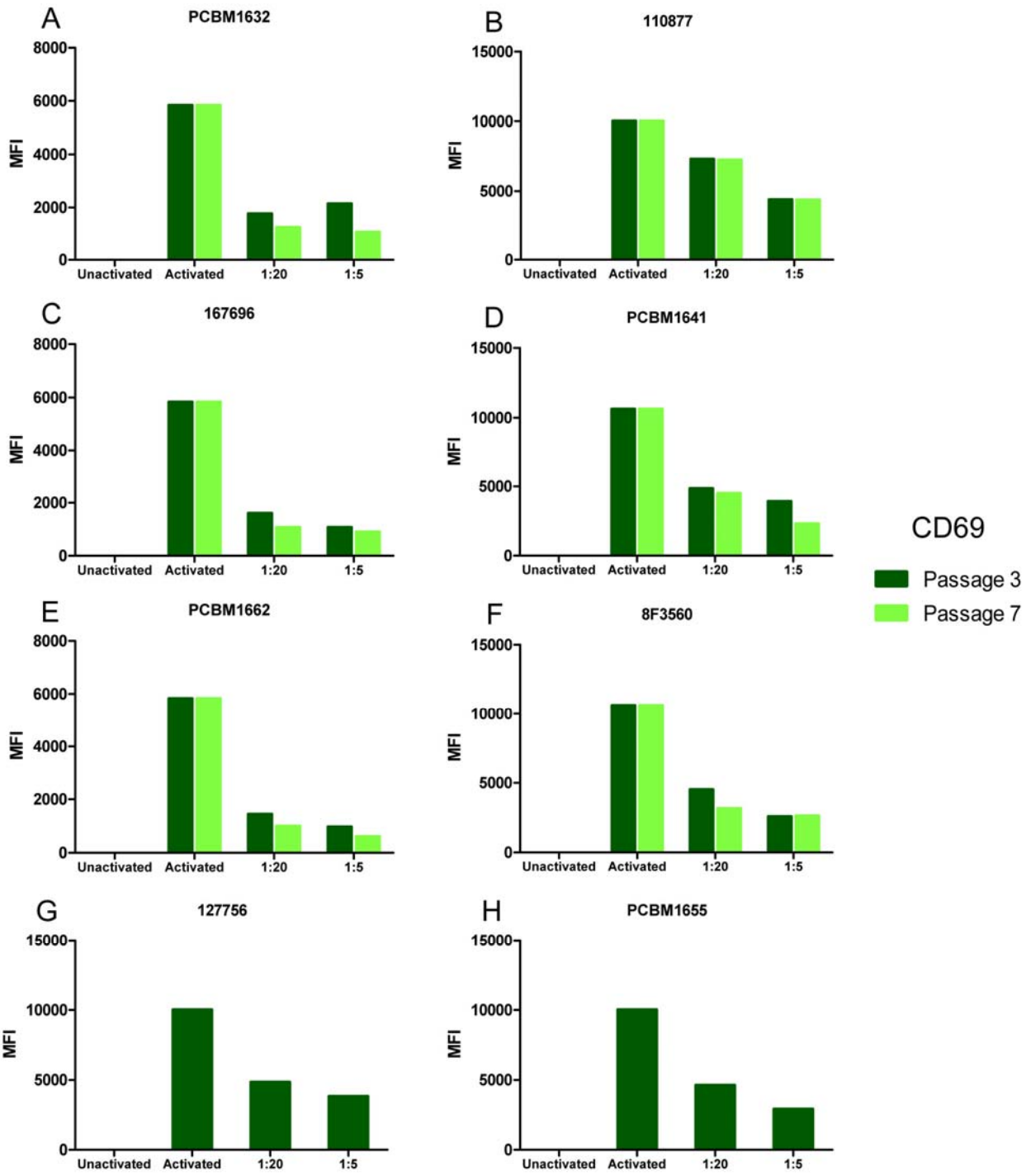

Figure 5-9. Co-culture of human MSCs with mouse T cells downregulates expression of CD69, and varies between passages. Changes in surface marker expression of CD69 in murine T cells following co-culture with human MSCs were measured by flow cytometry. Data is expressed as mean fluorescence intensity (MFI), n=1. Ratios indicate the number of MSCs:murine T cells. (A) PCBM1632 (B) 110877 (C) 167696 (D) PCBM1641 (E) PCBM1662 (F) 8F3560 (G) 127756 (H) PCBM1655.

5.3.4 MSCs inhibit secretion of pro-inflammatory cytokines TNF-α and IFN-γ

It has been previously demonstrated that MSCs are capable of inhibiting cytokine secretion by T cells both *in vitro* and *in vivo* (145). To assess donor and passage differences, we evaluated supernatants following 72 hours of co-culture with murine T cells by a Th1/Th2 multiplex ELISA assay. As anticipated, secreted levels in activated samples were very high compared to unstimulated samples. Following co-culture with MSCs, murine T cells showed marked decreases in secretion of both TNF-α and IFN-γ in culture supernatants in a dose-dependent manner (Figures 5-10 and 5-11).

Inhibition of cytokine secretion by MSCs is variable between donors and passages. Inhibition of TNF-α secretion by MSCs shows there is a dose-dependent response in most cell lines and passages. With regard to IFN-γ, the extent of inhibition and lack of differences at different dilutions suggests further dilutions will be required to see a dose-dependent response. To graphically represent differences between donors, experimental groups with MSCs at both dilutions were normalized to activated sample values and plotted as percent activated, or an activation index (Figures 5-12 and 5-13). Data for most cell lines suggest that P7 may improve inhibition of cytokine secretion by murine T cells. Conversely, cell line PCBM1641 and PCBM1662 for IFN-γ (Figures 5-11D and 5-11E) and TNF-α (Figures 5-10D and 5-10E) 1:5 suggests P3 is more immunosuppressive by cytokine secretion. Overall, MSCs from all donors inhibit secretion of pro-inflammatory cytokines IFN-γ and TNF-α by murine T cells.

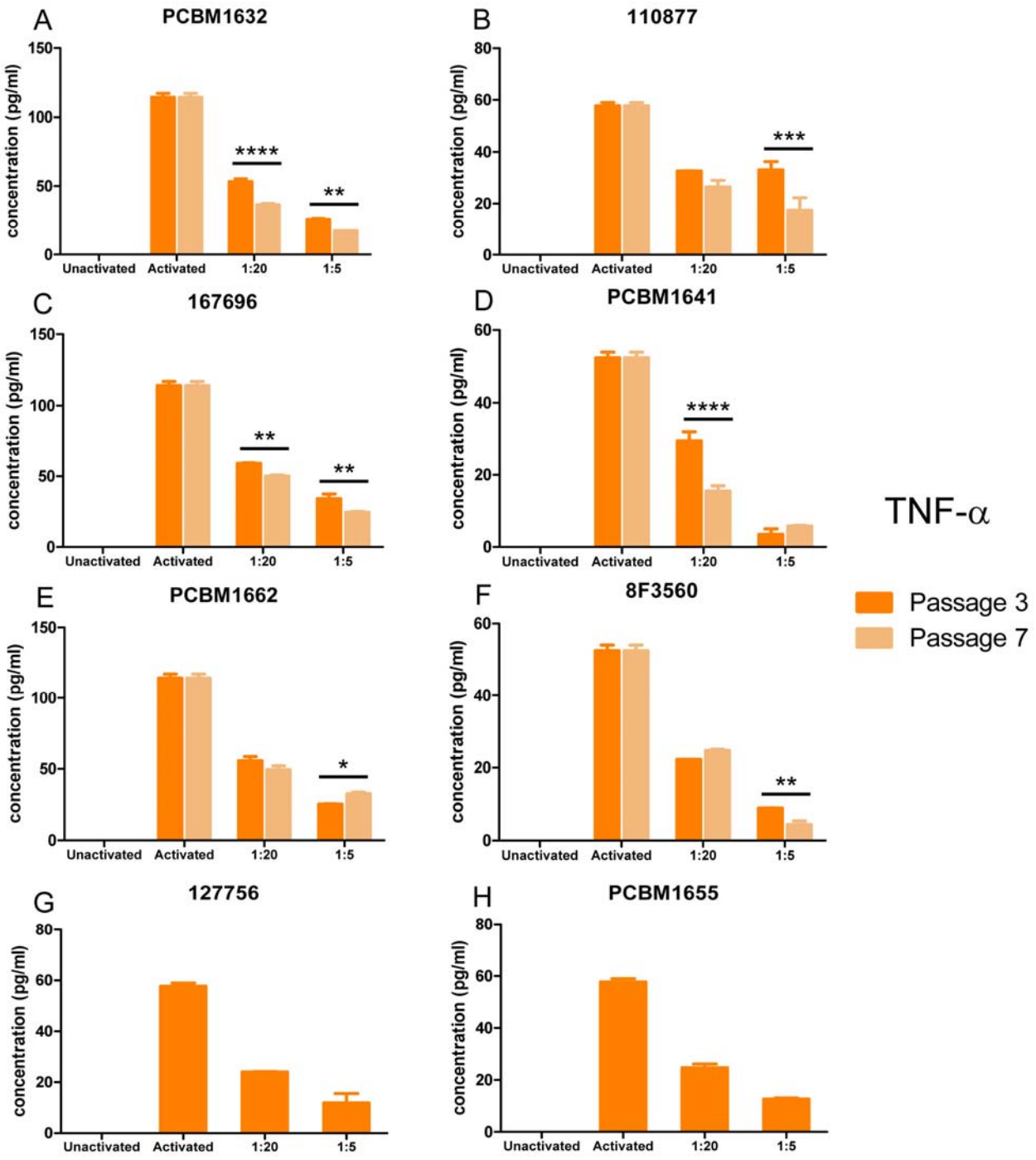

Figure 5-10. Co-culture of human MSCs with mouse T cells inhibits secretion of pro-inflammatory cytokine TNF-α. Changes in cytokine secretion of TNF-α in murine T cells following co-culture with human MSCs were measured by an ELISA. Data is expressed as mean concentration (pg/ml) ± standard deviation (n=2); *p<0.05, **p<0.01, ***p<0.001, ****p<0.0001. Ratios indicate the number of MSCs:murine T cells. (A) PCBM1632 (B) 110877 (C) 167696 (D) PCBM1641 (E) PCBM1662 (F) 8F3560 (G) 127756 (H) PCBM1655.

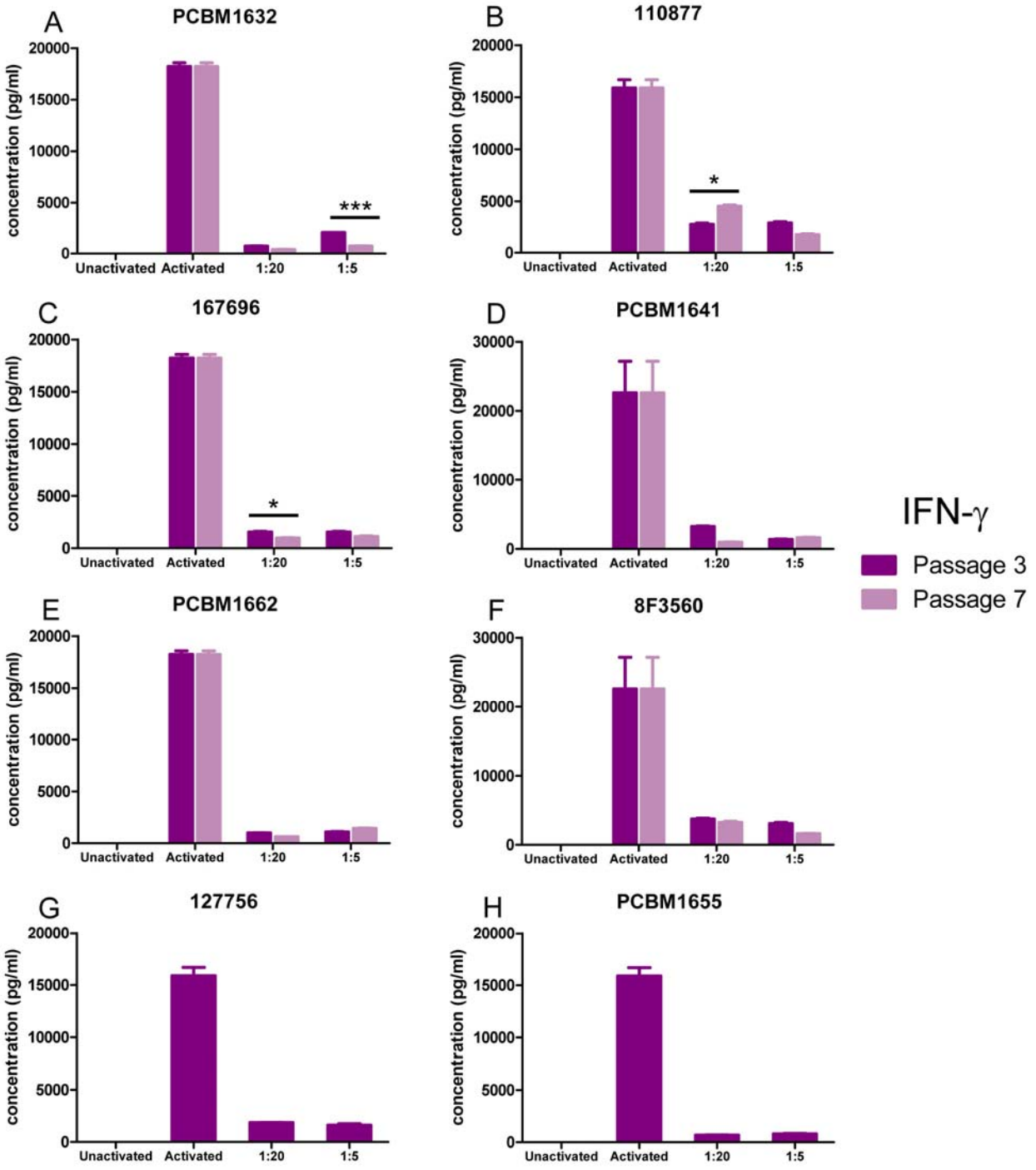

Figure 5-11. Co-culture of human MSCs with mouse T cells inhibits secretion of pro-inflammatory cytokine IFN-γ. Changes in cytokine secretion of IFN-γ in murine T cells following co-culture with human MSCs were measured by an ELISA. Data is expressed as mean concentration (pg/ml), ± standard deviation (n=2); *p<0.05, **p<0.01, ***p<0.001, ****p<0.0001. Ratios indicate the number of MSCs:murine T cells. (A) PCBM1632 (B) 110877 (C) 167696 (D) PCBM1641 (E) PCBM1662 (F) 8F3560 (G) 127756 (H) PCBM1655.

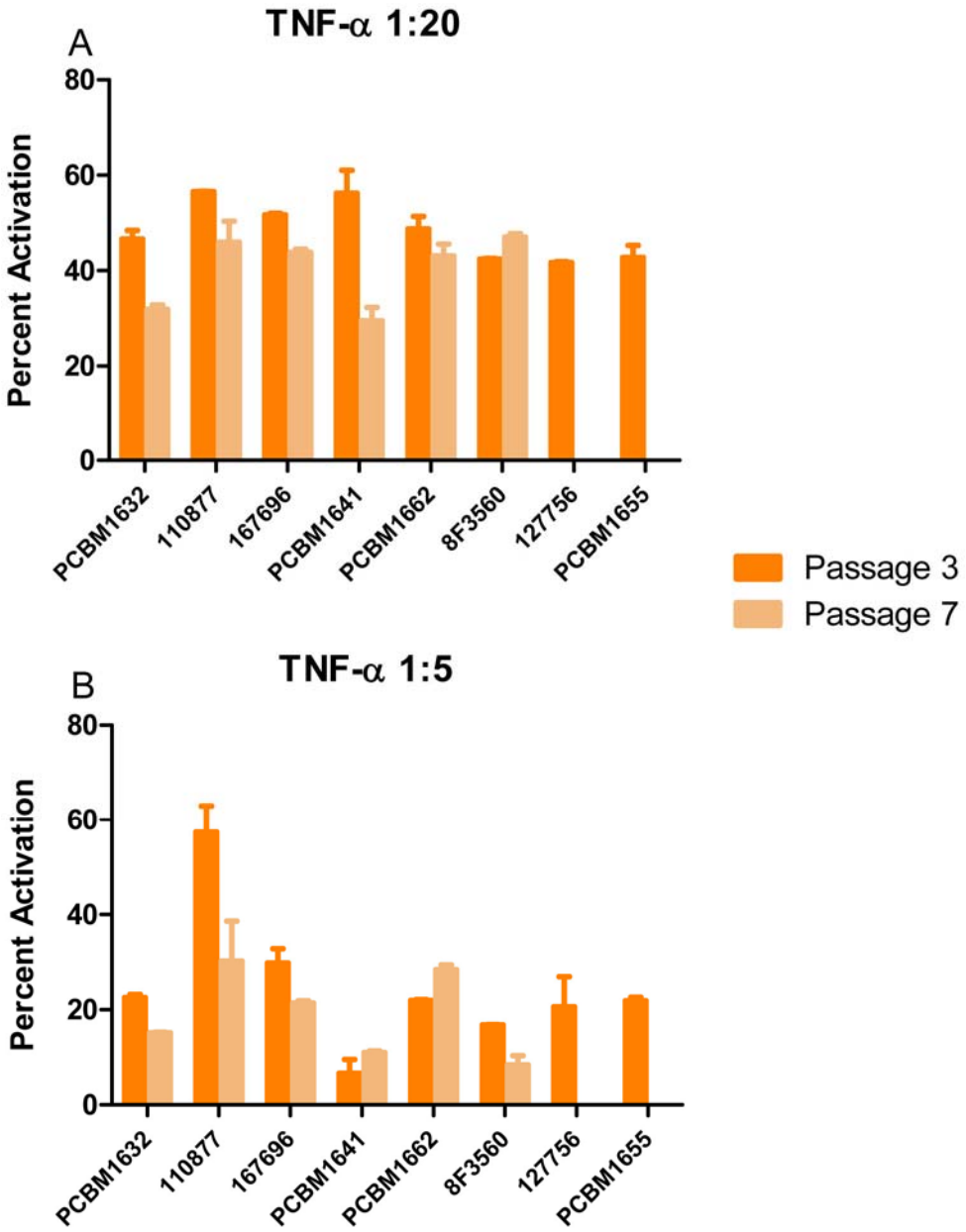

Figure 5-12. Inhibition of TNF-α secretion may be donor- and/or passage-dependent. Secretion concentrations were normalized to activated sample values to obtain a donor comparison, and plotted as mean percent activation ± standard deviation, n=2. (A) TNF-α 1:20 (B) TNF-α 1:5.

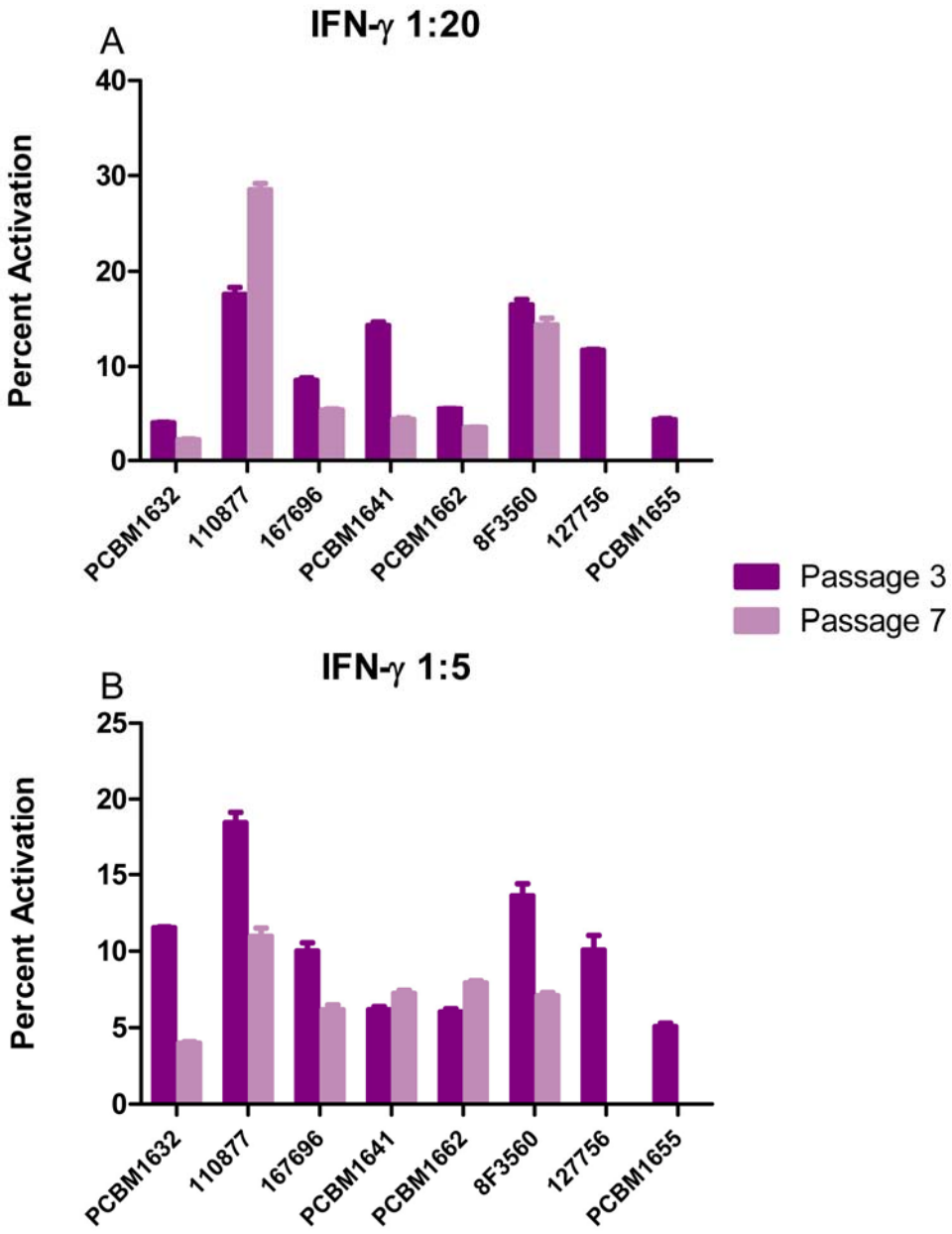

Figure 5-13. Inhibition of IFN-γ secretion may be donor- and/or passage-dependent. Secretion concentrations were normalized to the activated sample values to obtain a donor comparison, and plotted as mean percent activation ± standard deviation, n=2. (A) IFN-γ 1:20 (B) IFN-γ 1:5.

5.4 DISCUSSION

Based on their ability to immunosuppress, MSCs have been utilized in several clinical trials to treat many diseases including Crohn's Disease, GvHD, multiple sclerosis and others (132,138,145,146). Due to the potential for MSCs from several donors to treat many patients, there is a need to understand the role of donor differences through quantitative *in vitro* bioassays capable of predicting *in vivo* outcomes. However, there are currently no *in vitro* bioassays that are suitable to detect differences in immunosuppressive activity in MSCs from different donors or passages. Current assessment of immunosuppressive activity in MSCs is typically examined using a mixed lymphocyte reaction (MLR) assay using allogeneic, polyclonal peripheral blood T cells, which inherently ignores donor/recipient MHC class mismatch, making it difficult to assess and quantify a donor's ability to immunosuppress.

It has been previously established that MSCs can be used allogeneically, and further, may exert an effect in a xenogeneic setting, where human MSCs have been shown to home to injured sites and exert a function in mouse and rat *in vivo* models (147-151). Therefore, the ability of human MSCs to exert their immunosuppressive effect on murine T cells in an *in vitro* model system was examined. Once this was established and shown to be successful (Nazarov and Lo Surdo *et al.*, submitted), we expanded this methodology to assess immunosuppressive activity in various donors and passages. The advantages of this *in vitro* assay system include elimination of genetic and age variations between human T cell donors, while utilizing mouse T cells with monoclonal TCRs with known antigen specificity. We have demonstrated that MSCs can exert an immunosuppressive effect not only across MHC mismatches, but also across species, making this model system ideal for measuring MSC function as it relates to immunosuppression.

Here, this methodology was extended to additional donors and passages to better understand the role of donor variability and *in vitro* expansion on immunosuppressive capacity. Based on endpoints studied here, including changes in gene expression, flow cytometry and cytokine secretion, we have shown that most donors can modulate expression of activation markers. However, the data suggests some donors are more immunosuppressive than others. Based on Tbet and GATA3 expression, cell line PCBM1632 appears to downregulate expression of these markers based on their relative activated expression. Flow-based endpoints showing decreased expression of CD25, CD62L and CD69, as well as inhibition of pro-inflammatory cytokine secretion, confirm these findings, and suggest that cell line PCBM1632 may be a more potent immunomodulator. Conversely, cell line 110877 appears to be less immunosuppressive in our model system. Data shows less downregulation of activation markers relative to stimulated (activated) samples. Taken together, this data suggests there may be donor variability in immunosuppressive capacity that can be detected in our *in vitro* assay system.

The reason for potential donor differences detected here may be due to the disease status of the donor, or other biological factors. We currently do not know the disease status of the donors from which our cell lines were derived. Cell lines obtained from donors having an autoimmune disease may be less potent than those derived from healthy donors, and may ultimately alter their immunosuppressive function. Further, even cell lines derived from healthy donors may show donor-to-donor variability. Francois *et al* described the relationship between indoleamine 2,3-Dioxygenase (IDO) upregulation through IFN-γ and TNF-α stimulation and immunosuppressive capacity by human MSCs in MSC/activated PBMC co-culture experiments. Interestingly, upon cytokine stimulation with the above mentioned factors, MSCs differed in their level of expression of IDO, and expression of IDO directly correlated with

immunosuppressive capacity based on T cell suppression. This study suggests that MSCs from a variety of healthy donors may also demonstrate a wide range of immunosuppressive capacity.

Another potential source of functional variability may be due to *in vitro* expansion of MSCs to obtain sufficient numbers for treatment. A recent review by Jacques Galipeau suggests a role in expansion and subsequent cryopreservation of MSCs through a comparison of clinical treatment of GvHD in the United States and Europe. Interestingly, clinical trials treating GvHD in Europe minimize cell expansion by deriving many different cell lines from many donors with success. In the US, MSCs from very few donors are expanded extensively to obtain similar numbers for treatment, which has shown negative results (140). Further, clinical data from the Karolinska Institute has shown less expansion may improve survival rates in patients with GvHD. Those treated with low passage MSCs (passage 1-2) had a one year survival rate of 75%, compared to those who were treated with later passage MSCs (passage 3-4) who had only a 14% survival rate (143). Taken together, this suggests a negative role of extensive *in vitro* expansion in the immunoregulatory function in MSCs.

Interestingly, our data suggests a slight improvement in immunosuppressive function from P3 to P7, pointing to a potential secretory role of MSCs in immunoregulation in our *in vitro* system. However, future experiments to determine whether or not this effect in our system is valid can include IFN-γ/TNF-α stimulation and subsequent regulation of IDO expression as described by Francois *et al* (152). Further, it is necessary to correlate our *in vitro* data with *in vivo* outcomes, which are currently being explored in a murine autoimmune type I diabetes model.

5.5 CONCLUSION

We have demonstrated human MSCs can be immunosuppressive in a xenogeneic *in vitro* model system, making it an ideal system to study human MSCs from several donors and passages. However, more work needs to be done to correlate these *in vitro* data with *in vivo* outcomes, to better understand the role of donor variation and passaging on immunosuppressive capacity in MSCs. A better understanding of the mechanism of action of immunosuppressive activity may help identify novel therapeutic targets for cellular therapies to enhance immunomodulatory function in MSCs.

6.0 OVERALL CONCLUSIONS

MSCs hold great therapeutic potential, however MSC heterogeneity between donors and within populations of MSCs necessitate a better understanding underlying the mechanisms of and influence on MSC function that ultimately could be related to clinical outcome. Further, *in vitro* expansion is inherently required as the fraction of MSCs in the bone marrow is low. As discussed in Chapter 1, the overarching goal of this work was to improve characterization of bone marrow-derived MSCs through the use of quantitative bioassays. As MSCs have several facets of clinical relevancy, these quantitative functional assays must address their ability to proliferate, differentiate, and provide an immunomodulatory function. It is the hope that these quantitative bioassays can correlate with *in vivo* outcomes. In Chapters 2, 3 and 5, we addressed these properties of MSCs through the use of both existing and novel bioassays to measure MSC functional activity. Due to the inherent heterogeneity of MSCs, in Chapter 4 we took advantage of these heterogeneities and morphological differences by enriching based on cell size using two different techniques.

In this work, we utilized MSCs from eight different donors to better understand the role of donor variability in MSC function. Based on our data, it is clear that *in vitro* potential is donor and endpoint specific. In Chapter 2, we assessed the biologic activity of the eight cell lines through existing bioassays, including CFUs, proliferation, and marker phenotype expression by flow cytometry. Further, we also documented by several methods that MSCs

increase in cell size with passage, and that this may correlate with decreased potential. Interestingly, decreased proliferative and CFU capacity do correlate with this increase in cell size. Of note, however, is that expression of commonly used MSC markers to identify MSCs do not change with passage or between donors. While the ISCT put forth a white paper defining MSCs through expression of CD73, CD90 and CD105, we clearly demonstrate that this does not correlate with decreased potential or function as shown by other endpoints. Therefore, although these markers may be necessary to identify an MSC, they do not correlate with changes in biological functions between donors or with *in vitro* culture.

There has been little effort to quantify differentiation capacity in MSCs. Quantitative measurements of differentiation are necessary to assess biological activity between populations of MSCs derived from different donors. Further, due to MSC heterogeneity, it is important that these quantitative bioassays measure activity on a per cell basis. In Chapter 3, we measured changes in adipogenic and osteogenic potential using novel quantitative assays that can measure differentiation on a per cell basis. While we were able to show differences between 2 donors using a limiting dilution assay, we moved toward more objective, high-throughput measurements using automated microscopy. Through this methodology, we were able to identify donor and passage differences in adipo- and osteogenic potential in a quantitative readout. These methods will have utility in donor screening to assess differentiation capacity quantitatively. Further, these quantitative measurements could be used to make precise measurements that allow for comparisons of differentiation potential in a variety of different *in vitro* growth conditions and determine the influence of many other factors that could affect MSC biological function. Once established, these quantitative methods to measure differentiation provide a toolbox so that other researchers can measure differentiation capacity in MSCs. While we assessed chondrogenic

differentiation capacity qualitatively, future work will focus on using similar automated methods to improve quantification of chondrogenesis *in vitro.*

As shown in Chapter 2, and elsewhere in the literature, MSCs are highly heterogeneous (64,153). Much of this heterogeneity may be tied to morphological differences within a population of MSCs. We documented these changes in cell size through passaging, demonstrating an increase in size and granularity by flow cytometry, and an increase in cell diameter though cellometer measurements. We took advantage of these cell size heterogeneities and used cell size as a metric that can be used to enrich MSCs, and to study these cell size populations separately. We initially used flow cytometry as a means to separate cells based on their FSC/SSC properties. Due to the required time out of culture to perform a cell sorting experiment, we wanted to design a simpler, faster way to separate cells by size. In Chapter 4, we designed a simple filtering apparatus that can accommodate filter sizes of our choosing to sequentially separate cells by size. Based on proliferation, CFU and differentiation measurements, we were able to enrich for early progenitors in MSCs as shown by their enhanced ability to proliferate and differentiate. Enrichment based on cell size may therefore be a mechanism by which to diminish heterogeneity and enhance biological function in MSCs. Further, separation by cell size will allow us to better understand the molecular signature associated with the small cell phenotype. Future work using global gene expression analyses on the small and large cell subpopulations may allow for the identification of novel biomarkers that have yet to be discovered in MSCs.

In Chapter 5, we addressed the immunosuppressive potential of MSCs from different cell lines and passages using a novel *in vitro* model system. This approach is ideal in that we use clonal T cells specific for known peptide antigens, which reduces variability typically seen in

traditional polyclonal mixed lymphocyte reaction assays. In doing so, using endpoints assessing changes in gene expression of Tbet and GATA3, expression of activation markers by PCR, and cytokine secretion, we determined that our model system successfully assesses immunosuppression by MSCs. Further, our data suggests that there may be donor and passage differences in immunosuppressive potential of donors used here. Future work will correlate these *in vitro* assay outcomes with an *in vivo* model system to better correlate and predict the role of donor variability and passaging in immunosuppressive capacity.

Overall, we have extensively characterized MSC cell lines derived from eight human donors using both existing and novel quantifiable endpoints. Interestingly, it appears as though all endpoints are not necessarily correlative, and that individual *in vitro* bioassay outcomes are donor and passage specific. In other words, for example, proliferative potential does not necessarily predict the ability to undergo adipogenic or osteogenic differentiation, nor the ability of MSCs to immunosuppress. Therefore, identification of biomarkers that are more predictive of *in vitro* and *in vivo* outcomes will certainly benefit the field. A collective effort to further improve characterization of MSCs is currently being pursued at the FDA through the use of proteomics, and genetic and epigenetic-based discovery tools, which will help identify novel biomarkers that may better identify the MSCs used in this study. An improved understanding of the MSC phenotype and more quantitative bioassays will aid in the discovery of novel biomarkers that may improve characterization and clinical outcome using MSCs.

APPENDIX A

CHANGES IN GENE EXPRESSION FOLLOWING TRILINEAGE DIFFERENTIATION – A CELL LINE COMPARISON

Changes in gene expression following adipogenic, osteogenic, and chondrogenic differentiation were reported in section 3.3.4. Here, we report the same data, however compiled onto one graph to better visualize cell line differences in response to differentiation induction.

A.1 ADIPOGENESIS

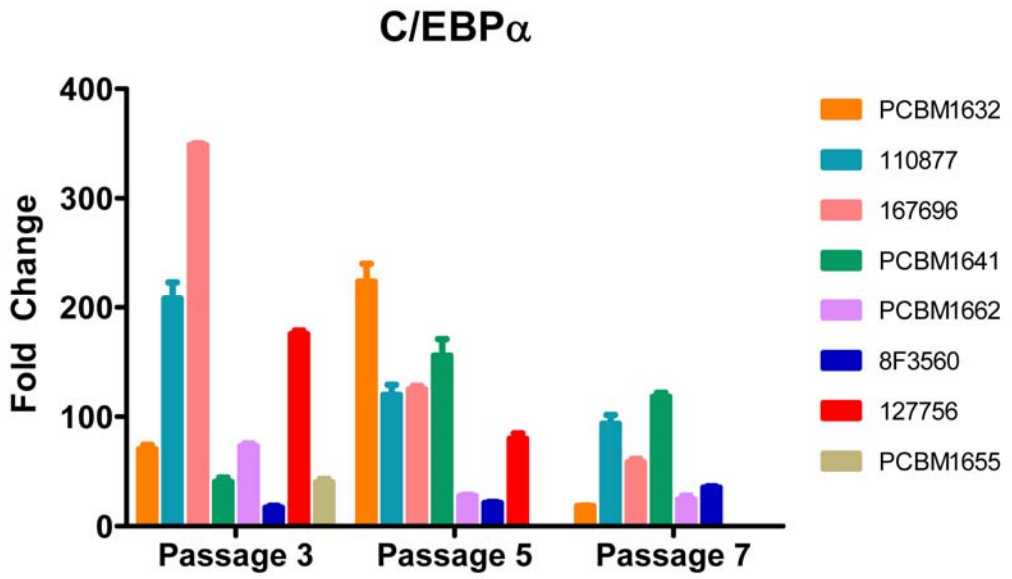

Figure A-1-1. Change in C/EBPα expression following adipogenic stimulation is donor- and passage-dependent. MSCs from all cell lines were cultured for 14 days in adipogenic differentiation medium, and assessed for expression of C/EBPα by qRT-PCR. Data is expressed as mean ± standard deviation.

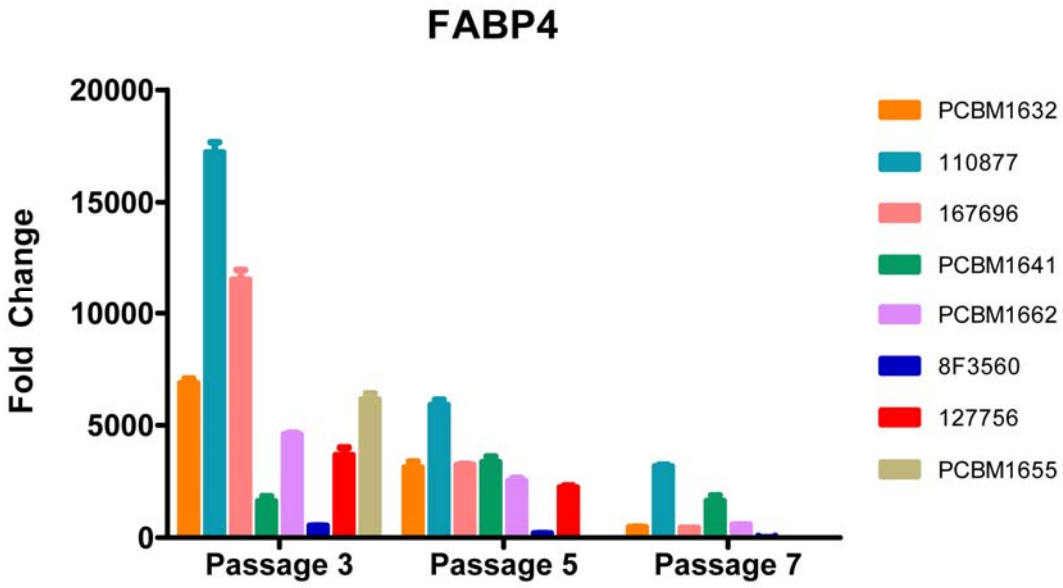

Figure A-1-2. Change in FABP4 expression following adipogenic stimulation is donor- and passage-dependent. MSCs from all cell lines were cultured for 14 days in adipogenic differentiation medium, and assessed for expression of FABP4 by qRT-PCR. Data is expressed as mean ± standard deviation.

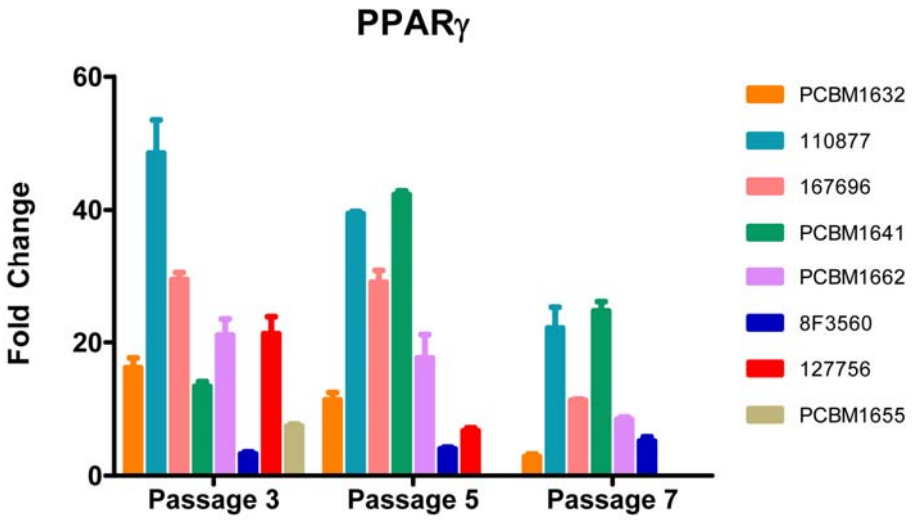

Figure A-1-3. Change in PPARγ expression following adipogenic stimulation is donor- and passage-dependent. MSCs from all cell lines were cultured for 14 days in adipogenic differentiation medium, and assessed for expression of PPARγ by qRT-PCR. Data is expressed as mean ± standard deviation.

A.2 OSTEOGENESIS

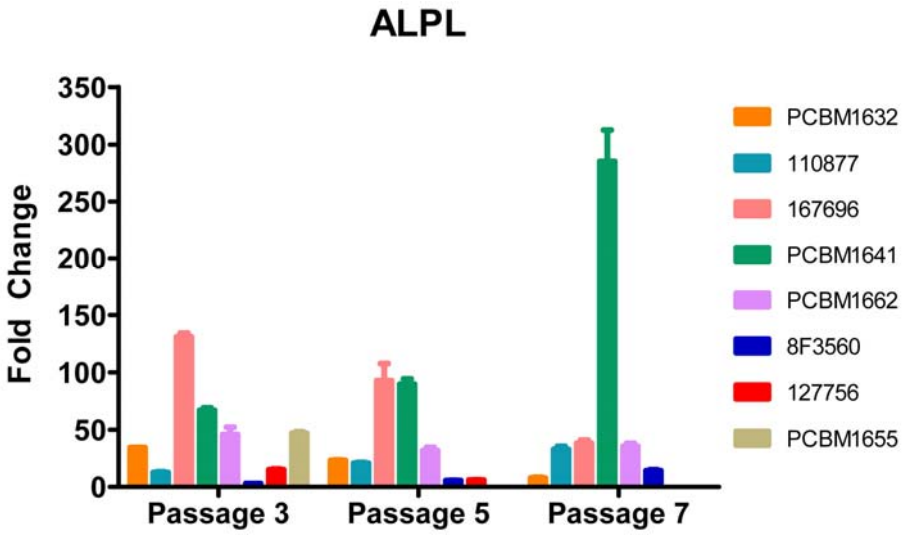

Figure A-2-1. Change in ALPL expression following osteogenic stimulation is donor- and passage-dependent. MSCs from all cell lines were cultured for 14 days in osteogenic differentiation medium, and assessed for expression of ALPL by qRT-PCR. Data is expressed as mean ± standard deviation.

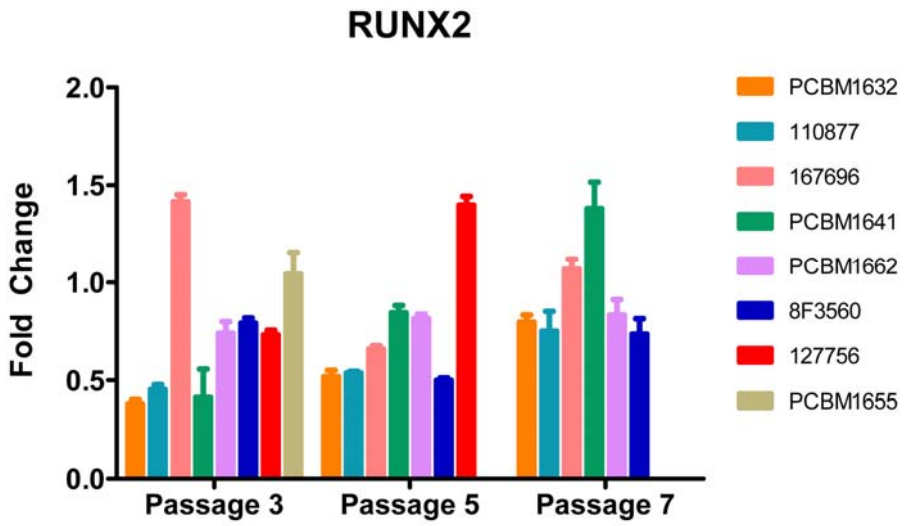

Figure A-2-2. Change in RUNX2 expression following osteogenic stimulation is donor- and passage-dependent. MSCs from all cell lines were cultured for 14 days in osteogenic differentiation medium, and assessed for expression of RUNX2 by qRT-PCR. Data is expressed as mean ± standard deviation.

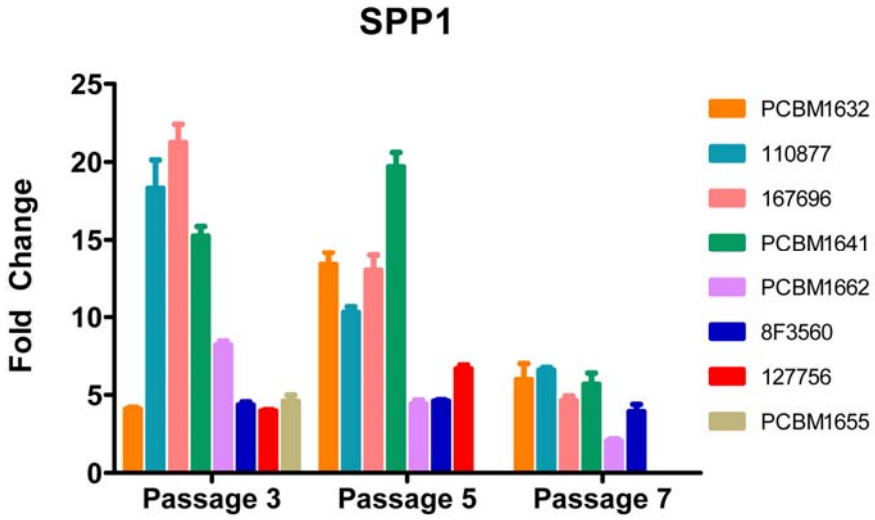

Figure A-2-3. Change in SPP1 expression following osteogenic stimulation is donor- and passage-dependent. MSCs from all cell lines were cultured for 14 days in osteogenic differentiation medium, and assessed for expression of SPP1 by qRT-PCR. Data is expressed as mean ± standard deviation.

A.3 CHONDROGENESIS

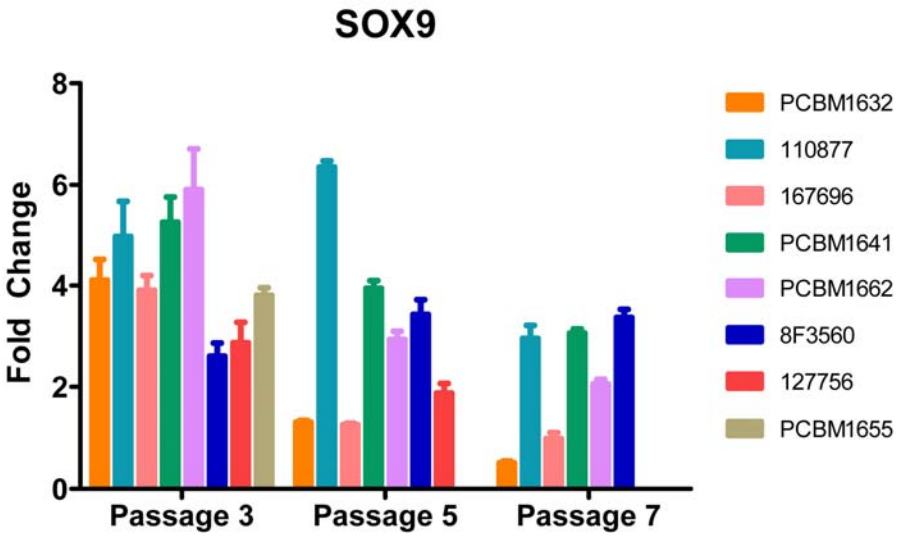

Figure A-3-1. Change in SOX9 expression following chondrogenic stimulation is donor- and passage-dependent. MSCs from all cell lines were cultured for 15 days in chondrogenic differentiation medium, and assessed for expression of SOX9 by qRT-PCR. Data is expressed as mean ± standard deviation.

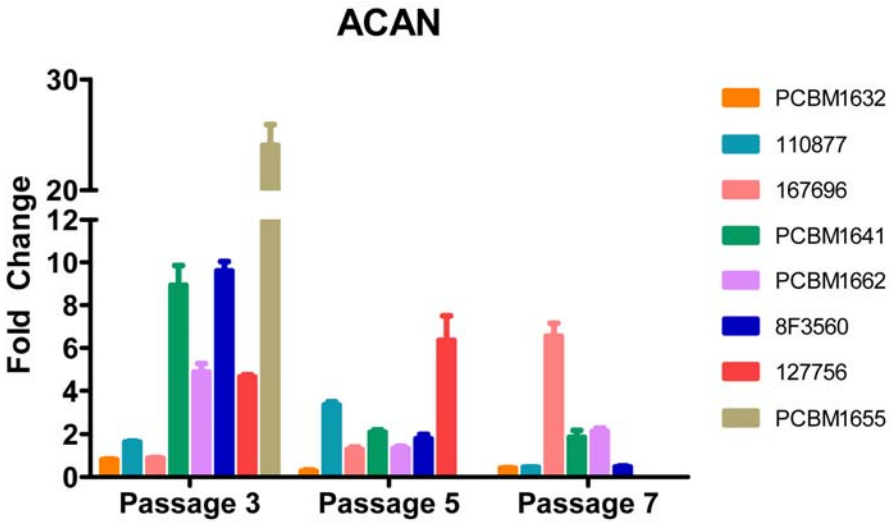

Figure A-3-2. Change in ACAN expression following chondrogenic stimulation is donor- and passage-dependent. MSCs from all cell lines were cultured for 15 days in chondrogenic differentiation medium, and assessed for expression of ACAN by qRT-PCR. Data is expressed as mean ± standard deviation.

APPENDIX B

MACRO SCRIPT TO QUANTIFY ADIPOGENESIS

As described in Section 3.3.1.2, we quantified adipogenesis using Nile Red fluorescence measurements. Following image acquisition, the percent Nile Red positive cells and nuclei counts were quantified using a macro written for Nikon Elements software. The macro script used to quantify adipogenesis following automated microscopy is annotated in the table below (Table B-1).

Table B-1. Macro script and annotation utilized to quantify adipogenesis following automated microscopy.

Elements Command	Explanation
ClearBinary();	Clears any previous binaries (thresholds) that have been applied to an image
Zoom(100.0);	Brings the image to 100% image resolution (this isn't needed for the program, however, it gives the user a better view of how the macro proceeds.
ViewComponents("10");	Selects the first fluorescence channel (of a multichannel image) to be viewed only
RegionalMaxima(16,3,0,1,0,7);	This is an image processing function that looks at a pixel, or group of pixels, and compares this to the surrounding pixels to determine where the most intensity lies as a way of enhancing the peaks of an image relative to its immediate surroundings. This is particularly useful for bringing out region-based contrast and can be

Table B-1 (Continued)

	particularly useful for separation of features.
DefineThresholdMCHOperation(1); DefineThresholdMCHChannel(0,20,255,0); DefineThresholdMCHChannel(1,1,0,0); DefineThresholdProcessing(0,0,0); DefineThresholdRestrictionSize(0,0.000000,845.000000); DefineThresholdRestrictionCircularity(0,0.000000,1.000000); ThresholdND(1,1,1);	This group of commands defines the threshold with which a binary (mask) will be applied to the image. This "all-in-one" function has the ability to define the intensity range that the binary will represent, and also can incorporate size and circularity restrictions should the user wish to implement them here. Although restrictions in this case were done subsequently.
ViewComponents("10");	Selects the first fluorescence channel (of a multichannel image) to be viewed only
FillHolesND(1,1,1);	Once a binary has been applied, it may occur that one object (binary) can have areas within it, where there are no pixels selected. In certain circumstances, the user may wish to fill in these holes as a step towards the final segmentation
MorphoSeparateObjectsND(15,2,1,1,1);	This function has many traditional names such as "watershed". The basic function of this command is to cleave a bottleneck between objects that the user wishes to be separated. The degree or "aggressiveness" of this function, is user selectable by selected the size of the cluster of pixels analyzed, as well as the number of iterations performed and can be experimented with to ensure the most accuracy of the function for the desired analysis.
Restrictions("Area",1,1,100,99999999);	Each binary can be made up of many individual objects. This function allows the software to exclude or include these individual objects depending on their size. It should be noted that once this command is executed, the objects are not yet discarded, however, the objects that do not make it into the specified size limits are "flagged" for further action.
ScanObjectsND(1,1,1);	Upon execution of this command, the software will look through the entire dataset and take a measurement of the size of each object that has been detected through segmentation at this point of the macro.

Table B-1 (Continued)

GenerateBinaryND(1,1,1);	Allows the software to implement the previous "restrictions" command by deleting any objects that have been flagged for exclusion via a previous command.
BinLayerStore("DAPI Cell Count","DAPI Count");	Takes the current binary and stores it for later use with the name specified.
ViewComponents("01");	Selects the second fluorescence channel (of a multichannel image) to be viewed only.
DefineThresholdMCHOperation(1);	This group of commands defines the threshold with which a binary, or mask, will be applied to the image. This "all-in-one" function has the ability to define the intensity range that the binary will represent, and also can incorporate size and circularity restrictions should the user wish to implement them here.
DefineThresholdMCHChannel(0,1,0,0);	
DefineThresholdMCHChannel(1,35,255,0);	
DefineThresholdProcessing(0,0,0);	
DefineThresholdRestrictionSize(0,0.000000,999999999);	
DefineThresholdRestrictionCircularity(0,0.000000,1.000000);	
ThresholdND(1,1,1);	
ViewComponents("01");	Selects the second channel of a multichannel image for viewing (only).
CloseBinaryND(1,4,1,1,1);	A close function is a combination of a certain sequence of dialations and erosions. Each object in the binary for example may be dialated by some number which will define the number of times a 1-pixel addition will be added to the outer perimeter of each object, followed by a erosion which will subtract 1 pixel (per each iteration) from the outer perimeter of each object. The result is that if two objects come into contact with each other by dialation, the subsequent erosion will only erode the outer perimeter's pixels, thus maintaining the original size of the components and leaving the connection intact. The purpose of this is normally, but not always, to connect objects that have been too aggressively separated by the macro so far and are more accurately defined as 1 object.
FillHolesND(1,1,1);	Once a binary has been applied, it may occur that one object (binary) can have areas within it, where there are no pixels selected. In certain circumstances, the user may wish to fill in these holes as a step towards the final segmentation which is what this function does.
ScanObjectsND(1,1,1);	Upon execution of this command, the software will look through the entire dataset and take a measurement of the size of each object that

Table B-1 (Continued)

	has been detected through segmentation at this point of the macro.
Restrictions("Area",1,1,100,1.00e+008);	Each binary image can be made up of many individual masks. This function allows the software to exclude or include these individual pieces depending on their size. It should be noted that once this command is executed, the objects are not yet completely deleted, however, the objects that do not make it into the specified size limits are "flagged" for further action.
GenerateBinaryND(1,1,1);	Allows the software to implement the previous "restrictions" command by deleting any objects that have been flagged for exclusion via a previous command.
ConvexHullND(1,1,1);	This function recognizes the shape of convex objects and fills the concavity to include this area in the mask. This is particularly useful in cases where there is cytosolic, but not nuclear localization of a particular probe, yet one would like to include the nuclear signal of all cells expressing a cytosolic probe as a means of counting positive expression of cells relative to total number.
BinLayerStore("Nile Red Positive","Threshold Nile Red");	Takes the current binary and stores it for later use with the name specified.
BinLayerMergeND("DAPI-Nile Red Intersection", "DAPI Cell Count, Nile Red Positive", 2, 1, 1, 1);	Merges two binary layers so that only the intersection of the two respective binary layers are now shown. This newly created binary is its own binary layer which can be utilized for analysis.
ScanObjectsND(1,1,1);	Upon execution of this command, the software will look through the entire dataset and take a measurement of the size of each object that has been detected through segmentation at this point of the macro.
Restrictions("Area",1,1,33.11,1.00e+008);	Each binary image can be made up of many individual masks. This function allows the software to exclude or include these individual pieces depending on their size. It should be noted that once this command is executed, the objects are not yet completely deleted, however, the objects that do not make it into the specified size limits are "flagged" for further action.

Table B-1 (Continued)

GenerateBinaryND(1,1,1);	Allows the software to implement the previous "restrictions" command by deleting any objects that have been flagged for exclusion via a previous command.
ViewComponents("11");	Selects both the first and second channels of a multichannel image for viewing.
OverlayTransparency(50);	Sets the transparency of the mask which is overlaying the image
BinLayerSelect("DAPI-Nile Red Intersection");	Selects a particular stored layer to be viewed

BIBLIOGRAPHY

1. Clinical Trials.gov, 2013.

2. Schofield R. The relationship between the spleen colony-forming cell and the haemopoietic stem cell. *Blood Cells* 1978;4:7-25.

3. Koller MR, Manchel I, Palsson BO. Importance of parenchymal:stromal cell ratio for the ex vivo reconstitution of human hematopoiesis. *Stem Cells* 1997;15:305-13.

4. Strobel ES, Gay RE, Greenberg PL. Characterization of the in vitro stromal microenvironment of human bone marrow. *Int J Cell Cloning* 1986;4:341-56.

5. Tavassoli M, Takahashi K. Morphological studies on long-term culture of marrow cells: characterization of the adherent stromal cells and their interactions in maintaining the proliferation of hemopoietic stem cells. *Am J Anat* 1982;164:91-111.

6. Friedenstein AJ, Gorskaja JF, Kulagina NN. Fibroblast precursors in normal and irradiated mouse hematopoietic organs. *Exp Hematol* 1976;4:267-74.

7. Jiang Y, Vaessen B, Lenvik Tet al. Multipotent progenitor cells can be isolated from postnatal murine bone marrow, muscle, and brain. *Exp Hematol* 2002;30:896-904.

8. Metcalf D. The unsolved enigmas of leukemia inhibitory factor. *Stem Cells* 2003;21:5-14.

9. Tsutsumi S, Shimazu A, Miyazaki Ket al. Retention of multilineage differentiation potential of mesenchymal cells during proliferation in response to FGF. *Biochem Biophys Res Commun* 2001;288:413-9.

10. Zaragosi LE, Ailhaud G, Dani C. Autocrine fibroblast growth factor 2 signaling is critical for self-renewal of human multipotent adipose-derived stem cells. *Stem Cells* 2006;24:2412-9.

11. Boland GM, Perkins G, Hall DJet al. Wnt 3a promotes proliferation and suppresses osteogenic differentiation of adult human mesenchymal stem cells. *J Cell Biochem* 2004;93:1210-30.

12. Kleber M, Sommer L. Wnt signaling and the regulation of stem cell function. *Curr Opin Cell Biol* 2004;16:681-7.

13. Colter DC, Sekiya I, Prockop DJ. Identification of a subpopulation of rapidly self-renewing and multipotential adult stem cells in colonies of human marrow stromal cells. *Proc Natl Acad Sci U S A* 2001;98:7841-5.

14. Banas A, Teratani T, Yamamoto Yet al. Adipose tissue-derived mesenchymal stem cells as a source of human hepatocytes. *Hepatology* 2007;46:219-28.

15. Brayfield C, Marra K, Rubin JP. Adipose stem cells for soft tissue regeneration. *Handchir Mikrochir Plast Chir* 2010;42:124-8.

16. Kokai LE, Rubin JP, Marra KG. The potential of adipose-derived adult stem cells as a source of neuronal progenitor cells. *Plast Reconstr Surg* 2005;116:1453-60.

17. Bellayr IH, Gharaibeh B, Huard Jet al. Skeletal muscle-derived stem cells differentiate into hepatocyte-like cells and aid in liver regeneration. *Int J Clin Exp Pathol* 2010;3:681-90.

18. Deasy BM, Jankowski RJ, Huard J. Muscle-derived stem cells: characterization and potential for cell-mediated therapy. *Blood Cells Mol Dis* 2001;27:924-33.

19. Gharaibeh B, Lu A, Tebbets Jet al. Isolation of a slowly adhering cell fraction containing stem cells from murine skeletal muscle by the preplate technique. *Nat Protoc* 2008;3:1501-9.

20. Huard J. Regenerative medicine based on muscle stem cells. *J Musculoskelet Neuronal Interact* 2008;8:337.

21. Bieback K, Kluter H. Mesenchymal stromal cells from umbilical cord blood. *Curr Stem Cell Res Ther* 2007;2:310-23.

22. Jager M, Zilkens C, Bittersohl Bet al. Cord blood--an alternative source for bone regeneration. *Stem Cell Rev* 2009;5:266-77.

23. Koponen JK, Kekarainen T, S EHet al. Umbilical cord blood-derived progenitor cells enhance muscle regeneration in mouse hindlimb ischemia model. *Mol Ther* 2007;15:2172-7.

24. Manca MF, Zwart I, Beo Jet al. Characterization of mesenchymal stromal cells derived from full-term umbilical cord blood. *Cytotherapy* 2008;10:54-68.

25. Huang GT, Gronthos S, Shi S. Mesenchymal stem cells derived from dental tissues vs. those from other sources: their biology and role in regenerative medicine. *J Dent Res* 2009;88:792-806.

26. Mrozik KM, Zilm PS, Bagley CJet al. Proteomic characterization of mesenchymal stem cell-like populations derived from ovine periodontal ligament, dental pulp, and bone marrow: analysis of differentially expressed proteins. *Stem Cells Dev* 2010;19:1485-99.

27. Pivoriuunas A, Surovas A, Borutinskaite Vet al. Proteomic analysis of stromal cells derived from the dental pulp of human exfoliated deciduous teeth. *Stem Cells Dev* 2009;19:1081-93.

28. Woods EJ, Perry BC, Hockema JJet al. Optimized cryopreservation method for human dental pulp-derived stem cells and their tissues of origin for banking and clinical use. *Cryobiology* 2009;59:150-7.

29. Dominici M, Le Blanc K, Mueller Iet al. Minimal criteria for defining multipotent mesenchymal stromal cells. The International Society for Cellular Therapy position statement. *Cytotherapy* 2006;8:315-7.

30. Yeh YC, Lin HH, Tang MJ. A tale of two collagen receptors, integrin beta1 and discoidin domain receptor 1, in epithelial cell differentiation. *Am J Physiol Cell Physiol* 2012;303:C1207-17.

31. Gunthert U. CD44: a multitude of isoforms with diverse functions. *Curr Top Microbiol Immunol* 1993;184:47-63.

32. Baum CM, Weissman IL, Tsukamoto ASet al. Isolation of a candidate human hematopoietic stem-cell population. *Proc Natl Acad Sci U S A* 1992;89:2804-8.

33. Ge AZ, Butcher EC. Cloning and expression of a cDNA encoding mouse endoglin, an endothelial cell TGF-beta ligand. *Gene* 1994;138:201-6.

34. Carter RA, Wicks IP. Vascular cell adhesion molecule 1 (CD106): a multifaceted regulator of joint inflammation. *Arthritis Rheum* 2001;44:985-94.

35. Aruffo A, Bowen MA, Patel DDet al. CD6-ligand interactions: a paradigm for SRCR domain function? *Immunol Today* 1997;18:498-504.

36. Gronthos S, Graves SE, Ohta Set al. The STRO-1+ fraction of adult human bone marrow contains the osteogenic precursors. *Blood* 1994;84:4164-73.

37. Gronthos S, Zannettino AC, Hay SJet al. Molecular and cellular characterisation of highly purified stromal stem cells derived from human bone marrow. *J Cell Sci* 2003;116:1827-35.

38. Buhring HJ, Battula VL, Treml Set al. Novel markers for the prospective isolation of human MSC. *Ann N Y Acad Sci* 2007;1106:262-71.

39. Churchman SM, Ponchel F, Boxall SAet al. Transcriptional profile of native CD271+ multipotential stromal cells: evidence for multiple fates, with prominent osteogenic and Wnt pathway signaling activity. *Arthritis Rheum*;64:2632-43.

40. Crigler L, Robey RC, Asawachaicharn Aet al. Human mesenchymal stem cell subpopulations express a variety of neuro-regulatory molecules and promote neuronal cell survival and neuritogenesis. *Exp Neurol* 2006;198:54-64.

41. Croft AP, Przyborski SA. Mesenchymal stem cells expressing neural antigens instruct a neurogenic cell fate on neural stem cells. *Exp Neurol* 2009;216:329-41.

42. Krampera M, Marconi S, Pasini Aet al. Induction of neural-like differentiation in human mesenchymal stem cells derived from bone marrow, fat, spleen and thymus. *Bone* 2007;40:382-90.

43. Lange C, Bassler P, Lioznov MVet al. Liver-specific gene expression in mesenchymal stem cells is induced by liver cells. *World J Gastroenterol* 2005;11:4497-504.

44. Sato Y, Araki H, Kato Jet al. Human mesenchymal stem cells xenografted directly to rat liver are differentiated into human hepatocytes without fusion. *Blood* 2005;106:756-63.

45. Saulnier N, Lattanzi W, Puglisi MAet al. Mesenchymal stromal cells multipotency and plasticity: induction toward the hepatic lineage. *Eur Rev Med Pharmacol Sci* 2009;13 Suppl 1:71-8.

46. Zuk PA, Zhu M, Ashjian Pet al. Human adipose tissue is a source of multipotent stem cells. *Mol Biol Cell* 2002;13:4279-95.

47. Lehmann JM, Lenhard JM, Oliver BBet al. Peroxisome proliferator-activated receptors alpha and gamma are activated by indomethacin and other non-steroidal anti-inflammatory drugs. *J Biol Chem* 1997;272:3406-10.

48. Leinninger GM, Backus C, Uhler MDet al. Phosphatidylinositol 3-kinase and Akt effectors mediate insulin-like growth factor-I neuroprotection in dorsal root ganglia neurons. *FASEB J* 2004;18:1544-6.

49. Rosen ED, MacDougald OA. Adipocyte differentiation from the inside out. *Nat Rev Mol Cell Biol* 2006;7:885-96.

50. Sekiya I, Larson BL, Vuoristo JTet al. Adipogenic differentiation of human adult stem cells from bone marrow stroma (MSCs). *J Bone Miner Res* 2004;19:256-64.

51. Rosen ED, Walkey CJ, Puigserver Pet al. Transcriptional regulation of adipogenesis. *Genes Dev* 2000;14:1293-307.

52. Odrowaz-Sypniewska G. Markers of pro-inflammatory and pro-thrombotic state in the diagnosis of metabolic syndrome. *Adv Med Sci* 2007;52:246-50.

53. Zippel N, Limbach CA, Ratajski Net al. Purinergic receptors influence the differentiation of human mesenchymal stem cells. *Stem Cells Dev*;21:884-900.

54. Gupta A, Leong DT, Bai HFet al. Osteo-maturation of adipose-derived stem cells required the combined action of vitamin D3, beta-glycerophosphate, and ascorbic acid. *Biochem Biophys Res Commun* 2007;362:17-24.

55. Igarashi M, Kamiya N, Hasegawa Met al. Inductive effects of dexamethasone on the gene expression of Cbfa1, Osterix and bone matrix proteins during differentiation of cultured primary rat osteoblasts. *J Mol Histol* 2004;35:3-10.

56. Lee KS, Kim HJ, Li QLet al. Runx2 is a common target of transforming growth factor beta1 and bone morphogenetic protein 2, and cooperation between Runx2 and Smad5 induces osteoblast-specific gene expression in the pluripotent mesenchymal precursor cell line C2C12. *Mol Cell Biol* 2000;20:8783-92.

57. Lee MH, Kim YJ, Kim HJet al. BMP-2-induced Runx2 expression is mediated by Dlx5, and TGF-beta 1 opposes the BMP-2-induced osteoblast differentiation by suppression of Dlx5 expression. *J Biol Chem* 2003;278:34387-94.

58. Komori T. Regulation of osteoblast differentiation by transcription factors. *J Cell Biochem* 2006;99:1233-9.

59. Aubin JE, Liu F, Malaval Let al. Osteoblast and chondroblast differentiation. *Bone* 1995;17:77S-83S.

60. Nakashima K, Zhou X, Kunkel Get al. The novel zinc finger-containing transcription factor osterix is required for osteoblast differentiation and bone formation. *Cell* 2002;108:17-29.

61. Pavlin D, Dove SB, Zadro Ret al. Mechanical loading stimulates differentiation of periodontal osteoblasts in a mouse osteoinduction model: effect on type I collagen and alkaline phosphatase genes. *Calcif Tissue Int* 2000;67:163-72.

62. Pavlin D, Zadro R, Gluhak-Heinrich J. Temporal pattern of stimulation of osteoblast-associated genes during mechanically-induced osteogenesis in vivo: early responses of osteocalcin and type I collagen. *Connect Tissue Res* 2001;42:135-48.

63. Quintana L, zur Nieden NI, Semino CE. Morphogenetic and regulatory mechanisms during developmental chondrogenesis: new paradigms for cartilage tissue engineering. *Tissue Eng Part B Rev* 2009;15:29-41.

64. Pevsner-Fischer M, Levin S, Zipori D. The origins of mesenchymal stromal cell heterogeneity. *Stem Cell Rev* 2011;7:560-8.

65. Etheridge SL, Spencer GJ, Heath DJet al. Expression profiling and functional analysis of wnt signaling mechanisms in mesenchymal stem cells. *Stem Cells* 2004;22:849-60.

66. Dryden GW. Overview of stem cell therapy for Crohn's disease. *Expert Opin Biol Ther* 2009;9:841-7.

67. Iyer SS, Co C, Rojas M. Mesenchymal stem cells and inflammatory lung diseases. *Panminerva Med* 2009;51:5-16.

68. Tyndall A, Uccelli A. Multipotent mesenchymal stromal cells for autoimmune diseases: teaching new dogs old tricks. *Bone Marrow Transplant* 2009;43:821-8.

69. Yi T, Song SU. Immunomodulatory properties of mesenchymal stem cells and their therapeutic applications. *Arch Pharm Res*;35:213-21.

70. Ling L, Nurcombe V, Cool SM. Wnt signaling controls the fate of mesenchymal stem cells. *Gene* 2009;433:1-7.

71. de Boer J, Siddappa R, Gaspar Cet al. Wnt signaling inhibits osteogenic differentiation of human mesenchymal stem cells. *Bone* 2004;34:818-26.

72. Taipaleenmaki H, Abdallah BM, AlDahmash Aet al. Wnt signalling mediates the cross-talk between bone marrow derived pre-adipocytic and pre-osteoblastic cell populations. *Exp Cell Res* 2011;317:745-56.

73. Takada I, Kouzmenko AP, Kato S. Wnt and PPARgamma signaling in osteoblastogenesis and adipogenesis. *Nat Rev Rheumatol* 2009;5:442-7.

74. Lo Surdo J, Bauer SR. Quantitative approaches to detect donor and passage differences in adipogenic potential and clonogenicity in human bone marrow-derived mesenchymal stem cells. *Tissue Eng Part C Methods* 2012;18:877-89.

75. Prockop DJ, Sekiya I, Colter DC. Isolation and characterization of rapidly self-renewing stem cells from cultures of human marrow stromal cells. *Cytotherapy* 2001;3:393-6.

76. Stenderup K, Justesen J, Clausen Cet al. Aging is associated with decreased maximal life span and accelerated senescence of bone marrow stromal cells. *Bone* 2003;33:919-26.

77. Wagner W, Ho AD. Mesenchymal stem cell preparations--comparing apples and oranges. *Stem Cell Rev* 2007;3:239-48.

78. Caplan AI. The mesengenic process. *Clin Plast Surg* 1994;21:429-35.

79. Bonab MM, Alimoghaddam K, Talebian Fet al. Aging of mesenchymal stem cell in vitro. *BMC Cell Biol* 2006;7:14.

80. Dexheimer V, Mueller S, Braatz Fet al. Reduced reactivation from dormancy but maintained lineage choice of human mesenchymal stem cells with donor age. *PLoS One* 2011;6:e22980.

81. Psaltis PJ, Paton S, See Fet al. Enrichment for STRO-1 expression enhances the cardiovascular paracrine activity of human bone marrow-derived mesenchymal cell populations. *J Cell Physiol* 2010;223:530-40.

82. Arufe MC, De la Fuente A, Fuentes Iet al. Chondrogenic potential of subpopulations of cells expressing mesenchymal stem cell markers derived from human synovial membranes. *J Cell Biochem* 2010;111:834-45.

83. Jarocha D, Lukasiewicz E, Majka M. Adventage of mesenchymal stem cells (MSC) expansion directly from purified bone marrow CD105+ and CD271+ cells. *Folia Histochem Cytobiol* 2008;46:307-14.

84. Larson BL, Ylostalo J, Lee RHet al. Sox11 is expressed in early progenitor human multipotent stromal cells and decreases with extensive expansion of the cells. *Tissue Eng Part A* 2010;16:3385-94.

85. Carneiro J, Duarte L, Padovan E. Limiting dilution analysis of antigen-specific T cells. *Methods Mol Biol* 2009;514:95-105.

86. Frisan T, Levitsky V, Masucci M. Limiting dilution assay. *Methods Mol Biol* 2001;174:213-6.

87. Strijbosch LW, Buurman WA, Does RJet al. Limiting dilution assays. Experimental design and statistical analysis. *J Immunol Methods* 1987;97:133-40.

88. Taswell C. Limiting dilution assays for the determination of immunocompetent cell frequencies. I. Data analysis. *J Immunol* 1981;126:1614-9.

89. Kulterer B, Friedl G, Jandrositz Aet al. Gene expression profiling of human mesenchymal stem cells derived from bone marrow during expansion and osteoblast differentiation. *BMC Genomics* 2007;8:70.

90. Ragni E, Vigano M, Rebulla Pet al. What is beyond a qRT-PCR study on mesenchymal stem cell differentiation properties: how to choose the most reliable housekeeping genes. *J Cell Mol Med*;17:168-80.

91. Kode JA, Mukherjee S, Joglekar MVet al. Mesenchymal stem cells: immunobiology and role in immunomodulation and tissue regeneration. *Cytotherapy* 2009;11:377-91.

92. Schinkothe T, Bloch W, Schmidt A. In vitro secreting profile of human mesenchymal stem cells. *Stem Cells Dev* 2008;17:199-206.

93. Delorme B, Charbord P. Culture and characterization of human bone marrow mesenchymal stem cells. *Methods Mol Med* 2007;140:67-81.

94. Janderova L, McNeil M, Murrell ANet al. Human mesenchymal stem cells as an in vitro model for human adipogenesis. *Obes Res* 2003;11:65-74.

95. Post S, Abdallah BM, Bentzon JFet al. Demonstration of the presence of independent pre-osteoblastic and pre-adipocytic cell populations in bone marrow-derived mesenchymal stem cells. *Bone* 2008;43:32-9.

96. Strube P, Mehta M, Baerenwaldt Aet al. Sex-specific compromised bone healing in female rats might be associated with a decrease in mesenchymal stem cell quantity. *Bone* 2009;45:1065-72.

97. Corsi KA, Pollett JB, Phillippi JAet al. Osteogenic potential of postnatal skeletal muscle-derived stem cells is influenced by donor sex. *J Bone Miner Res* 2007;22:1592-602.

98. Meszaros LB, Usas A, Cooper GMet al. Effect of host sex and sex hormones on muscle-derived stem cell-mediated bone formation and defect healing. *Tissue Eng Part A*;18:1751-9.

99. Dudas JR, Losee JE, Penascino VMet al. Leporine-derived adipose precursor cells exhibit in vitro osteogenic potential. *J Craniofac Surg* 2008;19:360-8.

100. Ogawa R, Mizuno H, Watanabe Aet al. Adipogenic differentiation by adipose-derived stem cells harvested from GFP transgenic mice-including relationship of sex differences. *Biochem Biophys Res Commun* 2004;319:511-7.

101. Crisostomo PR, Wang M, Herring CMet al. Sex dimorphisms in activated mesenchymal stem cell function. *Shock* 2006;26:571-4.

102. Csete M. Gender issues in transplantation. *Anesth Analg* 2008;107:232-8.

103. Colter DC, Class R, DiGirolamo CMet al. Rapid expansion of recycling stem cells in cultures of plastic-adherent cells from human bone marrow. *Proc Natl Acad Sci U S A* 2000;97:3213-8.

104. Jiang Y, Mishima H, Sakai Set al. Gene expression analysis of major lineage-defining factors in human bone marrow cells: effect of aging, gender, and age-related disorders. *J Orthop Res* 2008;26:910-7.

105. Moerman EJ, Teng K, Lipschitz DAet al. Aging activates adipogenic and suppresses osteogenic programs in mesenchymal marrow stroma/stem cells: the role of PPAR-

gamma2 transcription factor and TGF-beta/BMP signaling pathways. *Aging Cell* 2004;3:379-89.

106. Kim M, Kim C, Choi YSet al. Age-related alterations in mesenchymal stem cells related to shift in differentiation from osteogenic to adipogenic potential: implication to age-associated bone diseases and defects. *Mech Ageing Dev* 2012;133:215-25.

107. Almeida M, Han L, Martin-Millan Met al. Oxidative stress antagonizes Wnt signaling in osteoblast precursors by diverting beta-catenin from T cell factor- to forkhead box O-mediated transcription. *J Biol Chem* 2007;282:27298-305.

108. Mets T, Verdonk G. In vitro aging of human bone marrow derived stromal cells. *Mech Ageing Dev* 1981;16:81-9.

109. Moldes M, Zuo Y, Morrison RFet al. Peroxisome-proliferator-activated receptor gamma suppresses Wnt/beta-catenin signalling during adipogenesis. *Biochem J* 2003;376:607-13.

110. Rawadi G, Vayssiere B, Dunn Fet al. BMP-2 controls alkaline phosphatase expression and osteoblast mineralization by a Wnt autocrine loop. *J Bone Miner Res* 2003;18:1842-53.

111. Fu M, Rao M, Bouras Tet al. Cyclin D1 inhibits peroxisome proliferator-activated receptor gamma-mediated adipogenesis through histone deacetylase recruitment. *J Biol Chem* 2005;280:16934-41.

112. Tetsu O, McCormick F. Beta-catenin regulates expression of cyclin D1 in colon carcinoma cells. *Nature* 1999;398:422-6.

113. De Boer J, Wang HJ, Van Blitterswijk C. Effects of Wnt signaling on proliferation and differentiation of human mesenchymal stem cells. *Tissue Eng* 2004;10:393-401.

114. Gong Y, Slee RB, Fukai Net al. LDL receptor-related protein 5 (LRP5) affects bone accrual and eye development. *Cell* 2001;107:513-23.

115. Qiu W, Andersen TE, Bollerslev Jet al. Patients with high bone mass phenotype exhibit enhanced osteoblast differentiation and inhibition of adipogenesis of human mesenchymal stem cells. *J Bone Miner Res* 2007;22:1720-31.

116. Eijken M, Meijer IM, Westbroek Ietal. Wnt signaling acts and is regulated in a human osteoblast differentiation dependent manner. *J Cell Biochem* 2008;104:568-79.

117. Kahler RA, Galindo M, Lian Jet al. Lymphocyte enhancer-binding factor 1 (Lef1) inhibits terminal differentiation of osteoblasts. *J Cell Biochem* 2006;97:969-83.

118. Kahler RA, Westendorf JJ. Lymphoid enhancer factor-1 and beta-catenin inhibit Runx2-dependent transcriptional activation of the osteocalcin promoter. *J Biol Chem* 2003;278:11937-44.

119. Ryu JH, Kim SJ, Kim SHet al. Regulation of the chondrocyte phenotype by beta-catenin. *Development* 2002;129:5541-50.

120. Uren A, Reichsman F, Anest Vet al. Secreted frizzled-related protein-1 binds directly to Wingless and is a biphasic modulator of Wnt signaling. *J Biol Chem* 2000;275:4374-82.

121. Bafico A, Gazit A, Pramila Tet al. Interaction of frizzled related protein (FRP) with Wnt ligands and the frizzled receptor suggests alternative mechanisms for FRP inhibition of Wnt signaling. *J Biol Chem* 1999;274:16180-7.

122. Alfaro MP, Pagni M, Vincent Aet al. The Wnt modulator sFRP2 enhances mesenchymal stem cell engraftment, granulation tissue formation and myocardial repair. *Proc Natl Acad Sci U S A* 2008;105:18366-71.

123. Mirotsou M, Zhang Z, Deb Aet al. Secreted frizzled related protein 2 (Sfrp2) is the key Akt-mesenchymal stem cell-released paracrine factor mediating myocardial survival and repair. *Proc Natl Acad Sci U S A* 2007;104:1643-8.

124. Gopalsamy A, Shi M, Stauffer Bet al. Identification of diarylsulfone sulfonamides as secreted frizzled related protein-1 (sFRP-1) inhibitors. *J Med Chem* 2008;51:7670-2.

125. Lee RH, Seo MJ, Pulin AAet al. The CD34-like protein PODXL and alpha6-integrin (CD49f) identify early progenitor MSCs with increased clonogenicity and migration to infarcted heart in mice. *Blood* 2009;113:816-26.

126. Diefenderfer DL, Osyczka AM, Reilly GCet al. BMP responsiveness in human mesenchymal stem cells. *Connect Tissue Res* 2003;44 Suppl 1:305-11.

127. Mei Y, Bian C, Li Jet al. miR-21 modulates the ERK-MAPK signaling pathway by regulating SPRY2 expression during human mesenchymal stem cell differentiation. *J Cell Biochem.*

128. Aksu AE, Horibe E, Sacks Jet al. Co-infusion of donor bone marrow with host mesenchymal stem cells treats GVHD and promotes vascularized skin allograft survival in rats. *Clin Immunol* 2008;127:348-58.

129. Bensidhoum M, Chapel A, Francois Set al. Homing of in vitro expanded Stro-1- or Stro-1+ human mesenchymal stem cells into the NOD/SCID mouse and their role in supporting human CD34 cell engraftment. *Blood* 2004;103:3313-9.

130. Chen X, Armstrong MA, Li G. Mesenchymal stem cells in immunoregulation. *Immunol Cell Biol* 2006;84:413-21.

131. Du YY, Zhou SH, Zhou Tet al. Immuno-inflammatory regulation effect of mesenchymal stem cell transplantation in a rat model of myocardial infarction. *Cytotherapy* 2008;10:469-78.

132. Wang L, Zhao RC. Mesenchymal stem cells targeting the GVHD. *Sci China C Life Sci* 2009;52:603-9.

133. Huang K, Huang SL, Zhou DHet al. [Experiment study of efficacy on hematopoietic reconstitution and GVHD prophylaxis after mesenchymal cell infused by intra-bone marrow cavity or intravenous in rat BMT models]. *Zhonghua Xue Ye Xue Za Zhi* 2007;28:87-92.

134. von Bonin M, Stolzel F, Goedecke Aet al. Treatment of refractory acute GVHD with third-party MSC expanded in platelet lysate-containing medium. *Bone Marrow Transplant* 2009;43:245-51.

135. Fouillard L, Bensidhoum M, Bories Det al. Engraftment of allogeneic mesenchymal stem cells in the bone marrow of a patient with severe idiopathic aplastic anemia improves stroma. *Leukemia* 2003;17:474-6.

136. Le Blanc K, Tammik L, Sundberg Bet al. Mesenchymal stem cells inhibit and stimulate mixed lymphocyte cultures and mitogenic responses independently of the major histocompatibility complex. *Scand J Immunol* 2003;57:11-20.

137. Rasmusson I, Ringden O, Sundberg Bet al. Mesenchymal stem cells inhibit lymphocyte proliferation by mitogens and alloantigens by different mechanisms. *Exp Cell Res* 2005;305:33-41.

138. Aggarwal S, Pittenger MF. Human mesenchymal stem cells modulate allogeneic immune cell responses. *Blood* 2005;105:1815-22.

139. Krampera M. Mesenchymal stromal cell 'licensing': a multistep process. *Leukemia*;25:1408-14.

140. Galipeau J. The mesenchymal stromal cells dilemma--does a negative phase III trial of random donor mesenchymal stromal cells in steroid-resistant graft-versus-host disease represent a death knell or a bump in the road? *Cytotherapy*;15:2-8.

141. Bernardo ME, Zaffaroni N, Novara Fet al. Human bone marrow derived mesenchymal stem cells do not undergo transformation after long-term in vitro culture and do not exhibit telomere maintenance mechanisms. *Cancer Res* 2007;67:9142-9.

142. Moll G, Rasmusson-Duprez I, von Bahr Let al. Are therapeutic human mesenchymal stromal cells compatible with human blood? *Stem Cells*;30:1565-74.

143. von Bahr L, Sundberg B, Lonnies Let al. Long-term complications, immunologic effects, and role of passage for outcome in mesenchymal stromal cell therapy. *Biol Blood Marrow Transplant*;18:557-64.

144. Haskins K, Portas M, Bradley Bet al. T-lymphocyte clone specific for pancreatic islet antigen. *Diabetes* 1988;37:1444-8.

145. Abumaree M, Al Jumah M, Pace RAet al. Immunosuppressive properties of mesenchymal stem cells. *Stem Cell Rev*;8:375-92.

146. Siegel G, Schafer R, Dazzi F. The immunosuppressive properties of mesenchymal stem cells. *Transplantation* 2009;87:S45-9.

147. Bai L, Lennon DP, Eaton Vet al. Human bone marrow-derived mesenchymal stem cells induce Th2-polarized immune response and promote endogenous repair in animal models of multiple sclerosis. *Glia* 2009;57:1192-203.

148. Lee RH, Seo MJ, Reger RLet al. Multipotent stromal cells from human marrow home to and promote repair of pancreatic islets and renal glomeruli in diabetic NOD/scid mice. *Proc Natl Acad Sci U S A* 2006;103:17438-43.

149. Omori Y, Honmou O, Harada Ket al. Optimization of a therapeutic protocol for intravenous injection of human mesenchymal stem cells after cerebral ischemia in adult rats. *Brain Res* 2008;1236:30-8.

150. Onda T, Honmou O, Harada Ket al. Therapeutic benefits by human mesenchymal stem cells (hMSCs) and Ang-1 gene-modified hMSCs after cerebral ischemia. *J Cereb Blood Flow Metab* 2008;28:329-40.

151. Zhou K, Zhang H, Jin Oet al. Transplantation of human bone marrow mesenchymal stem cell ameliorates the autoimmune pathogenesis in MRL/lpr mice. *Cell Mol Immunol* 2008;5:417-24.

152. Francois M, Romieu-Mourez R, Li Met al. Human MSC suppression correlates with cytokine induction of indoleamine 2,3-dioxygenase and bystander M2 macrophage differentiation. *Mol Ther*;20:187-95.

153. Dominici M, Paolucci P, Conte Pet al. Heterogeneity of multipotent mesenchymal stromal cells: from stromal cells to stem cells and vice versa. *Transplantation* 2009;87:S36-42.